DEGRADATION OF COHERENCE AND CORRELATION WHEN SOUND FROM A MOVING SOURCE IS REFLECTED FROM SOLID SURFACES

by

JAMES PATRICK HUTTON
B.Sc., ROYAL ROADS MILITARY COLLEGE, 1979

A THESIS SUBMITTED IN PARTIAL FULFILLMENT
OF THE REQUIREMENTS FOR THE DEGREE OF
MASTER OF SCIENCE
in the Department
of
Physics

ACCEPTED
FACULTY OF GRADUATE STUDIES
[redacted]
DATE June 1982

We accept this thesis as conforming
to the required standard

[redacted]
W.M. Barss

[redacted]
G.H. Brooke

[redacted]
W.K. Hastings

[redacted]
A. Watton

UNIVERSITY OF VICTORIA
July 1981

Supervisor: Professor W.M. Barss

ABSTRACT

The propagation of a sound in ice-covered Arctic waters is complicated by the sound's repeated encounters with the under surface of the ice. This study addresses itself to sound propagation in the Arctic by investigating the influence of model reflecting surfaces on the coherence and cross correlation of sound, transmitted from a moving source and received by two remotely located sensors.

The signals from the sensors, for different reflecting surfaces, are processed in real time by a commercial spectrum analyser to determine which factors degrade the coherence most severely. The study shows that, when the sound reaches the sensors by reflection from an irregular solid surface, the degradation may be attributed to changes in the Doppler shifted components of the sounds at the sensors and to changes in acoustic interference patterns. In addition, the study compares cross correlation and coherence and concludes that the effects of the irregular reflecting surface may be less severe for cross correlation.

Examiners:

[redacted]
W.M. Barss

[redacted]
G.H. Brooke

[redacted]
W.K. Hastings

[redacted]
A. Watton

TABLE OF CONTENTS

TABLE OF CONTENTS (con't)

TABLE OF CONTENTS (con't)

TABLE OF CONTENTS (con't)

LIST OF TABLES

LIST OF FIGURES

LIST OF FIGURES (con't)

LIST OF FIGURES (con't)

LIST OF FIGURES (con't)

LIST OF FIGURES (con't)

LIST OF FIGURES (con't)

LIST OF FIGURES (con't)

LIST OF FIGURES (con't)

LIST OF SYMBOLS

Symbol	Definition	Units
c	Sound speed	m/s
C_k	Cross correlation of a digital sequence	
$C(\tau)$	Cross correlation of a continuous series	
d_n	Depth of the n^{th} well in a quadratic residue diffusor	m
D	The separation of the sensors	m
f	Frequency	Hz
f_k	A digital time sequence	
F_n	The Fourier transform of the digital time sequence f_k	
$f(t)$	A continuous time series	
$F(\omega)$	The Fourier transform of the continuous time series $f(t)$	
g	The sound speed gradient	s^{-1}
g_k	A digital time sequence	
G_n	The Fourier transform of the digital time sequence g_k	
$g(t)$	A continuous time series	
$G(\omega)$	The Fourier transform of the continuous time series $g(t)$	
j	$(-1)^{\frac{1}{2}}$	
m	The number of samplings made of a time series in producing coherence	
N	The number of samples obtained in one sampling of a time series	

LIST OF SYMBOLS (con't)

Symbol	Definition	Units
P	A power sequence	
r	The distance from the source to the array	m
R	The radius of curvature of a sound ray	m
S	The path difference between the sound rays arriving at the two microphones	m
T	The period of a time series	s
Δt	The time interval between samples in a digital sequence	s
v	The velocity of the source	m/s
z	The specific acoustic impedance	kg/m^2s
α	An angle in general	rad
β	Some small grazing angle	rad
γ_n	The coherence of a digital sequence	
θ	The angle defined by the intersection of the line through the array and the line from the source to the midpoint of the array	degree
λ	Wavelength	m
τ	Time difference or time delay	s
ϕ	The phase difference between the sounds arriving at each microphone	rad
ϕ_n	The phase difference that results when a sound wave travels down and up the n^{th} well of a quadratic residue diffusor	rad

LIST OF SYMBOLS (con't)

Symbol	Definition	Units
Ω	The angular velocity of the source	rad/s
ω	Angular frequency	rad/s

ACKNOWLEDGEMENTS

I wish to express my gratitude to Dr. W.M. Barss for his skillful supervision of this project and for his many constructive critiques that have served to heighten the educational rewards of this research.

I also wish to thank the Defence Research Establishment (Pacific) for providing major capital equipment for this project and the University of Victoria for providing graduate fellowships.

DEDICATION

I dedicate this thesis to MWO Charles G. Mackinnon who, through his example and encouragement, inspired this high school dropout to continue his education, and to my wife Patricia Anne for her constant encouragement and understanding, and for her many sacrifices over the past ten years which have enabled this pursuit of knowledge.

1. INTRODUCTION

1.1 The Arctic Propagation Problem

The transmission of sound between a source and a receiver in ice-covered waters is much more complicated than that in air. The acoustic energy emitted from a source in the ocean does not travel in a straight line but, rather, propagates along many curved paths which are determined by local velocity gradients (see Appendix A1). Unless the receiver is in the vicinity of the source, these curved paths often result in the sound's being reflected from the surface and/or bottom, before arriving at the receiver.

These reflections are of particular interest in ice-covered Arctic waters, where most of the acoustic energy is confined to a shallow sound channel whose axis is at or near the surface (see Appendix A2). The velocity gradient in the Arctic causes the sound to be refracted upward, so that it is repeatedly reflected or scattered by the irregular surface of the ice. This combination of upward refraction and downward reflection results in propagation phenomena unique to polar oceans.

In addition, the polar transmission medium can behave like a bandpass filter. For example, in deep water, frequencies above 30Hz are rapidly attenuated and scattered by the repeated encounters with the ice, while

frequencies below 15Hz are not effectively trapped in the channel and thus experience attenuation resulting from spherical divergence[1] (see Appendix A2). As a result, acoustic energy transmitted in the Arctic can undergo dramatic changes in character when propagating over long ranges. Acoustic energy from explosive sources has been observed to arrive at the receiver as almost sinusoidal oscillations,[2] rather than the many discrete pulses, ie. wideband energy, that are observed when a similar signal is transmitted in temperate oceans. As well, frequency dispersion can occur within the pass-band.[3] That is, in deep water, wave packets with different frequencies tend to travel with different group velocities, with low frequencies travelling faster than high ones.

As a result of these propagation characteristics, sound transmitted in the Arctic arrives at the receiver severely distorted and possessing few recognizable characteristics of the transmitted sound. Adding to the problem of detecting its arrival is the ever-present ambient noise which disguises the already distorted signal.

Under such conditions the transmitted sound can be more readily detected by comparing the signals arriving at two or more receivers having a constant separation

between them. The comparisons are commonly made by means of either the coherence or the cross correlation of the two signals. In the coherence method, the comparisons are made entirely in the frequency domain, while in the cross-correlation method the comparison is made in the time domain (as described in Chapter 5).

When the source is in motion, field observations indicate that the multiple reflections from the rough surface of the ice have a severe detrimental effect on the coherence of the sound at remotely located sensors. This research addresses itself to this problem by investigating coherence and cross correlation in a model environment. The study employs a commercial signal analyser to process the signals received at two microphones while a source is in motion in the presence of solid reflecting surfaces.

1.2 Related Studies

A number of articles have been published that deal with the primary elements involved in this problem (source motion and the presence of rough reflecting surfaces) on an individual basis.

The effects of sound reflection on cross correlation was investigated by D'Antoni and Hill[4] (1965). A model water tank was used to observe the effects of reflections from a wind driven surface on the cross correlation of

the electrical signal at the sound transmitter with that received at a single hydrophone. The study indicates a finite correlation between the transmitted and received signals. Although a considerable amount of distortion is introduced by the single reflection from the rough surface, the study concludes that the propagation path can be used for communication.

Clay and Medwin[5] (1969) use a similar model to show a significant correlation between the signals received at two hydrophones after being reflected from a wind driven surface. They suggest that, although a rough surface distorts the sound transmitted from a stationary source, the sound remains reasonably coherent.

Motion-induced degradation of coherence has been investigated by Gerlach[6] (1978), Flanagan and Weinberg[7] (1980) and Young[8] (1980). Gerlach's study, which is of particular interest to this investigation, concerns the degradation in cross correlation observed for sound arriving at a pair of sensors from a distant, moving source by direct paths in a homogeneous medium. Gerlach showed the correlation degradation to be a complex function involving the mean frequency of the source, the length of the analysis interval or correlation integration time and the motion of the source relative to the sensors. He further indicated that there is a characteristic

integration time T, determined by the geometry of the system, separating an initial period of slow decrease in correlation from a later period of more rapid decrease. Gerlach concludes that source motion creates an upper bound on the useful correlation integration time from the standpoint of maximizing processor gain. Thus, for the purposes of this study, correlation degradation induced solely by source motion can be minimized by exercising control over both the time required for analysis and the geometry of the system.

1.3 General Approach

A model environment simulating the field situation, is provided by an anechoic chamber 3.1m wide, 4.5m long and 2.1m high. The model consists of a sound source either stationary or travelling at constant speed along a predetermined path. The sound transmitted from the source is received at two sensors. The cross correlation and coherence of the electrical signals at the sensors are then computed with the aid of a dual channel spectrum analyser.

The Nicolet 660 dual channel spectrum analyser is employed in this study because of its availability. However it is not necessarily the best instrument for computing power spectral estimates. In particular its inability to perform certain data manipulation in the

frequency domain, such as spectrum smoothing as discussed by Jenkins and Watts,[9] severely limits the quality of the spectral estimates. Hence the coherence and possibility the correlation estimates are in turn limited by the capabilities of this analyser. (See also Thompson[10] on the advantages of Adaptive smoothing, Jenkins and Watts[11] on the difficulties in estimating coherence, and Kleiner, Martin and Thomson[12] for more sophisticated methods of estimating spectra.)

Studying this problem by means of a scale model provides several advantages that can not be realized in the deep ocean. Primarily the model allows the phenomenon to be observed in isolation, thus avoiding interference from other propagation phenomena associated with sound transmission in the open ocean.

In addition, the model permits the effects of refleection and source motion to be studied independently as well as in combination. The sequence followed is: (a) moving source without reflectors, ie., direct sound paths only; (b) stationary source and various reflectors, with the direct paths suppressed; and (c) moving source and various reflectors, again with the direct path suppressed.

2. CHOICE OF SUITABLE MODEL PARAMETERS

2.1 Field Parameters

The purpose of this chapter is to obtain appropriate scaling of microphone separation D, source frequency f and source velocity v. These scaled parameters will enable the degradation in coherence and cross correlation that has been observed in the field to be reproduced in the anechoic chamber.

To simplify the calculation of these parameters, consider the source travelling with velocity v in the system illustrated in Fig. 2.1. The microphone array is centered at the origin of a cartesian coordinate system and the motion of the source is confined to the horizontal x-y plane. The position of the source is conveniently described by the radius r and the polar angle θ with respect to the line through the microphones. Estimations of field parameters based on this geometry are shown in Table I.

2.2 Field Rates of Change

When the transducer separation is much less than the source distance, the two direct paths from the source have a path difference S which is approximately equal to D cos θ. The path difference changes at a rate given, on substituting v/r for $d\theta/dt$, by the expression

$$\dot{S} = (Dv/r) \sin \theta \qquad (2.1)$$

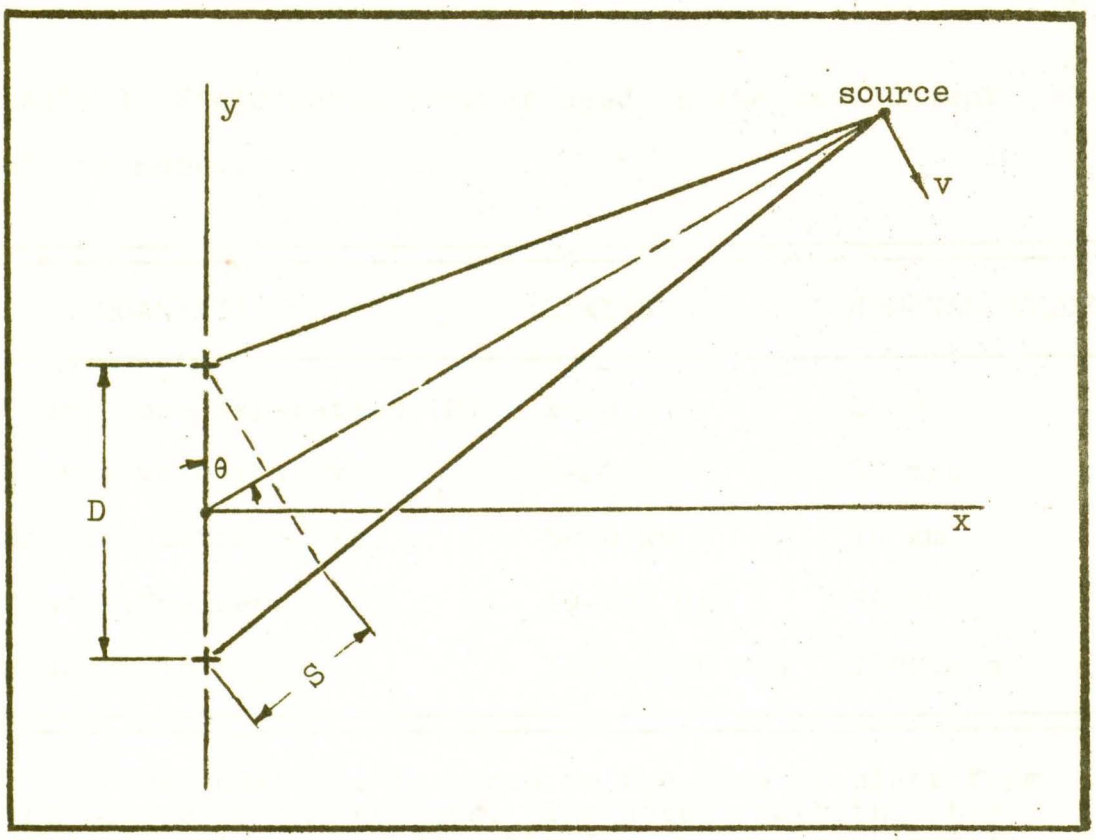

FIG. 2.1 Array source geometry showing the path difference that results when the source is displaced a distance of $r(\pi/2 - \theta)$ meters from the perpendicular bisector of the array.

TABLE I Field parameters as used in the development of the model.

QUANTITY	LIMITS	NOMINAL VALUE
Microphone separation (D)	1-60 m	10 m
Source velocity ($\bar{v}$)	0-20 m/s	10 m/s
Source distance[a] (r)	5-20 km	10 km
Source frequency (f)	10-200 Hz	50 hz
Sound velocity (c)	1455-1520 m/s	1500 m/s

[a]This distance is based on the line of sight from the source to the sensors. The actual path that the sound travels is considerably longer, as described in Appendix A.

Corresponding to the path difference is a propagation time difference τ given by $(D/c) \cos \theta$, where c is the sound velocity. The time-difference rate of change is therefore

$$\dot{\tau} = (Dv/rc) \sin \theta \qquad (2.2)$$

The difference in path length causes a sound to arrive at the two microphones with a phase difference $\phi = 2\pi S/\lambda = 2\pi fS/c$, where f is the frequency of the sound and λ its wavelength in the medium. The phase difference rate of change is then

$$\dot{\phi} = (2\pi fDv/rc) \sin \theta \qquad (2.3)$$

To ensure that the model parameters accurately

represent the conditions found in the field, it is necessary to include the maximum rates of change in these calculations. These essential rates of change are greatest when the source is 'broadside' to the line through the two transducers, ie. in the plane which bisects this line at right angles. These maximum rates of change found in the field are obtained by letting $\theta = \pi/2$ rad in Eqs. (2.1), (2.2) and (2.3) and are shown in Table II.

TABLE II The maximum field rates of change, from Eqs. (2.1)-(2.3). The minimum values shown were calculated using a sensor separation of 1 m, a source velocity of 1 m/s, a range of 20 km and a frequency of 10 Hz.

QUANTITY	LIMITS	NOMINAL VALUE
$\dot{S}$	50×10^{-6} - 0.24 m/s	0.01 m/s
$\dot{\tau}$	0.033 - 160 μs/s	6.67 μs/s
$\dot{\phi}$	2.6×10^{-6} - 0.3 rad/s	8.4×10^{-3} rad/s

2.3 Scaling the Field Parameters

The primary constraints in developing the laboratory models are the physical dimensions of the anechoic chamber and the velocity of sound in air (343 m/s). The relatively free variables are the microphone separation,

the source velocity and, when considering path- and time-difference criteria, the frequency.

As indicated in Eqs. (2.1) and (2.2), the path-difference and time-difference rates of change are independent of frequency. By substituting their nominal values (Table II) in Eqs. (2.1) and (2.2), expressions for nominal model source velocity can be obtained. Thus a path-difference rate of change of 0.01 m/s results in the model velocity being given by

$$v = 0.01 \frac{r}{D} \text{ m/s} \tag{2.4}$$

Similarly a time-difference rate of change of 6.7 μs/s results in a corresponding expression for model velocity given by

$$v = 6.7 \times 10^{-6} \frac{rc}{D} \text{ m/s} \tag{2.5}$$

Since r and c are known quantities, the field conditions can be simulated in the model by choosing values of v and D that satisfy either (2.4) or (2.5). These equations are represented by the "nominal" curves in Figs. 2.2 and 2.3. Also included are curves based on the maximum and minimum field rates of change. These curves represent extreme field conditions and hence their probability of occurrence is small. They have been included so that the full range of field conditions may be appreciated. However, calculations and laboratory experiments are based on the nominal values only.

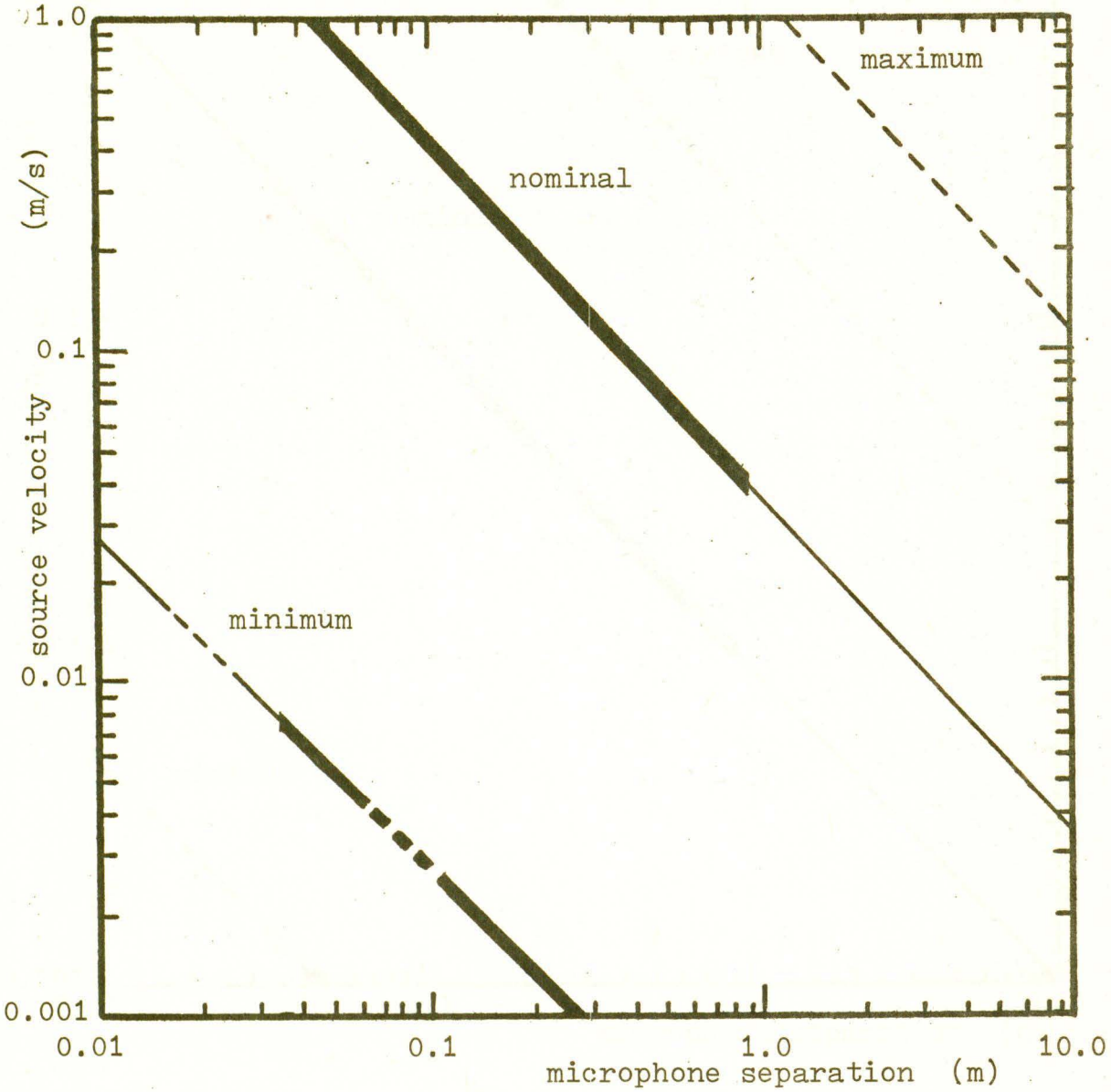

FIG. 2.2 Comparison between model source velocity and microphone separation based on field path-difference rates of change. The heavy black lines represent the physical limitations of the microphones and the anechoic chamber.

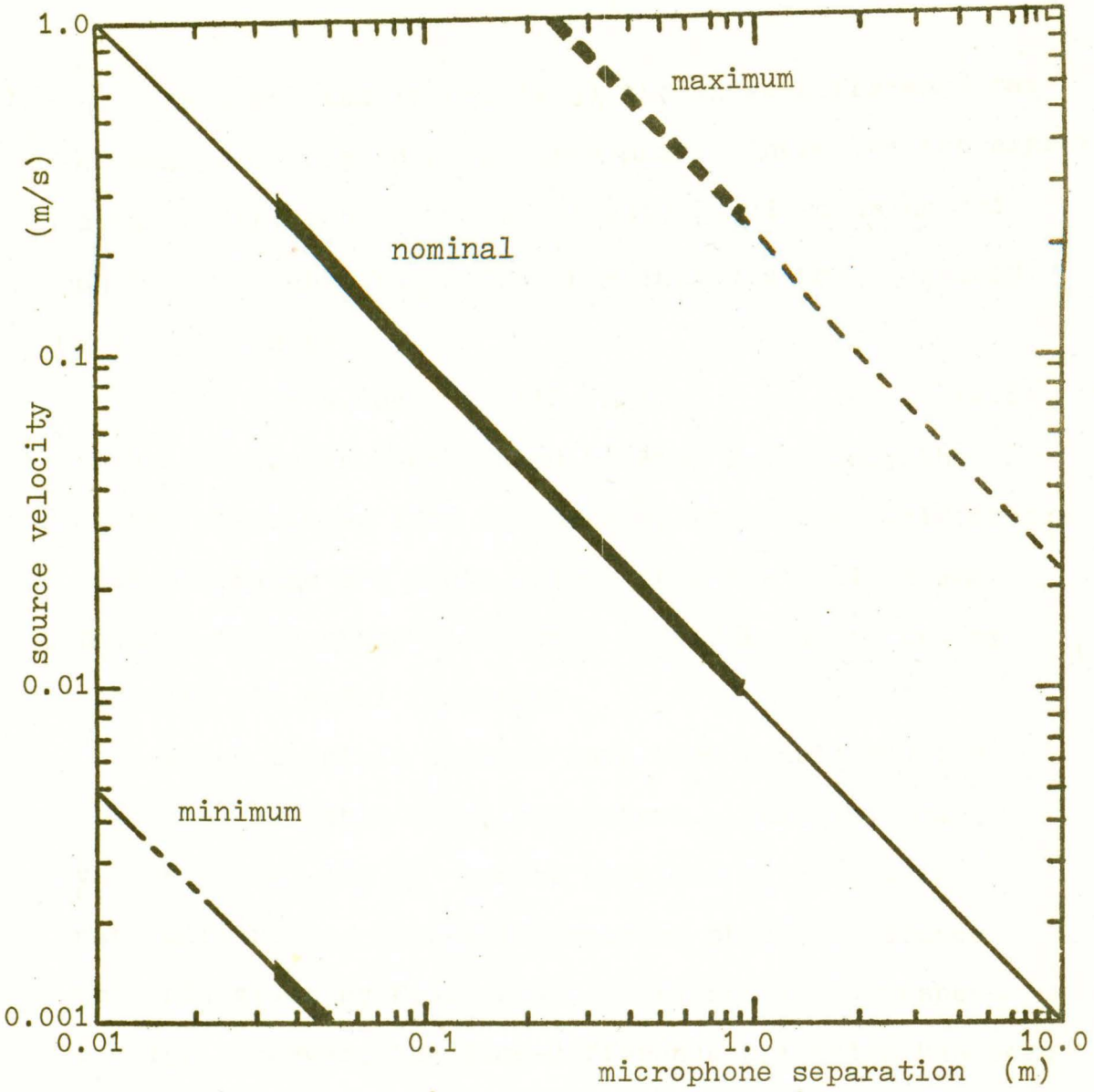

FIG. 2.3 Comparison between model source velocity and microphone separation based on field time-difference rates of change. The heavy black lines indicate the physical limitations of the microphones and the anechoic chamber.

As indicated in Eq. (2.3) the phase-difference rate of change is dependent on frequency. Therefore the expression for the model source velocity obtained using the phase-difference rate of change includes the frequency and is given by

$$v = 0.0084\ rc/2\pi fD \quad m/s \qquad (2.6)$$

This equation is represented by Fig. 2.4. Only the curves calculated from the nominal field phase-difference rate of change are shown, since both the minimum and maximum field phase-difference criteria can be met by altering the model frequency.

Three possible methods have been considered for obtaining suitable model parameters. That is, model values of v and D can be obtained by satisfying path-difference, time-difference or phase-difference criteria given by Eqs. (2.4), (2.5) and (2.6) respectively. However, the time-difference criterion has been chosen for this study because it leaves the frequency as a free variable and is appropriate to the use of the cross-correlation function as a measure of the relation between the signals from the two microphones.

2.4 Additional Considerations

When the physical size of the microphones is considered, a lower limit of their separation becomes apparent (approximately 0.03 m). As well, all calcula-

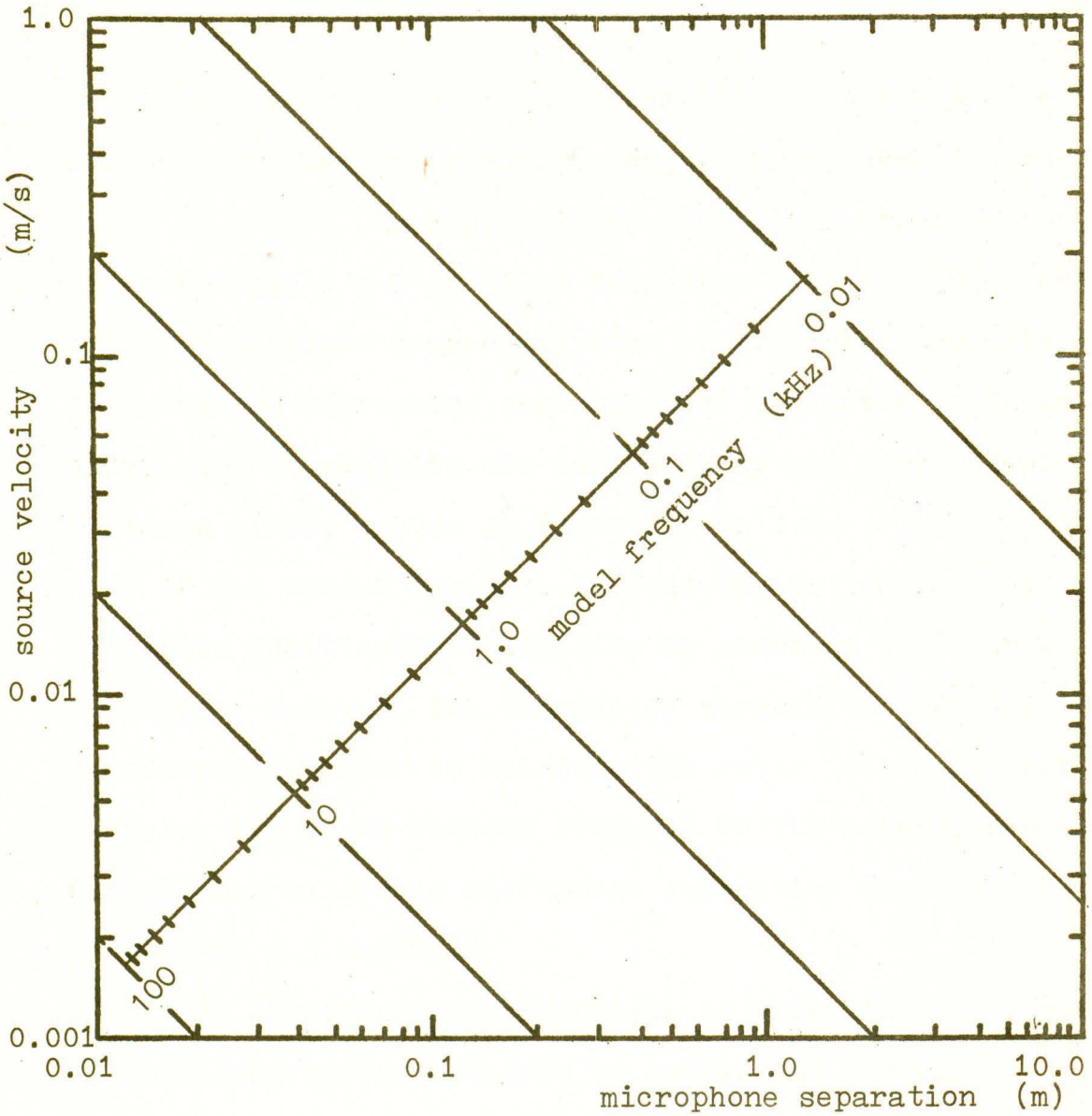

FIG. 2.2 Comparison between model source velocity and microphone separation based on nominal phase-difference rate of change.

tions have been based on the assumption that the source distance r is much greater than the transducer separation D. If D is kept less than $r/5$, the error in the approximation $S = D \cos \theta$ is less than 0.5% for θ near $\pi/2$. The maximum source distance of 4.5 meters results in a maximum microphone separation of 0.9 meters. These additional constraints are indicated by the heavy black portions of the curves in Figs. 2.2 to 2.4.

If the source distance is reduced, it is possible to obtain additional flexibility in choosing the source velocity. However, the transducer separation must also be reduced in order to maintain the ratio of r:D. For example, if r is reduced from 4.5 to 1.5 meters, then the maximum allowable microphone separation must also be reduced to 0.3 meters.

This additional consideration is shown in Fig. 2.5, in which the curves, obtained by satisfying the time-difference criterion, may be used to obtain values of source velocity, microphone separation and source distance. The ranges for the model parameters, taken from these curves, are tabulated in Table III.

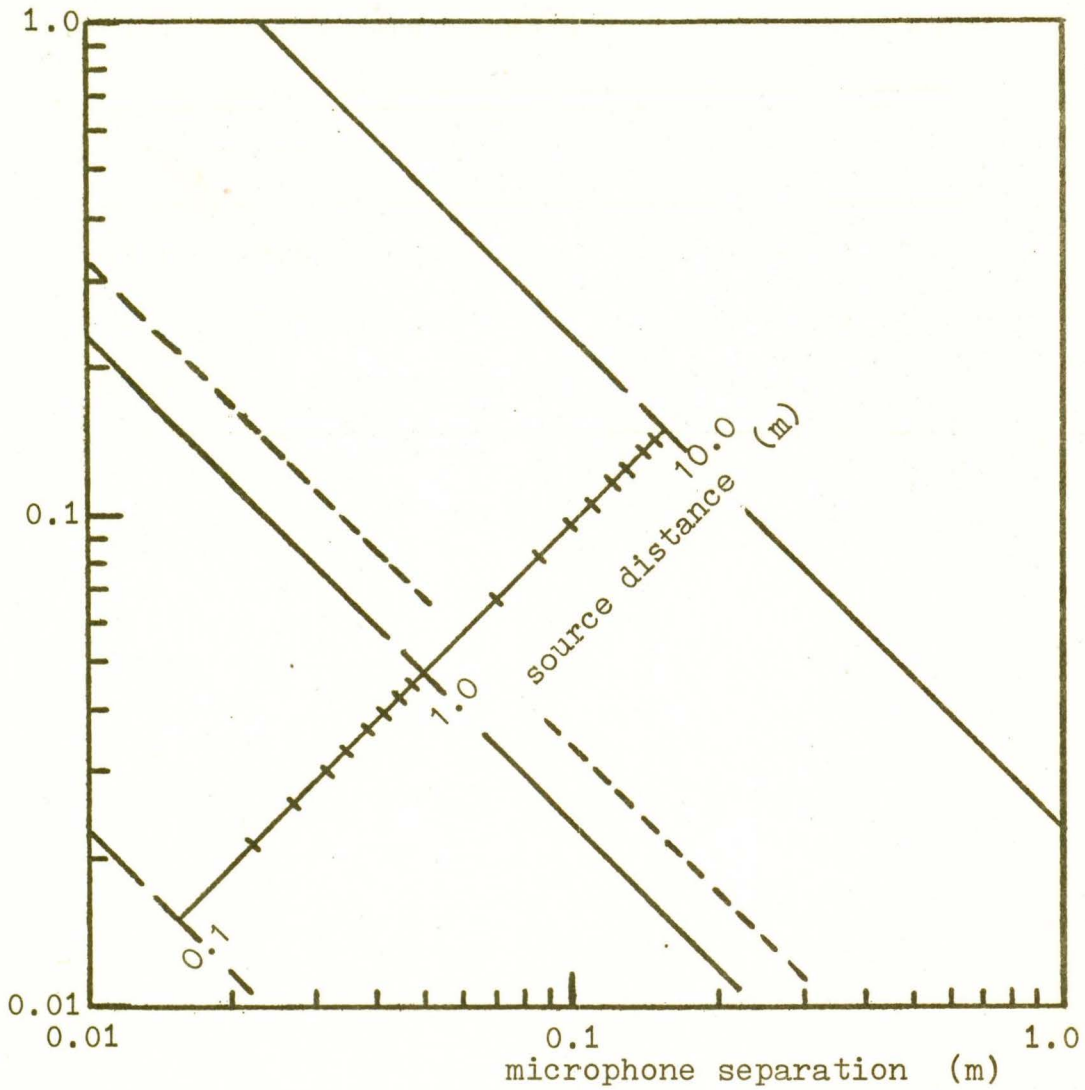

FIG. 2.5 Comparison between model source velocity and microphone separation for different values of source distance, with model calculations based on the nominal time-difference rate of change.

TABLE III Scaled parameters developed for the model.

QUANTITY	
Source velocity (v)	0.012-1.0 m/s
Source distance (r)	0.5-4.5 m
Transducer separation (D)	0.01-0.9 m

3. DESIGN OF MOVING SOURCE APPARATUS

3.1 Physical Criteria

The anechoic chamber in the Psychology Department provides an ideal environment for modeling the hydrophone array and moving source in air. The absence of unwanted reflections simplifies the experimental procedure and enhances the accuracy of the results. However, since this facility is shared with other researchers it is necessary to dismantle the model and remove all equipment on the completion of each allotted time period. It is therefore essential that the moving source apparatus be completely portable and capable of being re-positioned at the beginning of each experiment with some degree of accuracy.

It is also desirable to be able to repeat any experiment and duplicate previous results. Therefore, the apparatus must have the capability of reproducing the relative positions of the source and sensors during each successive run. Also, since it may be necessary to calculate these positions accurately for any instant in time it is desirable that the motion of the source be cyclic.

3.2 Model Criteria

The model parameters described in Chapter 2 (Table

III) were developed with the maximum possible source distance of 4.5 meters. However the simplest way to achieve the cyclic source motion described above is to have the source revolving about the sensors. This reduces the maximum allowable source distance to 1.5 meters. The corresponding maximum and minimum values of source velocity, taken from Fig. 2.5 are then 0.15 m/s and 0.01 m/s respectively.

The maximum rate at which the source is required to rotate about the sensors is given by

$$RPM_{(max)} = 60v/2\pi r \qquad (3.1)$$

The limiting values of angular velocity are obtained by substituting the maximum and minimum values of source velocity into this equation along with the source distance of 1.5 m. These values are 0.95 and 0.06 rpm. Hence the rotating source must be capable of achieving these limiting angular velocities in order to accurately satisfy the model requirements.

3.3 Description of the Apparatus

Several possible designs for the moving source apparatus were considered. Each of these designs satisfied the above mentioned physical and model criteria. However the design shown in Fig. 3.1 was selected for its simplicity and versatility.

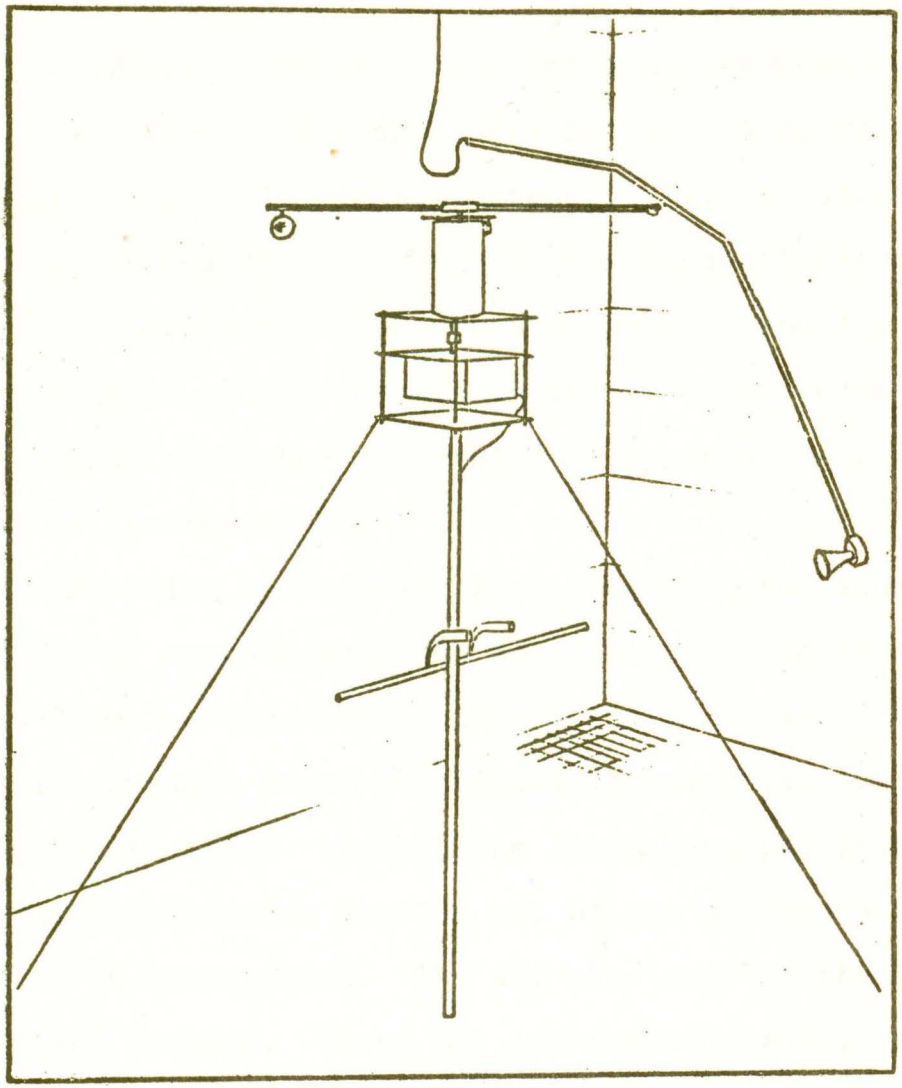

FIG. 3.1 A simplified drawing of the moving source apparatus set up in the anechoic chamber.

The source consists of a small horn-speaker mounted on one end of a rotating arm. The arm is driven by a 24 v reversible motor which is supported by a 1.5 cm diameter central shaft and held in place by three adjustable guy wires. The positions of the central support and guy wires have been clearly marked on the steel grate deck of the anechoic chamber to permit the accurate re-positioning of the apparatus.

The rotating arm is made from 1 cm diameter aluminum tubing and is counter-weighted to eliminate bending moments from the supporting shaft. Its flexible joints enable the speaker to be positioned either above or in the horizontal plane through the fixed sensors, while its variable extension enables all of the desired source distances to be achieved. The arm also carries the feed line to the speaker. Since the arm revolves slowly and its direction is reversible, the feed line does not require the use of a slip ring, but is simply suspended from the ceiling of the chamber at the axis of rotation of the arm.

The drive unit is shown in Fig. 3.2. The angular velocity of arm can be changed by replacing the first reduction gear, while its direction of rotation can be reversed by means of the switch shown in Fig. 3.2. For a detailed description of this unit refer to Appendix B.

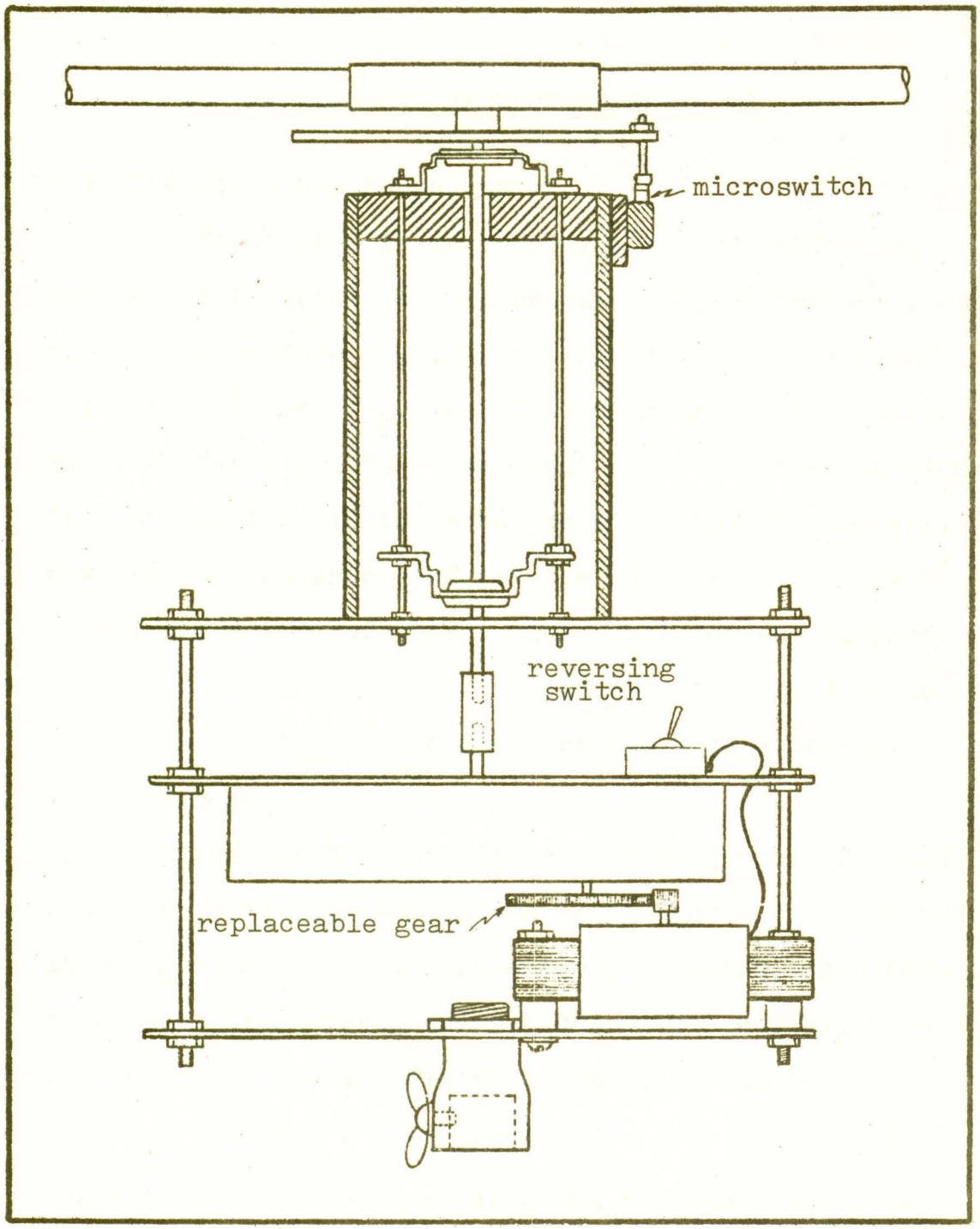

FIG. 3.2 A partial cut-away view of the drive unit. The combined gear ratio is 2400:1 as shown. This results in an angular velocity of 0.75 RPM.

4. APPROPRIATE REFLECTING SURFACES

4.1 The Field RMS Roughness

The first step in developing a scaled reflecting surface that reproduces the essential characteristics of the random surface found in the field is to establish its rms roughness σ_F. Results of experimental studies by H. W. Marsh and R. H. Mellen,[13] of sound reverberation from Arctic ice, indicate an rms roughness of 3 meters. However, the roughness of the ice is known to vary with location and time of year. Therefore, for the purposes of this study the field rms roughness is assumed to be within the range of 1 to 7 meters and have a nominal value of 3 meters.

Nominal field values for source frequency f_F and sound velocity c_F were given in Chapter 2 as 50 Hz and 1500 m/s respectively. These two parameters, when combined with the corresponding model values establish an rms roughness scaling factor as shown in Eq. (4.1).

$$\eta = \lambda_M/\lambda_F = c_M f_F / c_F f_M \tag{4.1}$$

The relationship between field rms roughness and model rms roughness is then given by

$$\sigma_M = \eta \sigma_F \tag{4.2}$$

The substitution of the values of sound velocity in the two media and the nominal value of field source frequency

results in the following linear relationship between model and field rms roughness:

$$\sigma_M = 11.43\ \sigma_F / f_M \qquad (4.3)$$

This relationship is also shown in Fig. 4.1 in the form of a convenient chart from which appropriate values of model rms roughness can be obtained from various field values. This chart indicates that the model surface should have a nominal roughness of approximately 0.34 cm when a model frequency of 10 kHz is used for the source.

4.2 Additional Surface Characteristics

Marsh and Mellen indicate that reflection from the ice surface is poor at grazing angles exceeding 13 degrees. Therefore for the purposes of developing a model of the ice surface it is assumed that sound arriving at the surface with grazing angles greater than 13 degrees is scattered diffusely. In addition, it is assumed that the surface behaves like a mirror for sound arriving with grazing angles less than 13 degrees.

Thus an ideal model of the ice surface would possess these reflecting characteristics and have an rms roughness of approximately 0.34 cm. To facilitate the calculation of its rms roughness it is also desirable that the surface have a simple mathematical approximation.

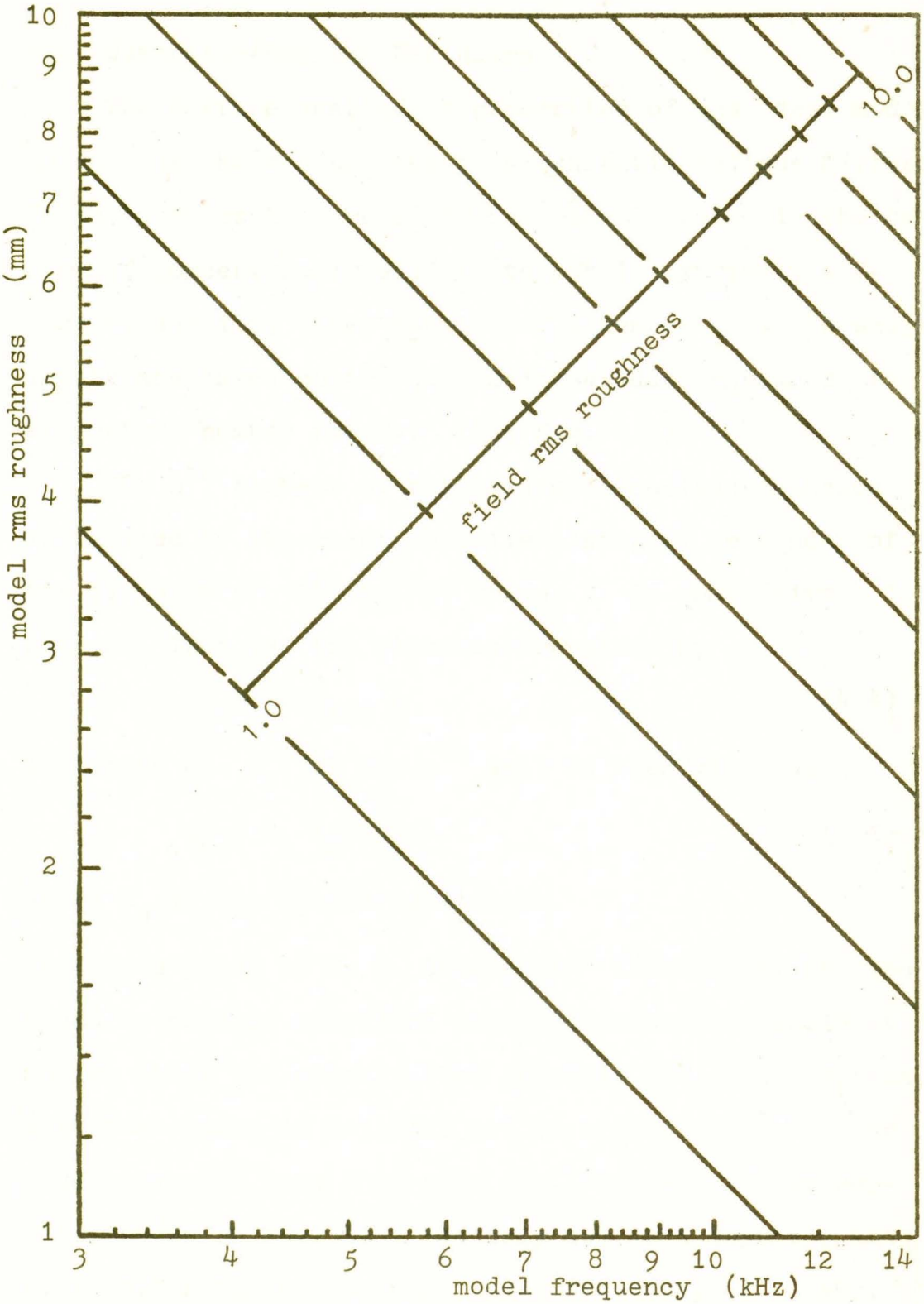

FIG. 4.1 Relationship between field and model rms roughness.

4.3 Quadratic-Residue Diffusors

The diffuse scattering properties of the ideal model surface can be represented by a quadratic-residue diffusor. These surfaces have recently been incorporated in the design of concert hall ceilings to obtain extremely diffuse reflection. They consist of a number of wells whose depths are based on the quadratic-residue sequences of elementary number theory. (See Fig. 4.2)

The n^{th} element of the quadratic-residue sequence is defined by the least positive (integer) remainder of the division of n^2 by N, where N is some prime number. That is, the elements are given by

$$S_n = (n)^2 \bmod N \tag{4.4}$$

The depth of d_n of the n^{th} well is then given by

$$d_n = S_n \lambda_o / 2N \tag{4.5}$$

where λ_o is the design wavelength.

In a study by M. R. Schroeder[14] these surfaces were found to produce excellent sound diffusion for incident angles about the normal. (See Appendix C1). In addition, a surface based on N=3 will act as a good reflector for grazing angles less than some small angle β. This surface, shown in Fig. 4.3, has only two well depths, 0 and 0.57 cm, for the center band model frequency of 10 kHz. It is apparent that β is a function of the well width w.

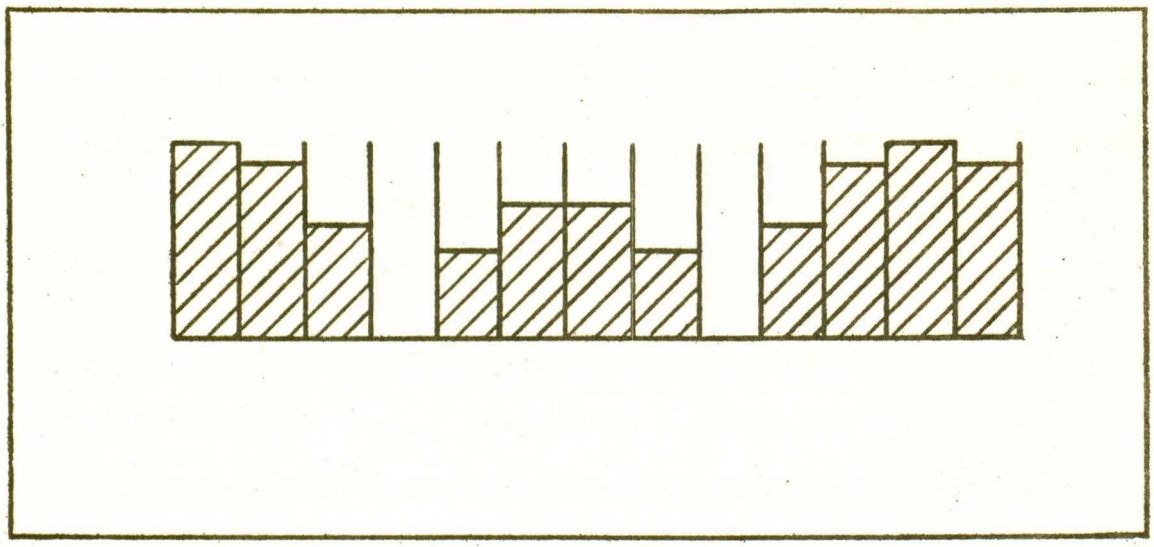

FIG. 4.2 Cross section of a surface based on the quadratic residue sequence for N = 11. From left to right the relative depths are; 0,1,4,9,5,3,3,5,9,4,1,0,1.

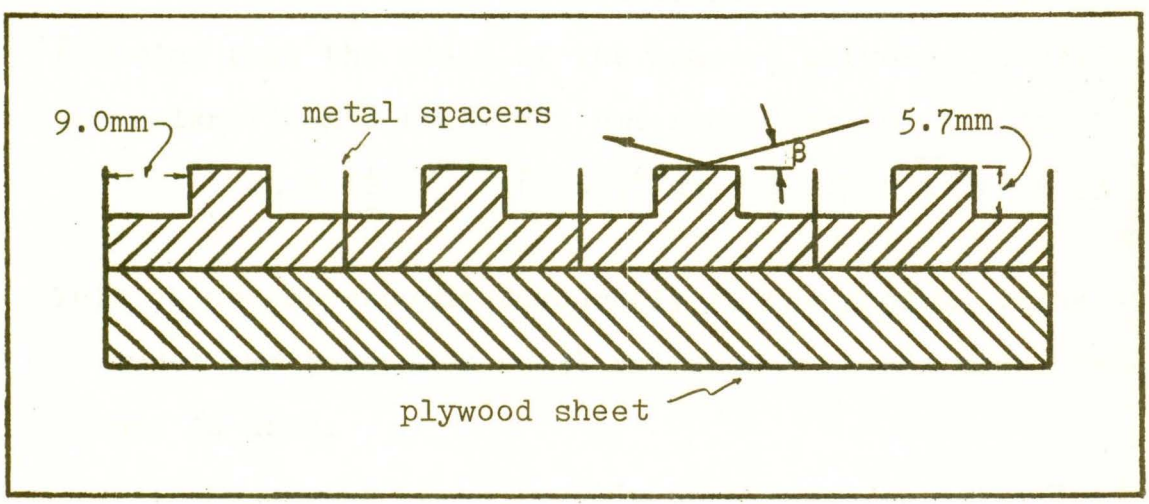

FIG. 4.3 Cross section of a reflector constructed on the quadratic-residue principles (N = 3). When the wells are extended in one direction as parallel groves, the surface exhibits its properties in one direction only.

Schroeder indicates that the well width is in turn related to the upper frequency limit for efficient scattering by the following relation:

$$w = c/2f_{max} \tag{4.6}$$

where c is the velocity of sound. Hence it is possible, by increasing f_{max} to obtain a value of β close to 13 degrees and therefore closely simulate the reflecting characteristics of the ice surface described by Marsh and Mellen.

The rms roughness of the model surface is given by

$$\sigma_M = \{\frac{1}{T} \int_0^T |f(x)|^2 \, dx\}^{\frac{1}{2}} \tag{4.7}$$

where $f(x)$ is some function describing the surface and T is the period of the quadratic-residue sequence. Assuming that the width of the spacers between the wells is insignificant, the model rms roughness for N=3 is

$$\sigma_M = \{\frac{1}{T} \int_0^{T/3} [0.57]^2 \, dx + \frac{1}{T} \int_{\frac{T}{3}}^{T} 0 dx\}^{\frac{1}{2}} = 0.33 \text{ cm.}$$

This value corresponds favourably to the nominal value of model rms roughness (0.34 cm) when a 10 kHz model frequency is used.

There appear to be certain advantages to employing a quadratic-residue surface as a reflector that could not be obtained by a random scattering surface. In particular, the quadratic-residue surface for N=3 can not only provide a mathematically determinable surface but

can also simulate the reflecting characteristics and rms roughness of the ice surface for appropriate choices of well width and model frequency. Hence the reflectors used in this study will be based on the quadratic-residue sequence for N=3.

4.4 Constructing the Reflectors

Two reflecting surfaces, based on the quadratic-residue sequence for N=3 are used in this study. The first reflector has wells running the entire length of the surface and exhibits the quadratic-residue properties in only one dimension. The wells in the second reflector have a length equal to their width and hence this surface will exhibit these properties in two dimensions. In addition, a third reflector with a smooth surface is used. Circular plywood sheets, of approximately 1 meter diameter, provided a basis for constructing the reflectors. The wells in the one-dimensional reflector were obtained by mounting wooden strips separated by metal spacers on the plywood sheet (see Fig. 4.3), while the wells in the two-dimensional surface were formed by filling appropriate segments of a plastic grid with plaster of paris (see Fig. 4.4). All reflectors were coated with a liquid plastic to enhance their reflecting properties.

When used with the moving source apparatus the re-

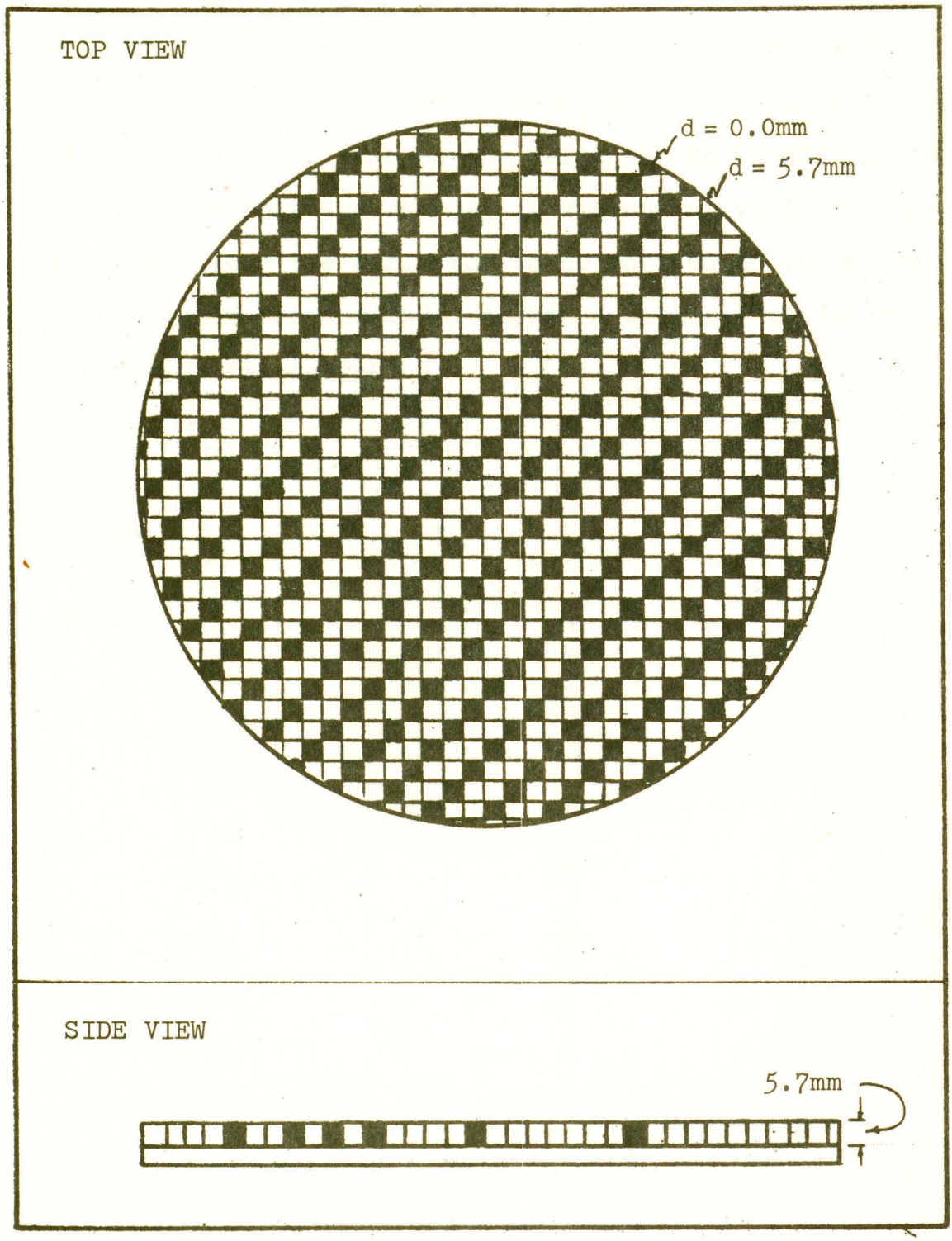

FIG. 4.4 Two-dimensional reflecting surface based on the quadratic-residue sequence for N=3. All wells are 9.0mm sq.

flectors are secured at their centers to a table with a variable-pitch top and adjustable height. This table shown in Fig. 4.5 enables the reflector to be positioned beneath the rotating source, at various elevations. As well it allows the reflector to be rotated in the plane of the table top and thus expose a slightly different profile to the source.

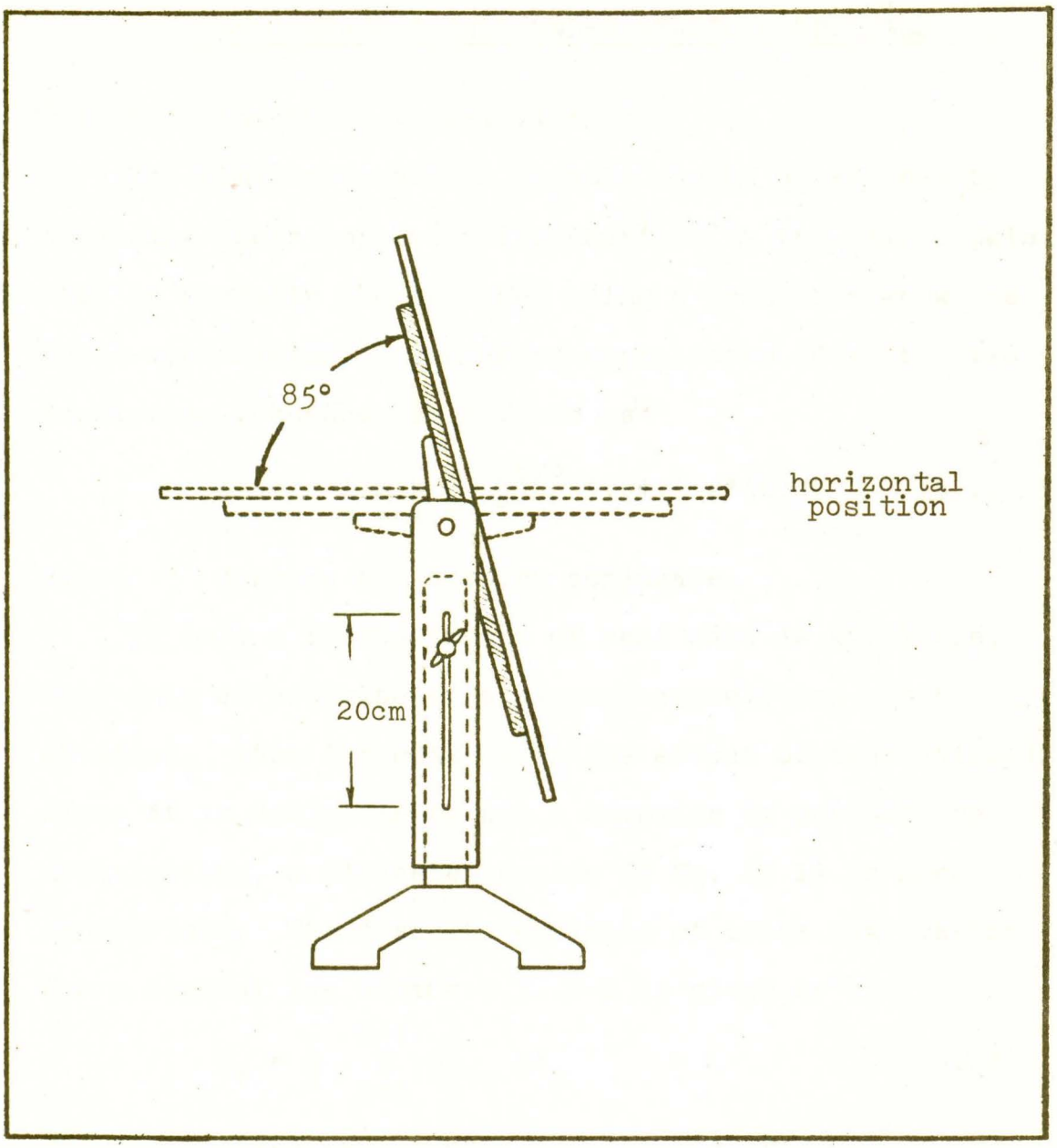

FIG. 4.5 Reflector board attached to the supporting table showing its variable pitch capabilities. The table is shown in its lowest position. There is a difference of approximately 20cm. between extreme elevations.

5. SAMPLE MEASUREMENTS UNDER STATIC CONDITIONS

5.1 Defining Cross-Correlation

The similarity of two signals can be determined by comparing their amplitude fluctuations in the time domain. This is normally accomplished using a technique known as cross-correlation.[a] The cross-correlation $C(\tau)$ for two continuous sequences is defined as[15]

$$C(\tau) = \lim_{T \to \infty} \frac{1}{T} \int_{-T/2}^{T/2} f(t+\tau)\, g^*(t)\, dt \qquad (5.1)$$

where $*$ denotes the complex conjugate.

If only a finite amount of real data is available, then only an estimate of the cross-correlation can be obtained. (See Appendix D1 on the effect of truncation.) Since it is desirable to use a computer to perform the calculations, a discrete version of Eq. (5.1) is more appropriate. The discrete estimate of cross-correlation for a digital lag of $|\tau| = 0,1..N-1$ is given by[16]

$$C_\tau = \frac{1}{N} \sum_{k=1}^{N-\tau} f_{k+\tau}\, g^*_k \qquad (5.2)$$

for $0 \leq |\tau| \leq N-1$ and where N is the number of data points in the discrete truncated sequence.

---

[a] The term cross-correlation should properly be applied to the normalized cross variance; however, it is commonly used for the unnormalized function, e.g. by the manufacturer of the analyser employed in this research.

The discrete definition of cross-power spectrum gives[17]

$$P_{ab} = \frac{1}{N} F_n \cdot G_n^* \qquad (5.3)$$

where F_n and G_n are obtained as the Fourier transforms of the time series f_k and g_k. The discrete Fourier transform is defined as

$$F_n = \sum_{k=0}^{N-1} f_k e^{-j2\pi n\, k/N}$$

and its inverse

$$f_k = \frac{1}{N} \sum_{n=0}^{N-1} F_n e^{j2\pi n\, k/N}.$$

The Wiener-Khintchine Theorem proves that the cross-power spectrum and the cross-correlation function are Fourier transform pairs. Therefore the cross-correlation can also be defined as[18]

$$C_\tau = \frac{1}{N} \sum_{n=0}^{N-1} \frac{1}{N} F_n G_n^* \, e^{j2\pi n\, \tau/N} \qquad (5.4)$$

The cross-correlation of the two time series f_k and g_k can be computed by either Eq. (5.2) or Eq. (5.4). However a rapid algorithm for calculating Fourier transforms, known as the Fast Fourier Transform (FFT), significantly reduces the computation time of Eq. (5.4) and thus has made it more popular. The signal analyser used in this study (Nicolet 660) employs the fast Fourier transform technique to produce power spectra and hence,

also uses this technique to compute cross correlation via Eq. (5.4). When the results of several time samples are to be averaged, this analyser permits the development of either the cross-power spectrum or the cross correlation to be observed, although the averaging is done only in the frequency domain.

5.2 Defining Coherence

The coherence is a modified cross-power spectrum, normalized so that all values lie in the range 0 to 1. Because of this normalization, which initially produces the value 1 at all frequencies, at least two successive time samplings must be obtained from each of the two signals being compared.

The sample coherence at the n^{th} point in the frequency spectrum, after m samplings have been accumulated, may be defined as[19]

$$\gamma_{nm} = \left| \sum_{i=1}^{m} P_{abi} \right|^2 / \left(\sum_{i=1}^{m} P_{ai} \right)\left(\sum_{i=1}^{m} P_{bi} \right) \qquad (5.5)$$

where the powers in the individual signals are $P_a = F_n \cdot F_n^*/N$ and $P_b = G_n \cdot G_n^*/N$, all at frequency n. It is to be noted that, although P_a and P_b are always real and positive, P_{ab} is a complex quantity and its summation is sensitive to changes of both relative amplitude and relative phase between the two signals (see Appendices D3 and D4).

Averaging, which is optional for cross correlation,

is essential for coherence. The signal analyser used in this study uses Eq. (5.5) to compute coherence and hence the power spectra are time averaged. A more normal definition of coherence requires an ensemble average. Thus the variations in the power spectra with respect to time should describe a statistically stationary process when Eq. (5.5) is used. However, it must be recognized that when the signals are transmitted from a moving source it is unlikely that this process is stationary. Hence unavoidable imperfections exist when computing coherence and cross correlation (with averaging), from signals transmitted from a moving source, with a signal analyser.

The dependence of the coherence on the relative power at the microphones may be illustrated by the following example in which, for simplicity, a single frequency is considered and the Fourier transforms of the two signals are assumed to possess only real components. Table IV shows how the coherence responds to moderate changes $\Delta(F_n/G_n)^2$ in the power ratio. Note that when this change remains zero (see m=6-9) the coherence slowly approaches unity.

The response of the coherence to change in the power ratio is determined by the number of samplings that have already been considered. This characteristic is demonstrated in Table V where the coherence computa-

tion for the same time series commences one sampling later than that in Table IV.

TABLE IV Numerical example of coherence showing the response to changes in the power ratio.

m	F_n^2	G_n^2	$(F_n/G_n)^2$	$\Delta(F_n/G_n)^2$	γ_n
1	25.10	80.82	0.310		1.00
2	22.10	85.91	0.257	0.053	0.997
3	69.20	10.10	6.851	6.594	0.643
4	51.20	49.20	1.040	5.811	0.721
5	26.01	84.64	0.307	0.733	0.749
6	26.01	84.64	0.307	0.00	0.774
7	26.01	84.64	0.307	0.00	0.795
8	26.01	84.64	0.307	0.00	0.812
9	26.01	84.64	0.307	0.00	0.827

TABLE V Numerical example of coherence showing the effect of the first sampling.

m	F_n^2	G_n^2	$(F_n/G_n)^2$	$\Delta(F_n/G_n)$	γ_n
1	22.10	85.91	0.257		1.00
2	69.20	10.10	6.851	6.594	0.559
3	51.20	49.20	1.040	5.811	0.698
4	26.01	84.64	0.307	0.773	0.721
5	26.01	84.64	0.307	0.00	0.749
6	26.01	84.64	0.307	0.00	0.774
7	26.01	84.64	0.307	0.00	0.795
8	26.01	84.64	0.307	0.00	0.812

The coherence computed in Tables IV and V is plotted as a function of time in Fig. 5.1. Note how the co-

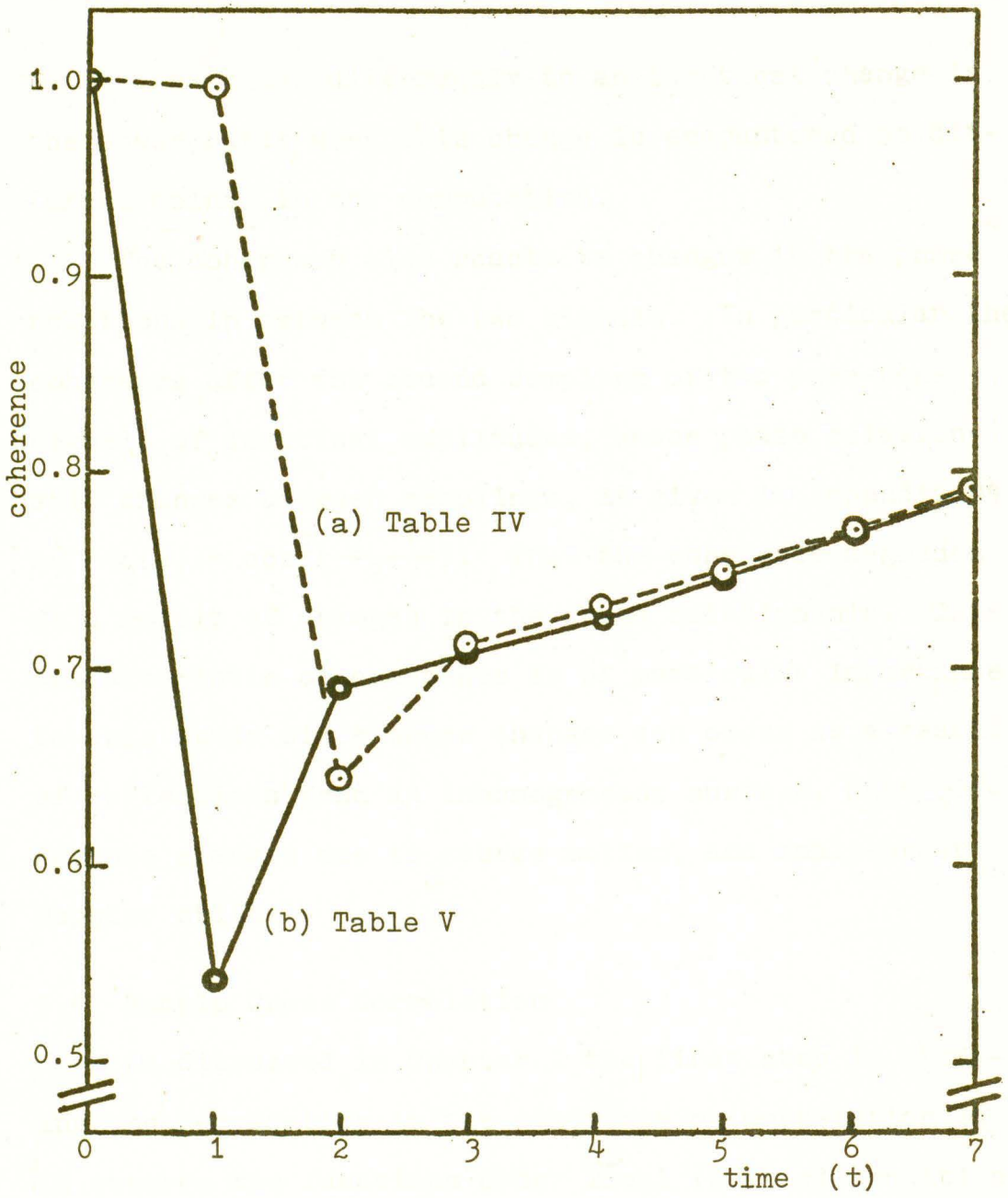

FIG. 5.1 Coherence as a function of time; (a) sampling begins at time t = 0, (b) sampling begins at time t = 1.

herence responds differently to an identical change in the power ratio when this change is encountered at different points in the computation.

The coherence also reacts to changes in the phase relationship between the two signals. In particular the coherence after the second sampling of two pure-tone signals of identical amplitudes, whose phase relationship changes between samplings, is given in Appendix D4 as $\gamma_2(\omega) = \cos^2(\frac{\phi_1 - \phi_2}{2})$. Thus the coherence degrades as a result of changes in the phase relationship. This characteristic of coherence is of particular importance to this study since these changes can occur as a result of reflections from an inhomogeneous surface, path-difference changes due to source motion, and small-order Doppler shifts.

5.4 Sample Cross Correlation

As discussed in Chapter 1 the first step in studying the degradation in the coherence or correlation is to observe the functions under ideal (static) conditions, both with and without reflecting surfaces. Figure 5.2 shows the positioning of the equipment in the anechoic chamber for obtaining the sample cross-correlation measurements. It is important to note that the directional characteristics of the source permit the analysing equipment to remain in the chamber during the experiment with-

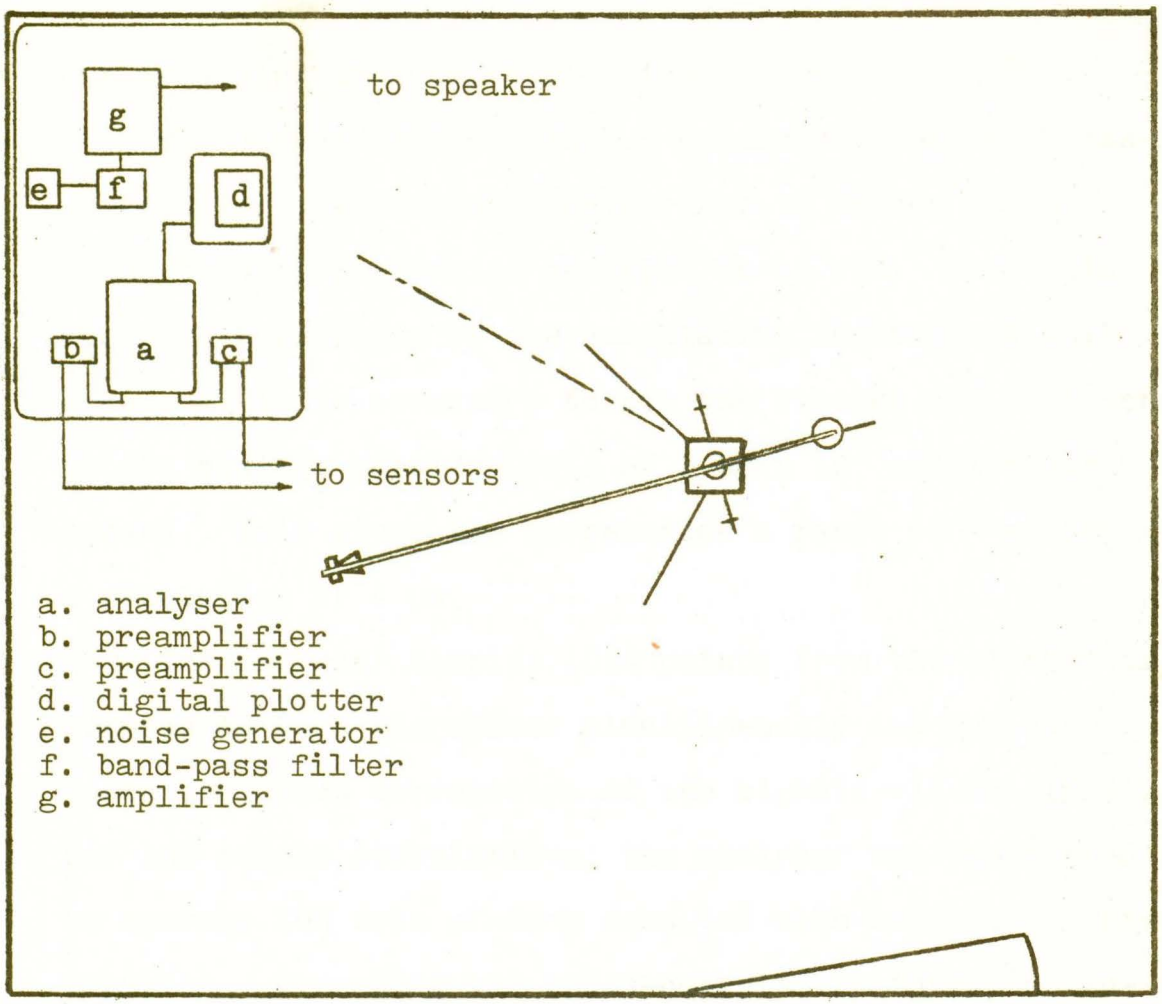

FIG. 5.2 Equipment set up in the anechoic chamber to produce sample correlations. The sound source is in the 90° position. The 45° position is indicated by the broken line. The maximum beamwidth of the source is approximately 60° at 8 kHz. Thus, the equipment can remain in the anechoic chamber during the experiments without producing unwanted reflections.

out producing unwanted reflections (see Appendix E1).

The source distance is 1.5 meters and for the cross-correlation measurements the speaker is driven by an 8 kHz band of pink noise centered at 10 kHz. To obtain adequate resolution of the correlation function at this frequency it is necessary to set the Nicolet 660 analyser at its maximum sampling rate of 2.56×10^5 samples per second. This gives the correlation a range of 4 ms and a resolution of 4 μs.

The analyser samples 1024 points from the electrical signals at each microphone simultaneously and then computes the cross correlation of the signals via Eq. (5.4). For the sample correlations, the analyser was programmed to average 100 sets of data computed with constant source position. Averaging the cross-correlation functions enhances the main correlation peak and minimizes apparent correlations that result from the random property of the noise source.

Sample cross correlations were first produced without the reflecting surface in position. These results are shown in Figs. 5.3 and 5.4 for the source in the 90 and 45 degree positions respectively. Note that the secondary correlation peaks are more pronounced when the rotating arm is at an angle of 45 degrees with respect to the array. This results from a difference in mutual interference between the microphones when the source is

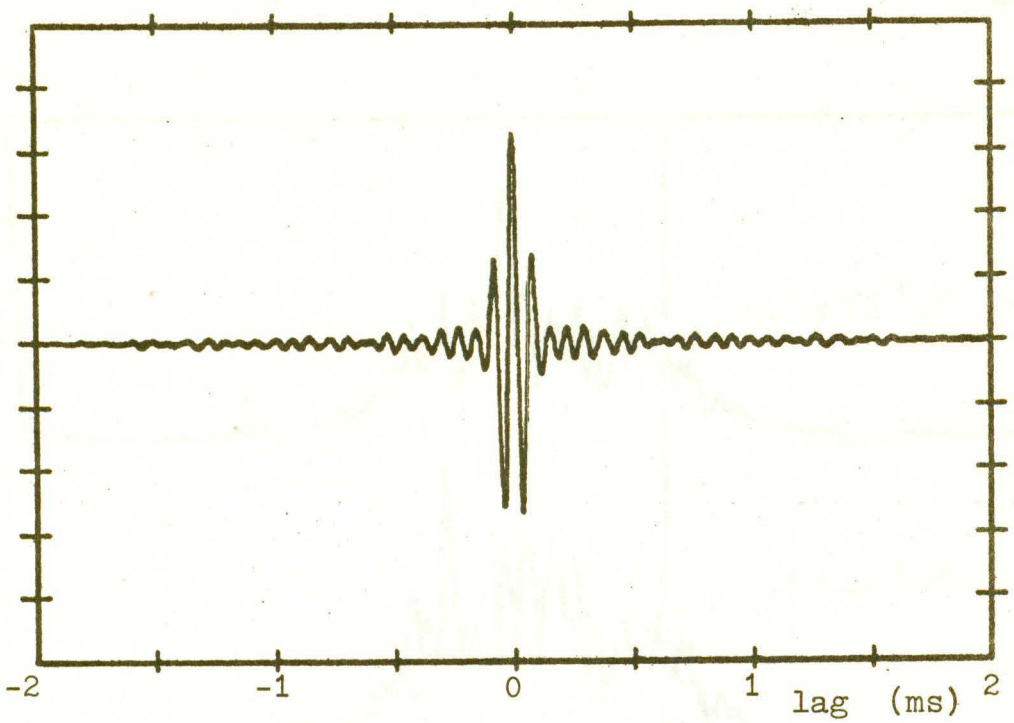

FIG. 5.3 Cross correlation obtained with the source in the 90° position and the microphones separated by 0.1 meters.

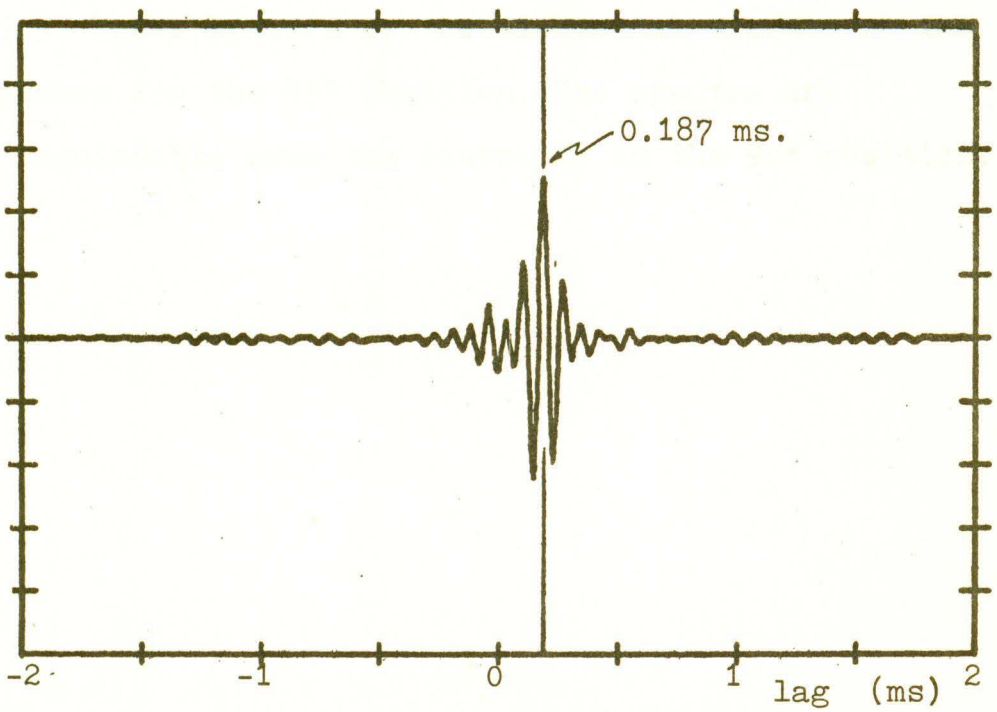

FIG. 5.4 Cross correlation obtained with the source in the 45° position and the microphones separated by 0.1 meters.

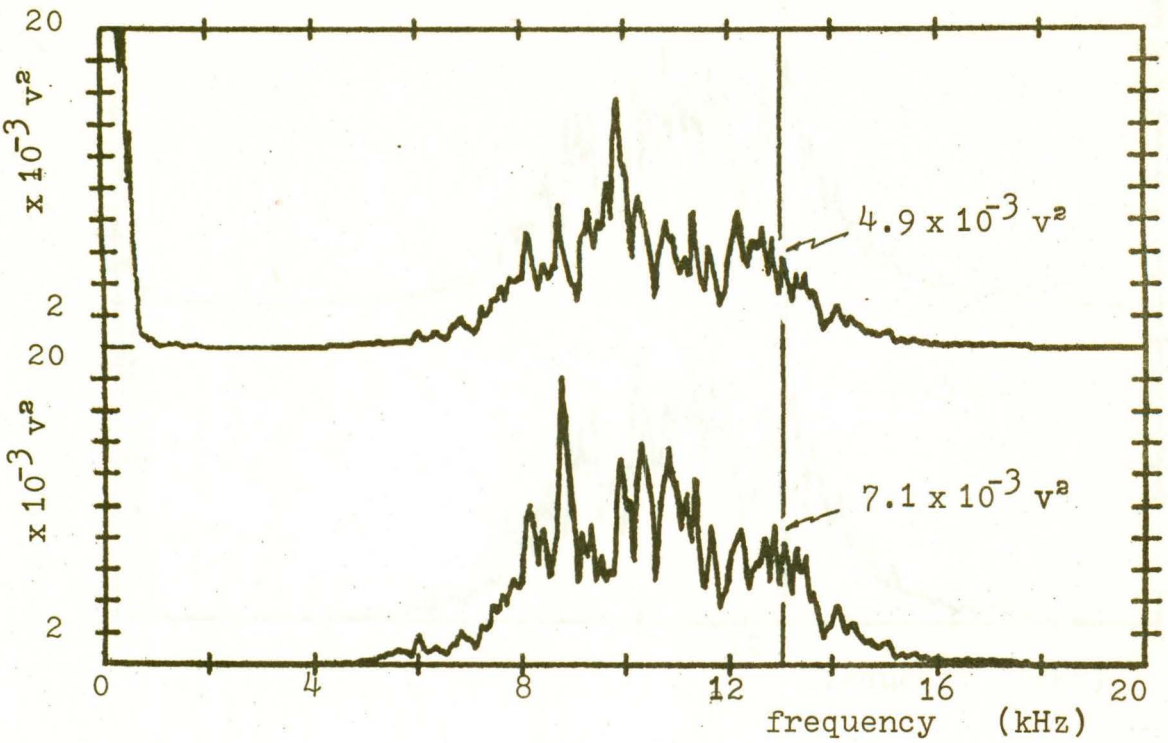

FIG. 5.5 Power spectra of the electrical signals at the microphones for the 45° position. The spectra are indistinguishable when the source is in the 90° position.

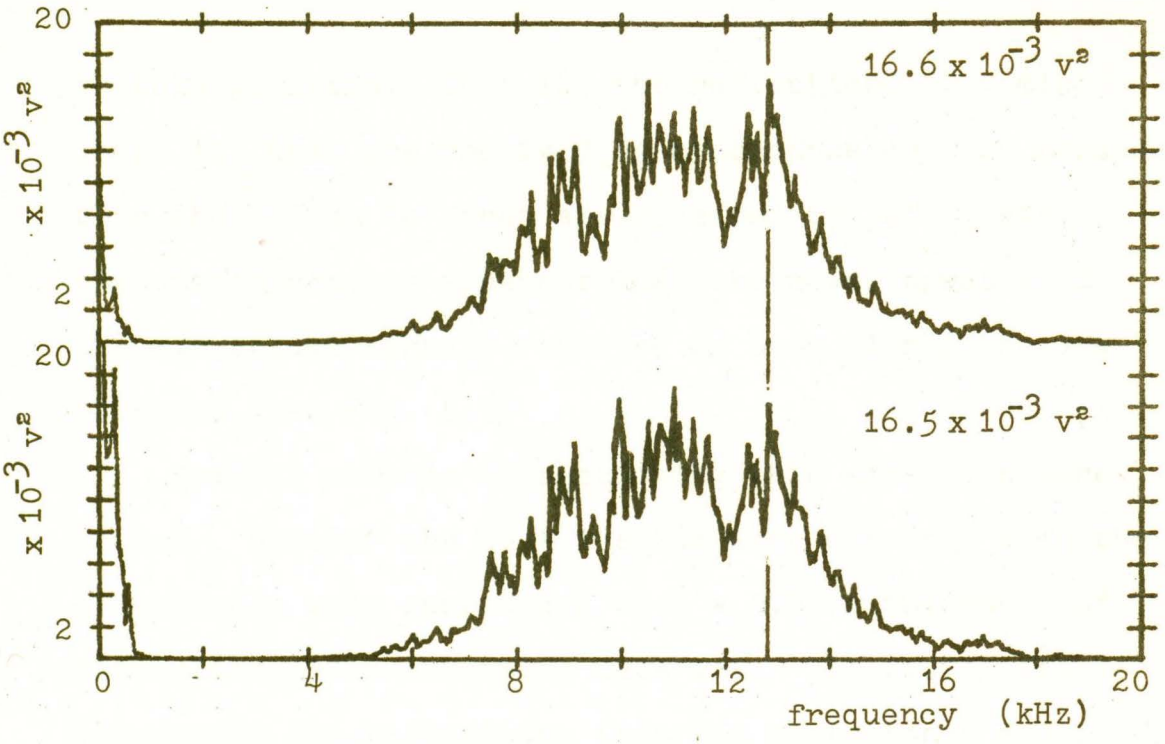

FIG. 5.6 Power spectra of the signals at the microphones for the 45° position, with the microphones surrounded with fibreglas sound-absorbing material. The intensity of the source has also been increased.

in this position. That is, the reflections from microphone 'a' that are received by microphone 'b' are greater than those from 'b' that are received by 'a'. This phenomenon becomes apparent when the power spectra of the electrical signals received by each microphone are observed (see Fig. 5.5).

Several methods of rectifying this situation were tested. However the best results were obtained when the microphones were surrounded with a 0.5 cm thickness of fibreglass sound-absorbing material. The fibreglass attenuates the reflections from the microphones and hence minimizes their mutual interference. The power spectra that result when this material is used are shown in Fig. 5.6. Note that the spectra are almost identical with only slight variations at the low end of the band. The resulting cross correlogram when the source is in the 45-degree position with the covered microphones has a signature similar to that shown in Fig. 5.3.

Figure 5.7(a) shows the cross-correlogram obtained with the plane reflector, the source in the 90-degree position, and the microphones separated by 35 mm. The secondary correlation peaks indicate that sound reaches each microphone by travelling along two different paths (direct and reflected). That is, one secondary peak results from the correlation of the reflected sound at

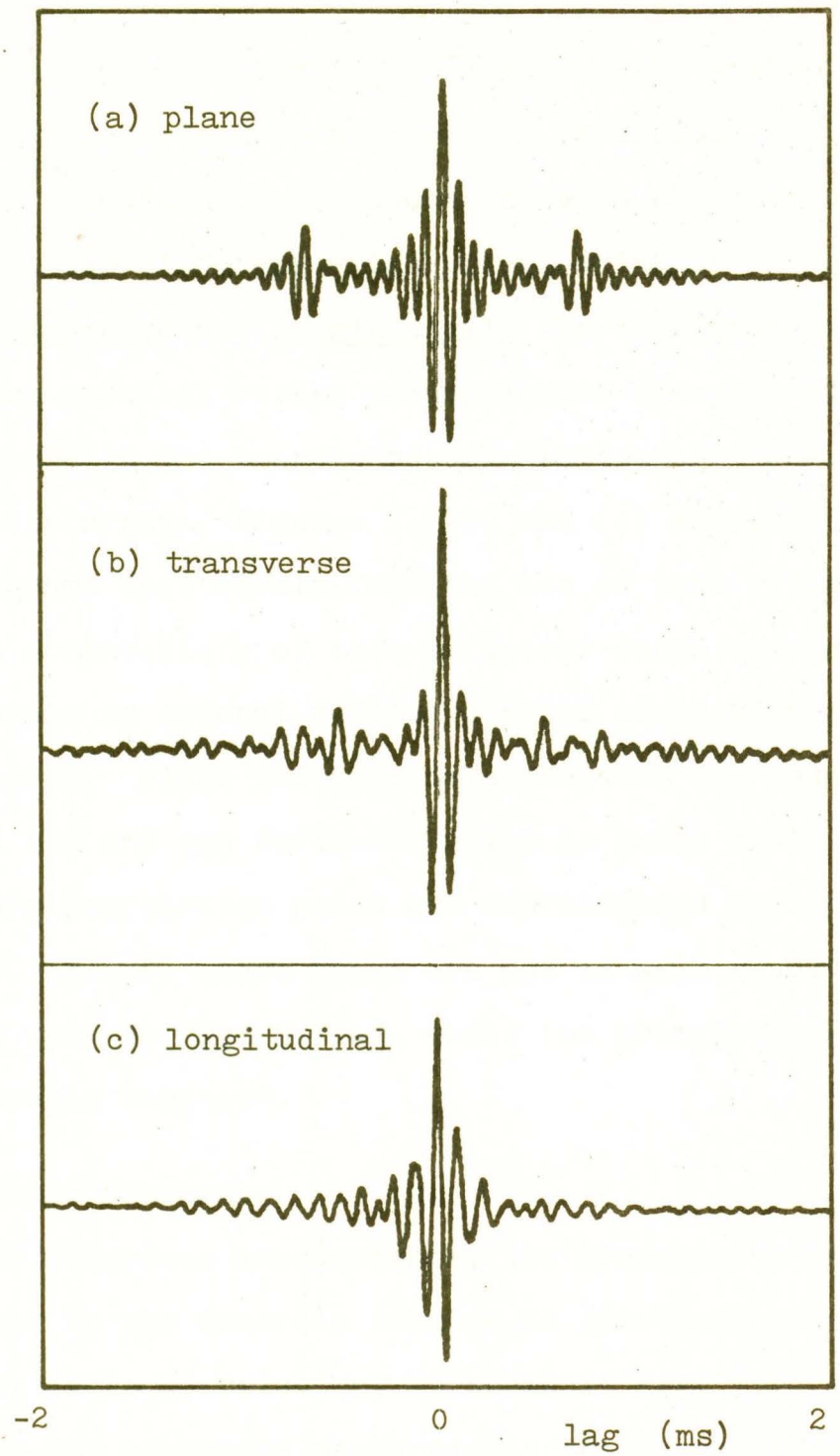

FIG. 5.7 Sample cross correlograms obtained with different reflectors, 40cm. below the source (in the 90° position) and a microphone separation of 35mm.

microphone 'a' with the direct sound at 'b' while the other peak results from the reverse situation.

The one-dimensional quadratic residue reflector is used with two different orientations which are referred to as transverse and longitudinal. In the latter the wells are parallel to the perpendicular bisector of the array while in the transverse orientation they are parallel to the array. Figures 5.7(b) and (c) show the cross correlograms that result from the use of this reflector. In both orientations of this reflector sound reaches the microphones by several reflected paths along with the direct path. Since the time delay between the sound's arrival via any two reflected paths is quite small the secondary correlation peaks are superimposed upon one another. Hence, these peaks are not as well resolved as they were in Fig. 5.7(a), while the primary peak is considerably enhanced.

5.5 Sample Coherence

For coherence measurements, the arrangement of the equipment in the anechoic chamber is identical to that used for cross correlation, as shown in Fig. 5.1. However for the coherence measurements the source is a pure tone at a frequency of 9.95 kHz and the time window is 20 ms rather than 4 ms as used for cross correlation.

The different time windows were chosen because they

provide the best resolution of each function. However the larger time window used for coherence results in a slight increase in the degradation (<1%) when the source is in motion (see Appendix D5).

As previously discussed, the coherence responds to the changes in the ratio of the power and/or changes in the phase relation at the microphones. Therefore since these sample measurements are obtained under static conditions the coherence remains at unity, even with the reflecting surfaces in position. This result is demonstrated by Fig. 5.8 where the coherence is shown after 100 samplings have been considered, (ie. m = 100) when the one-dimensional quadratic residue reflector is in position. The coherence at frequencies other than those about the source frequency of 9.95 kHz, is that of the electrical noise generated within the amplifiers.

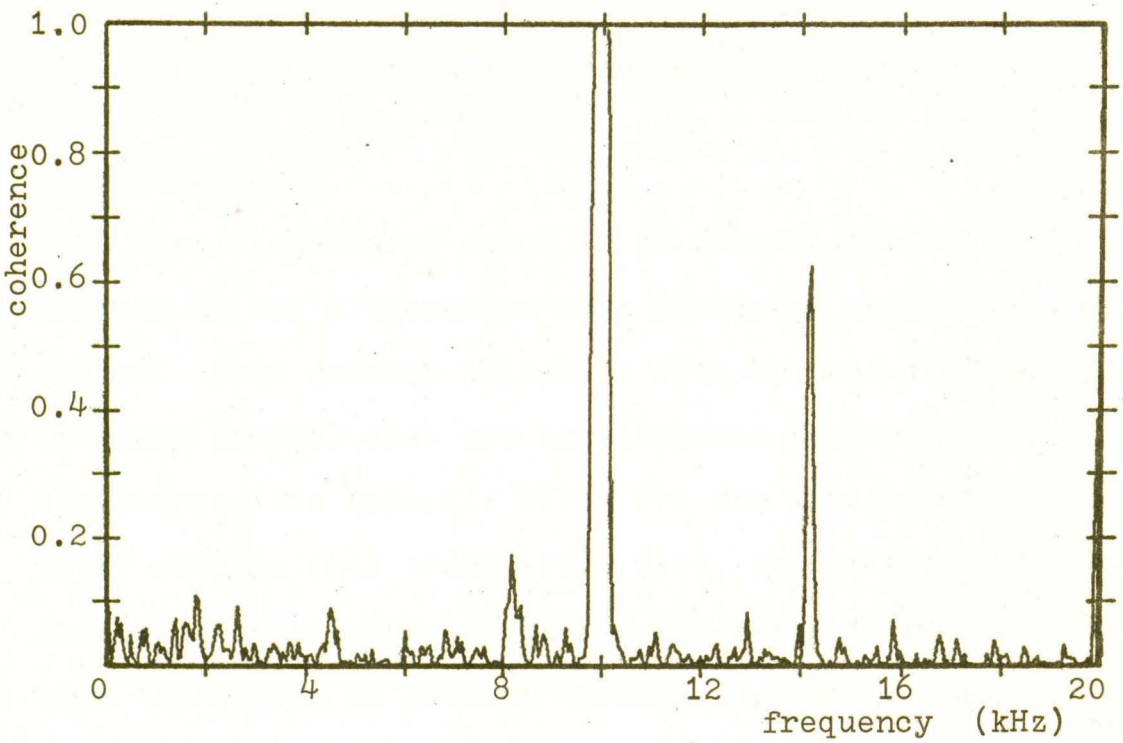

FIG. 5.8 Sample coherence obtained with the source in the 90° position and the microphones separated by 35mm. The signal shown at 14 kHz has a power which is 70 dB lower than that of the source at 10 kHz. This demonstrates the effectiveness of coherence in detecting very low level coherent sources.

6. CROSS CORRELATION AND COHERENCE, WITH SOURCE MOTION

6.1 Background

When a source of sound is in motion, the sound arrives at the microphones as a distorted version of the source. This results primarily from changes in frequency (Doppler shifts) that are attributable to the motion of the source (see Appendix F1). For the array-source geometry used in this study (Fig. 6.1), the effect of Doppler shifts on cross correlation and coherence is most severe when the source is passing through a point on the perpendicular bisector of the array (ie. $\theta = 90°$).

When the source is in this position the signal at microphone 'a' has a frequency given by

$$f_a = f_o(1 + \frac{v}{c}\cos\alpha_1) \qquad (6.1)$$

where f_o is the source frequency. The signal at microphone 'b' has a frequency given by

$$f_b = f_o(1 - \frac{v}{c}\cos\alpha_2) \qquad (6.2)$$

Therefore the frequency difference between the signals is

$$f_a - f_b = f_o \frac{v}{c}(\cos\alpha_2 - \cos\alpha_1) \qquad (6.3)$$

When $\alpha_1 = \alpha_2 = \alpha$ this difference can be expressed as

$$(f_a - f_b)_{max} = f_o \frac{vD}{rc}[1+(D/2r)^2]^{-\frac{1}{2}} \qquad (6.4)$$

The quantity vD/rc is a dimensionless constant (6.7×10^{-6}) when satisfying the time-difference criteria

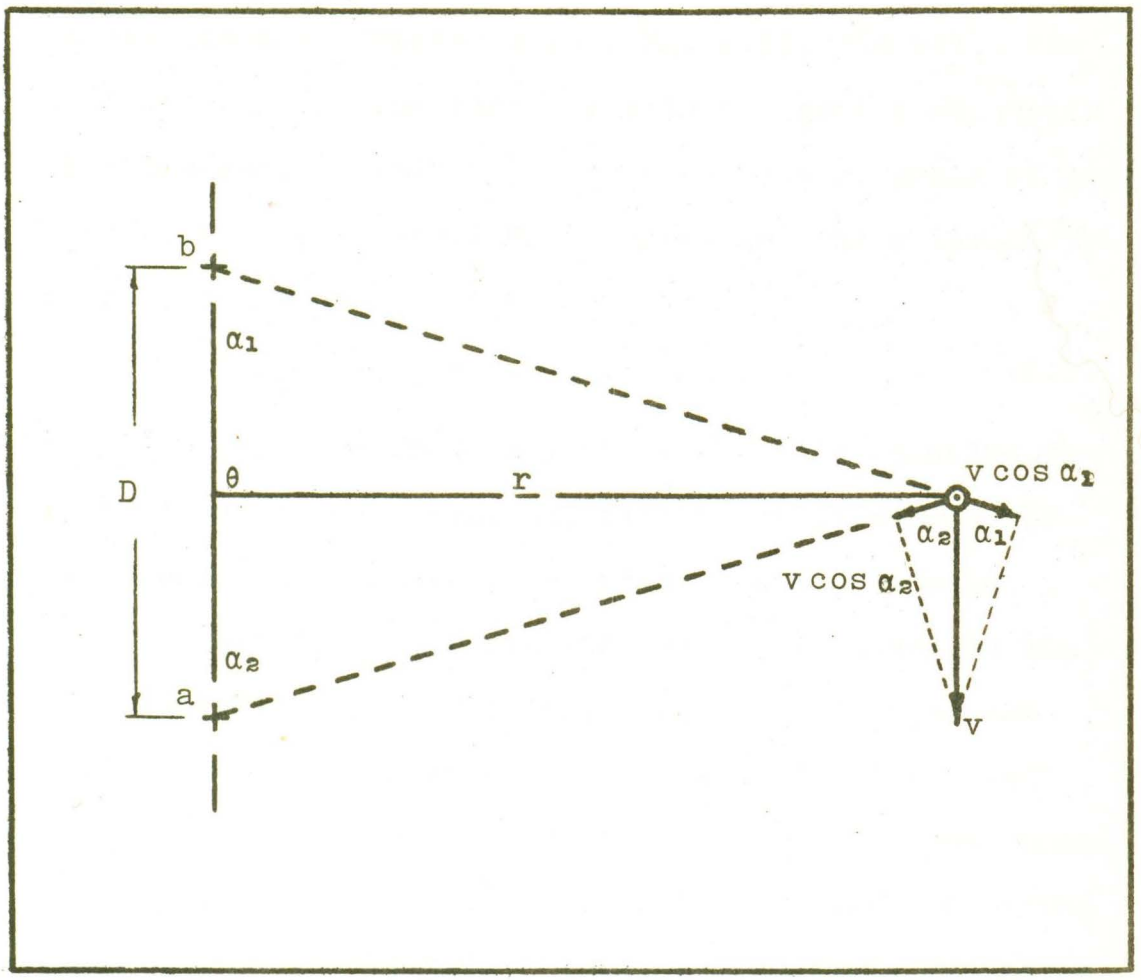

FIG. 6.1 Array-source geometry for calculating the maximum difference in signal frequency at the microphones.

as explained in Chapter 2 (see Eq. 2.5). As well, the truncation after the first term in the series expansion of the quantity $[1+(D/2r)^2]^{-\frac{1}{2}}$ introduces an error of less than 0.5% (see Appendix F2). Therefore the maximum frequency difference is given by

$$(f_a-f_b)_{max} = 6.7 \times 10^{-6} f_o \qquad (6.5)$$

For a center band frequency of 10 kHz this equation results in a maximum frequency difference of only 0.067 Hz between the signals received by the microphones.

An equation describing the expected change in the cross-correlation coefficient C(0) induced by source motion, is given in Appendix F3. When f_o=10 kHz and Δf=0.034 Hz this equation gives the change in the cross-correlation coefficient as $1.2 \times 10^{-8} A^2$, where A is the amplitude of the signals. Thus an observable change in this coefficient, resulting solely from the motion of the source, is not expected when only one sampling is obtained.

However this is not the case when measuring coherence, since coherence requires a number of samplings to be averaged. Degradation results from changes in the phase relationship of the signals that occur as a result of both changes in the angular position of the source and changes in Doppler shift. As discussed in Appendix D4 the coherence resulting from changes in source posi-

tion can be calculated and is shown in Fig. 6.8 as a comparison to the measured results.

6.2 Measuring the Velocity of the Source

Slight variations in the balance of the rotating arm may result in variations in its angular velocity during the cycle. It is not possible to maintain the apparatus in perfect balance at all times because of the movement of the sectionalized deck grating in the anechoic room. Therefore it is necessary to measure the velocity of the source at a particular point in its cycle.

This is accomplished with the aid of a small speaker mounted on the end of the rotating arm. The speaker is driven by a high frequency pure tone and the arm is set in motion at the approximate desired velocity. The pure tone is then sampled by the analyser when the arm is passing through the point at which an accurate measurement of its velocity is desired (see Fig. 6.2). A comparison of this Doppler-shifted signal to the original source signal allows the velocity of the source, at the point in question, to be calculated with the following relationship:

$$v = \Delta f \; c/f_o \qquad (6.6)$$

Figure 6.3(b) shows the shifted tone that results when the arm is rotated with an approximate velocity of 0.1 m/s. The use of the frequency translator option on the analyser allows the frequency of the tone to be

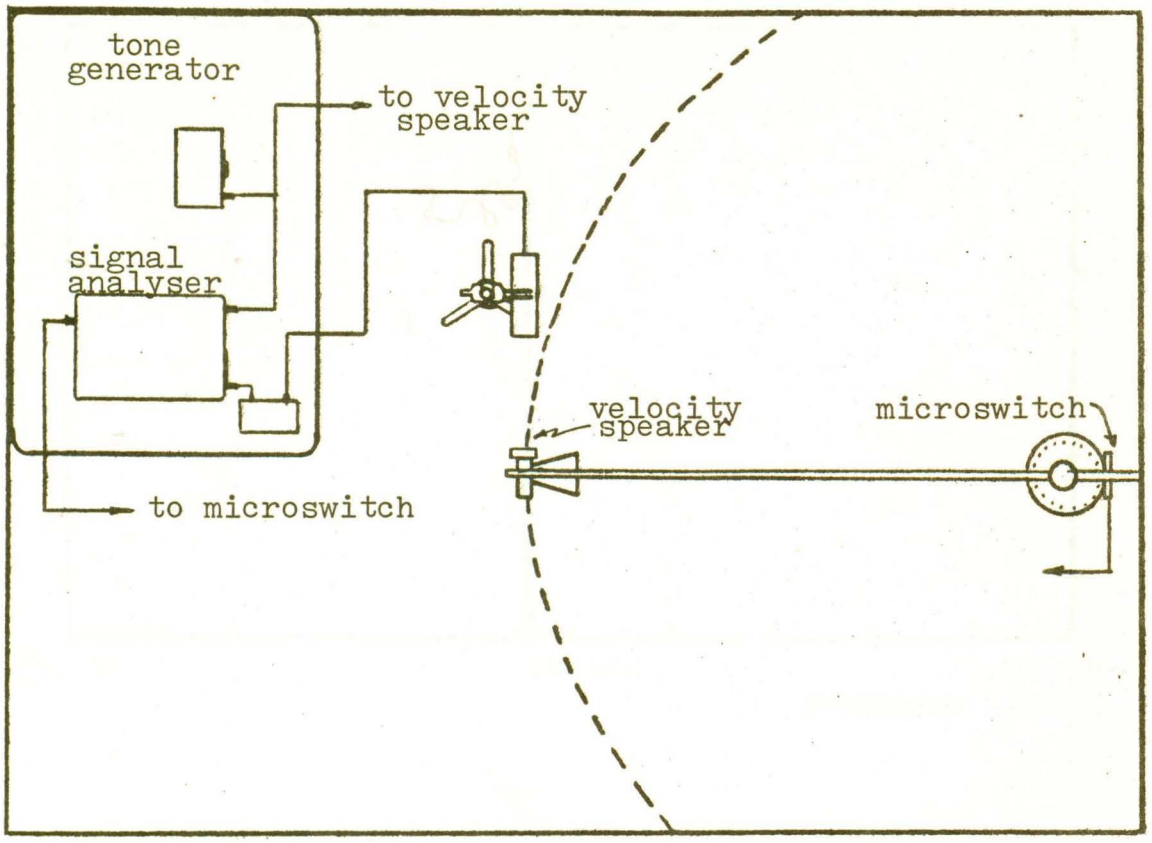

FIG. 6.2 Apparatus set to measure the velocity of the source as it passes through a point on its cycle. The analyser is triggered, when the source is passing through the desired point, by means of a microswitch which is activated by the rotating arm.

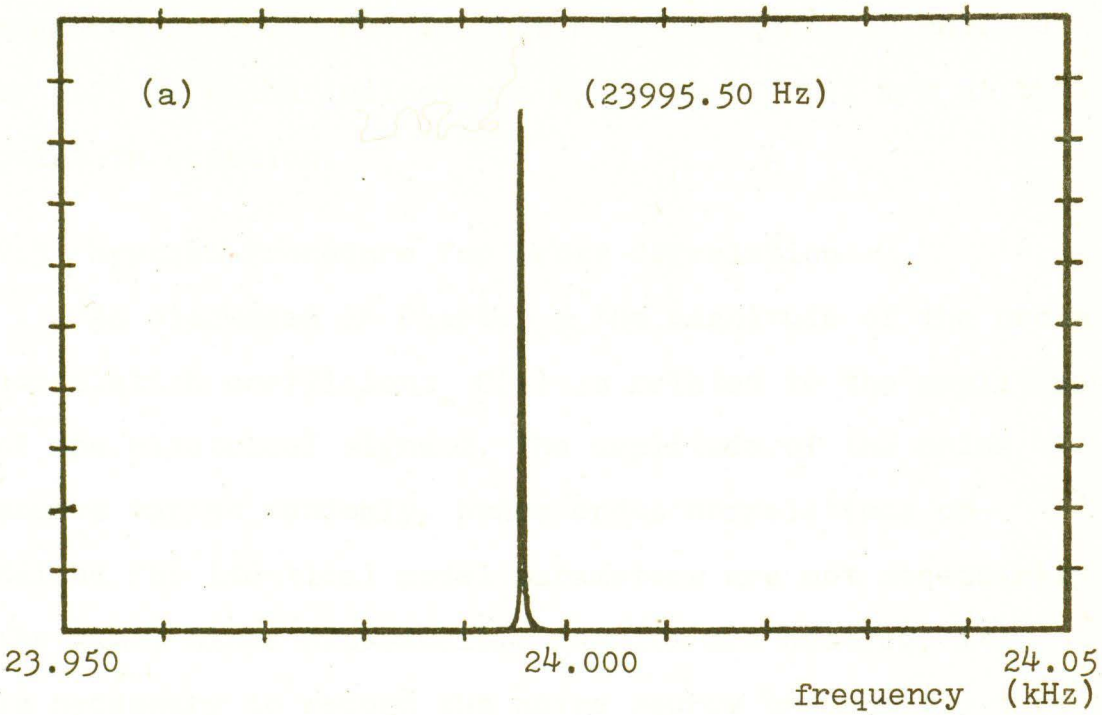

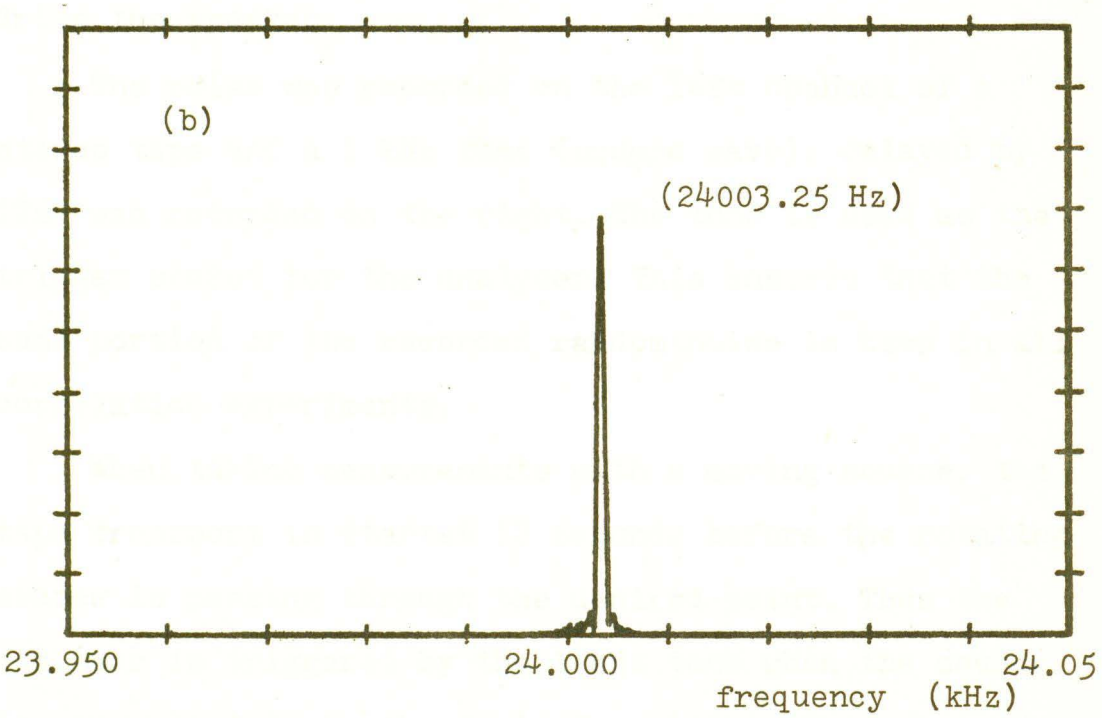

FIG. 6.3 Power spectra for, (a) signal applied to velocity speaker, (b) signal from fixed microphone along tangential path.

measured to 0.125 Hz. In this case the tone was shifted by 7.75 Hz which indicates a velocity of 0.11 m/s at the point in question.

6.3 Special Procedure for Cross Correlation

As discussed in Chapter 5, the magnitude of the cross-correlation coefficient C(0) is related to the amplitudes of the electrical signals. The amplitude of the noise source varies randomly, hence cross correlations obtained for identical model parameters are not necessarily the same. Since reproducible results are desired, it is necessary to record the noise source on magnetic tape and use the recording instead of the noise generator to drive the speaker.

The noise was recorded on the left channel of a stereo tape and a 1 kHz tone (square wave), delayed by 12s, was recorded on the right. The tone is used as the trigger source for the analyser. This ensures that the same portion of the recorded random noise is used in all correlation experiments.

When taking measurements with a moving source, the tape transport is started 12 seconds before the rotating source is passing through the desired point. Thus the analyser is triggered by the 1 kHz tone when the source is approximately in the desired position. The exact position the source was in, when the analyser was triggered, is obtained by measuring the lag in the cross-

correlation peak. The source is then manually placed in that position and a cross correlation is obtained under static conditions using the same section of the recorded noise tape as a source. Therefore differences in these two cross-correlations can be attributed to the motion of the source.

6.4 Cross-Correlation Results

Several cross correlations were obtained with the main speaker source in motion, and each compared with its static counterpart. Figure 6.4 shows a cross correlation obtained after one sampling, when the source was stationary. Note that the secondary or apparent correlation peaks are much more pronounced than the results obtained when several correlations are averaged (see Fig. 5.2). The correlations for both static and moving sources are for a source distance of 1.5 m and a microphone separation of 3.5 cm.

Figure 6.5 shows a typical result obtained for a source velocity of 0.11 m/s. Note the main correlation peak has the same magnitude as that obtained under static conditions. However it is slightly displaced in time. This is a result of an error in the manual placement of the source for the static test and is not related to the motion of the source. A close study of this cross correlation reveals that the secondary or apparent correla-

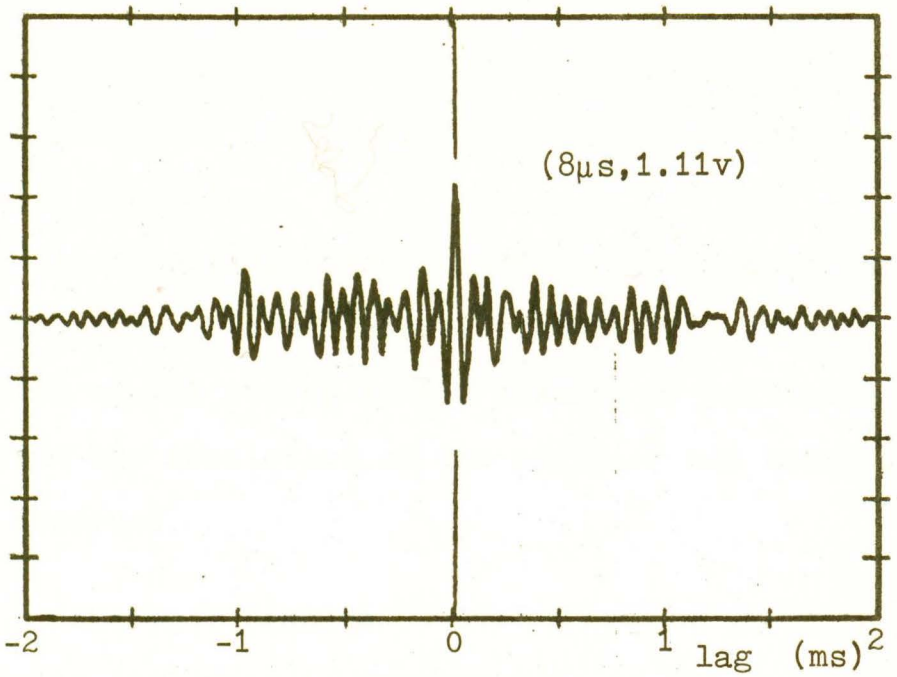

FIG. 6.4 Cross correlogram after 1 sampling of the electrical signals at the microphones with a stationary source.

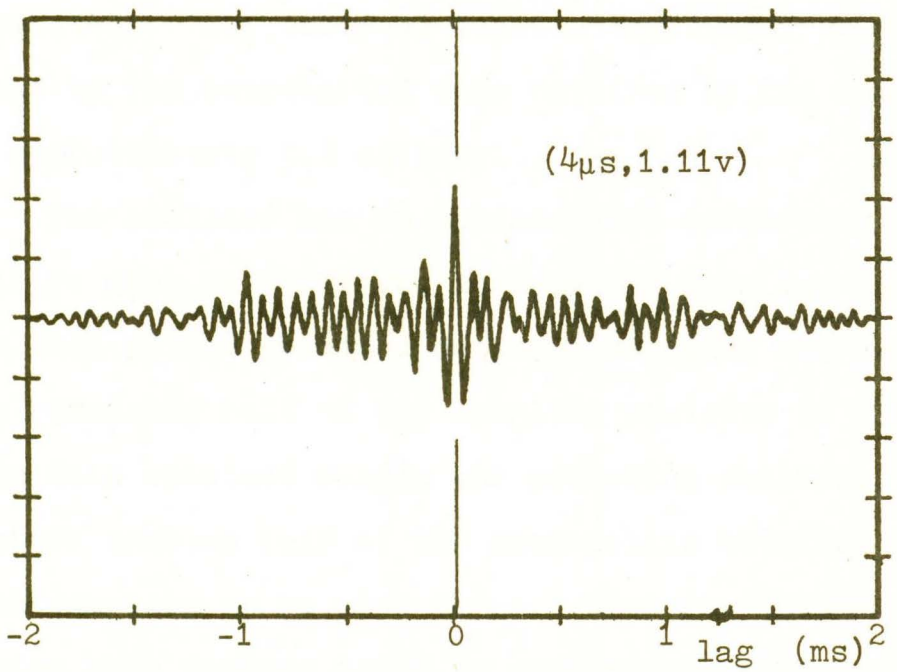

FIG. 6.5 Cross correlogram obtained when the source was moving with a velocity of 0.11 m/s.

tion peaks are also very similar to those obtained under static conditions.

As expected, these results indicate that the actual degradation in cross-correlation that is induced by the motion of the source in the absence of reflections is beyond the resolution of the analyser and hence can not be observed.

6.5 Coherence Results

As discussed in Chapter 5, it is necessary to compute the power spectra from a number of samplings in order to obtain the coherence. These samplings are obtained consecutively. The interval between samplings, as determined by the computation time required by the analyser is approximately 0.4 seconds.

The analyser has an optional 50% redundancy capability: when this feature is selected only one-half of the data points obtained during a sampling are used. The remaining half of the sampling register is filled with data obtained during the preceding sampling. This feature enables half of the data points obtained from each sampling to be used twice. When the source is in motion this feature tends to support the coherence of the source.

A pure tone at approximately 10 kHz is used for the coherence measurements. The first sampling of the elec-

trical signals at the microphones is made when the angle between the rotating arm and the array is approximately 72 degrees (see Fig. 6.6).

Figure 6.7 shows the coherence that results after various numbers of samplings have been considered. These coherence graphs indicate the existence of an optimum number of samplings. The coherence of the signal, relative to the coherence of the electrical noise, increases until approximately seven samplings have been considered.

This optimum number of samplings is analogous to the optimum correlation integration time found by Gerlach, as discussed in Chapter 1. In addition, the rapid decay of the signal coherence beyond this point is quite similar to that found by Gerlach for cross correlation. This result can be seen in Fig. 6.8 where the coherence of the signal is plotted as a function of time.

Figure 6.8 also demonstrates the effect of the analyser's 50% redundancy capability. This feature improves the apparent coherence of the signals by approximately 2 to 3% and is employed for the remainder of the study.

The coherence in the vicinity of 6 kHz, in Fig. 6.7, results from the acoustic energy generated by the drive motor and gear box. Since this energy is nearly the same for each channel the coherence at this frequency remains high.

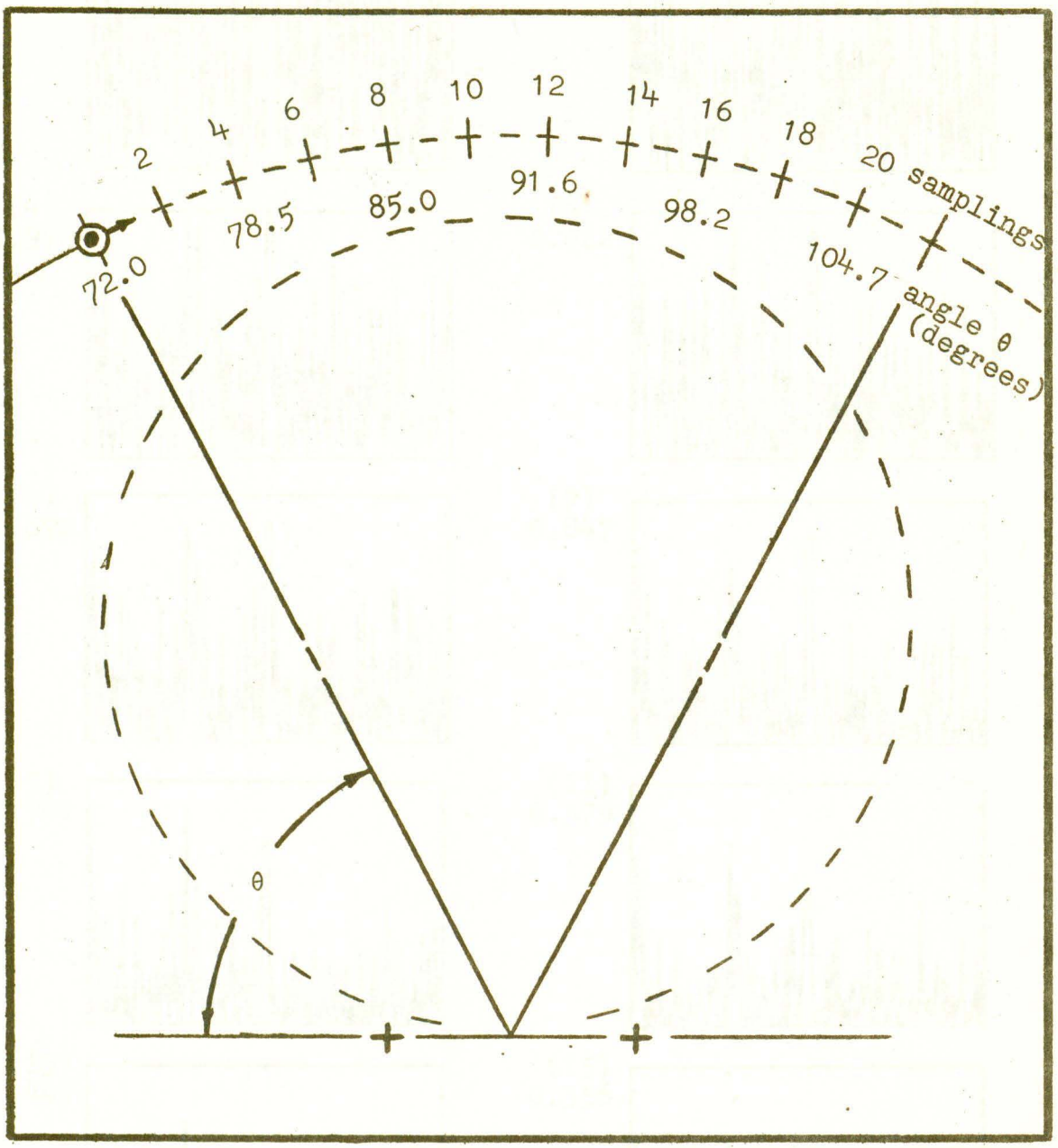

FIG. 6.6 The position of the source related to the sampling of the signals at the microphones. The broken circle indicates the position in which the reflecting surface will be placed for later experiments.

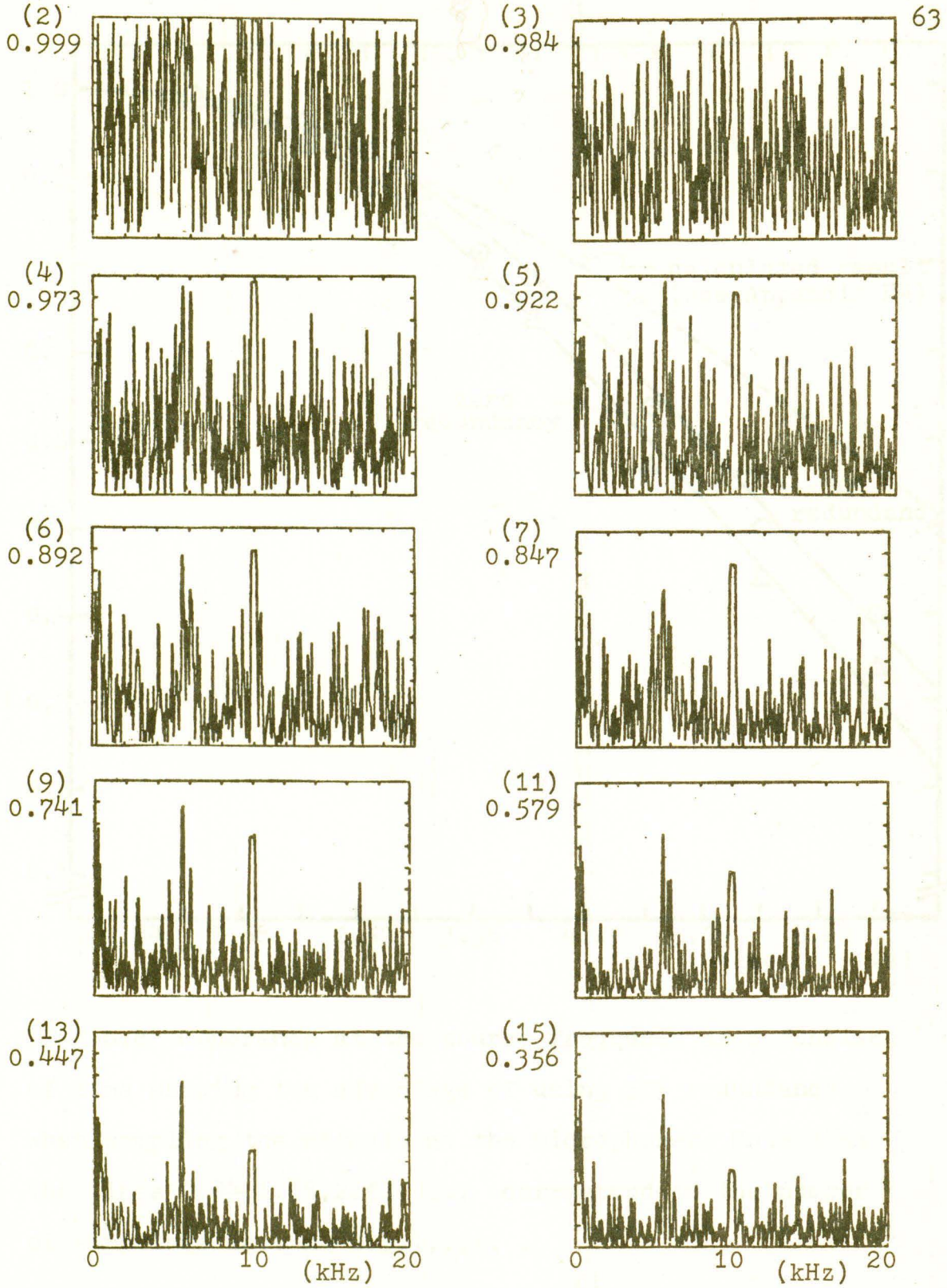

FIG. 6.7 Coherence with source motion. The number of samplings is shown in brackets with the source coherence below.

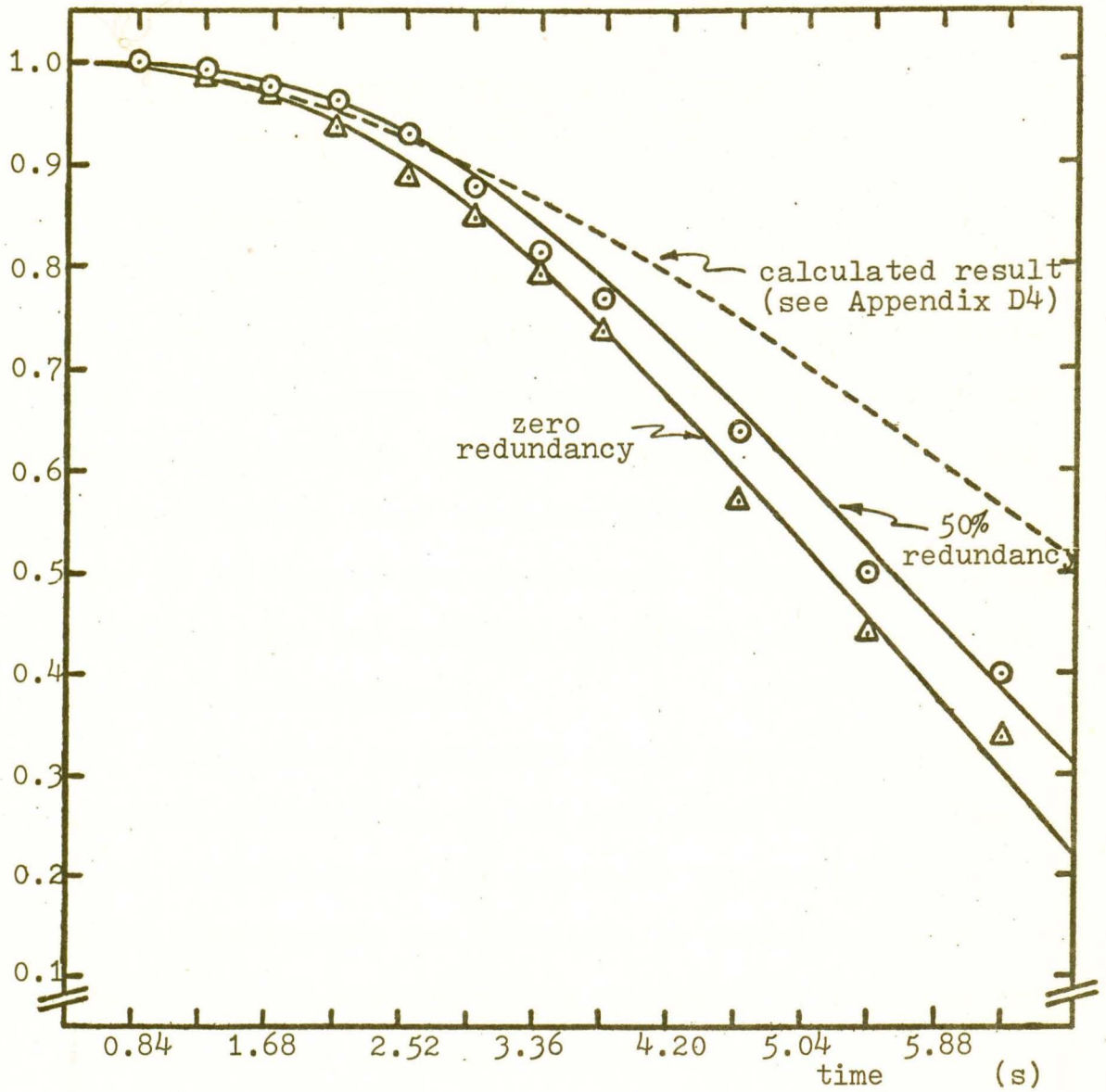

FIG. 6.8 Coherence at the source frequency as a function of time showing the advantage of using 50% redundancy when sampling the signals at the microphones. Note that the times 0.84,1.68,2.52. ... correspond to the number of samplings ie., m = 2,3,4,.... .

7. CROSS CORRELATION, WITH REFLECTORS AND A MOVING SOURCE

7.1 Introduction

The three reflecting surfaces described in Chapter 4 are introduced, one at a time, to observe their individual effect on cross correlation. The placement of the reflecting table is illustrated in Fig. 7.1. The table is shown in the "low" position with the reflecting surface 40 cm beneath the microphones. Experiments are also conducted with the board in the "high" position (20 cm beneath the microphones).

The speaker is slightly tilted downward to ensure complete illumination of the reflecting surface. The model parameters and the procedure for obtaining the cross correlograms are identical to those described in Chapter 6. As well, the same recording of band-limited random noise is used as a source.

7.2 Results

Figure 7.2(a) shows the cross correlogram that results when one 1024-point sampling is acquired with the plane reflecting surface in the 'low' position and a source velocity of 0.11 m/s. For comparison Fig. 7.2(b) shows the static result obtained with the same reflecting surface. Its relationship to the moving result is similar to that obtained without a reflecting surface present

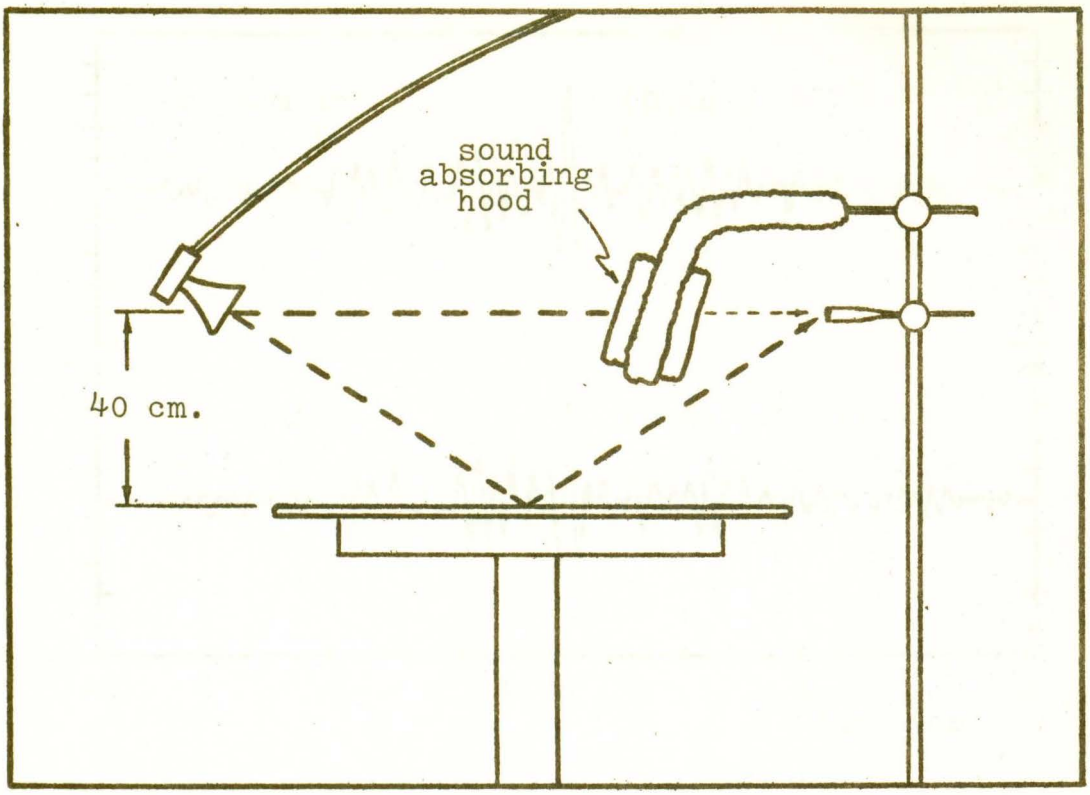

FIG. 7.1 Reflecting table set up in the anechoic chamber in the 'low' position. The sound-absorbing hood is a later addition and is not in place for the result shown in Fig. 7.2.

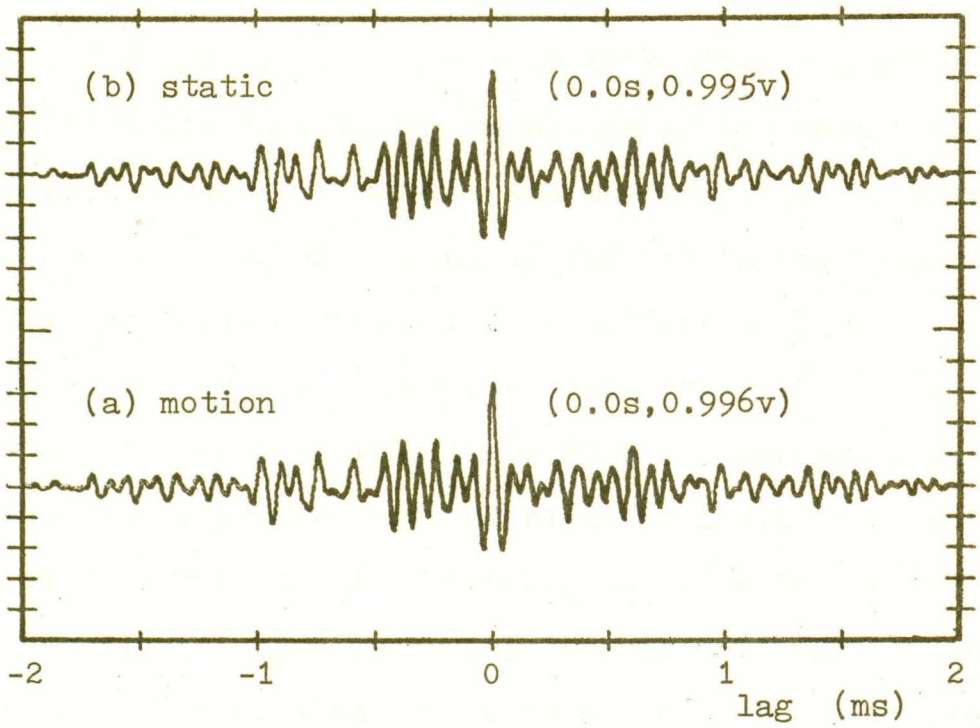

FIG. 7.2 Cross correlograms obtained with the plane reflecting surface in the 'low' position. Each correlogram results from a single sampling of the electrical signals at the microphones.

(Figs. 6.4 and 6.5). However in this situation there is a slight difference in the magnitude of the main correlation peak between the static and moving results. This difference, along with small variations in the secondary peaks, can be accounted for by considering the effect of interference between the direct and reflected sounds.

Interference between the direct and reflected waves results in alternate zones of high and low intensity in the vicinity of the microphones. For a perfectly level plane reflector, the intensity depends only on microphone height. However, with the textured reflectors it also varies with the horizontal position and depends on the angular position of the source. Because of small differences in the position of the static source and the effective position of the moving source (see Appendix G1), the intensity of the sound at the microphones for the static test will not necessarily be identical to that which existed when the moving result was obtained.

The interference between the direct and reflected waves can be minimized by attenuating the direct radiation received at the microphones. The attenuation is accomplished by placing a sound-absorbing hood in front of the microphones as shown in Fig. 7.1. The hood essentially eliminates the interference when the plane reflector is used.

When a textured reflector is used, however, the sound absorbing hood will generally not suppress all interference, because sound may still reach each microphone not only by specular reflection, but also by scattering from different parts of the reflector. Under these conditions, the signal from each microphone is very sensitive to small horizontal changes in source or microphone position, and comparisons between correlograms for static and moving sources become very difficult.

Figures 7.3 to 7.6 show the cross correlograms that result when the sound absorbing hood is used with different reflectors in position. The secondary correlation peaks in the correlograms with the moving source are almost identical to their static counterparts. However, the main correlation peak for the moving source result, in Fig. 7.4, has a larger magnitude than that obtained with the static source. This is a direct result of a spatial change in the interference pattern between the static and moving acquisitions. This result was observed with each of the quadratic residue reflectors, with approximately 40% of the static/moving comparisons showing larger magnitude correlation peaks in the moving result. Hence the degradation induced by source motion in the presence of the reflectors can not be determined with the present method of positioning the

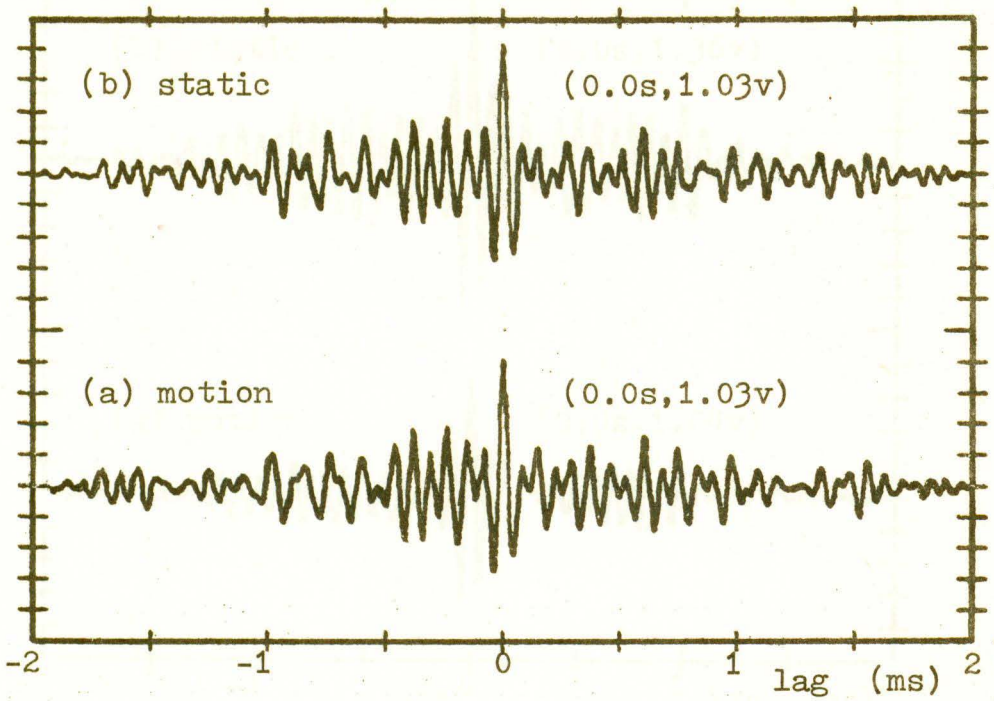

FIG. 7.3 Cross correlograms obtained with the plane reflector and the sound-absorbing hood ('low' position).

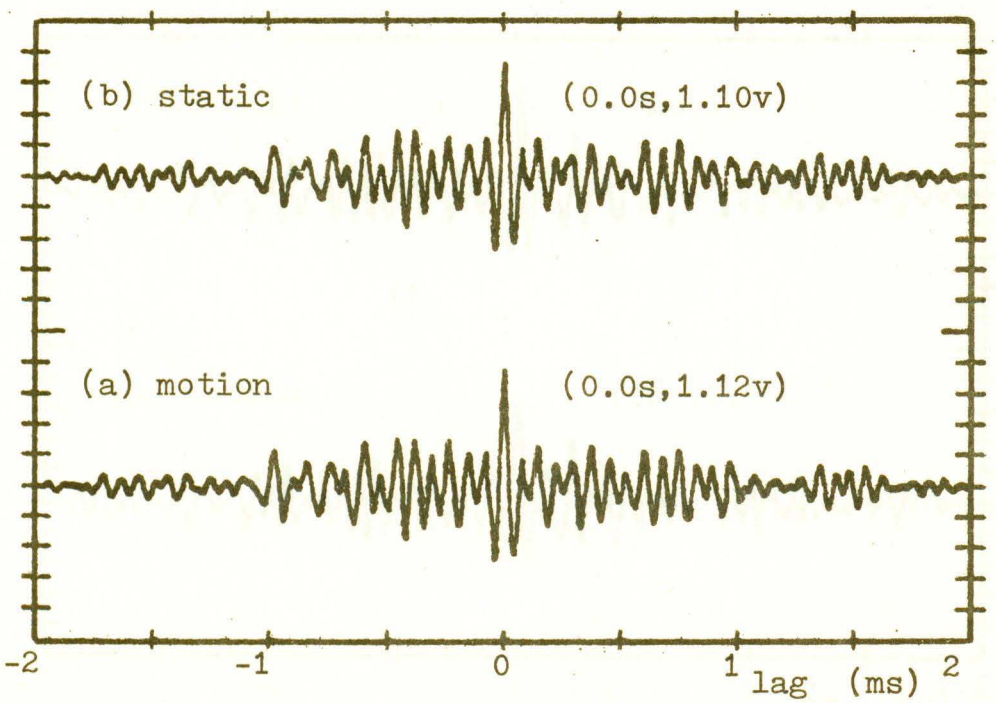

FIG.7.4 Cross correlograms obtained with the transverse reflector in the 'low' position and sound-absorbing hood.

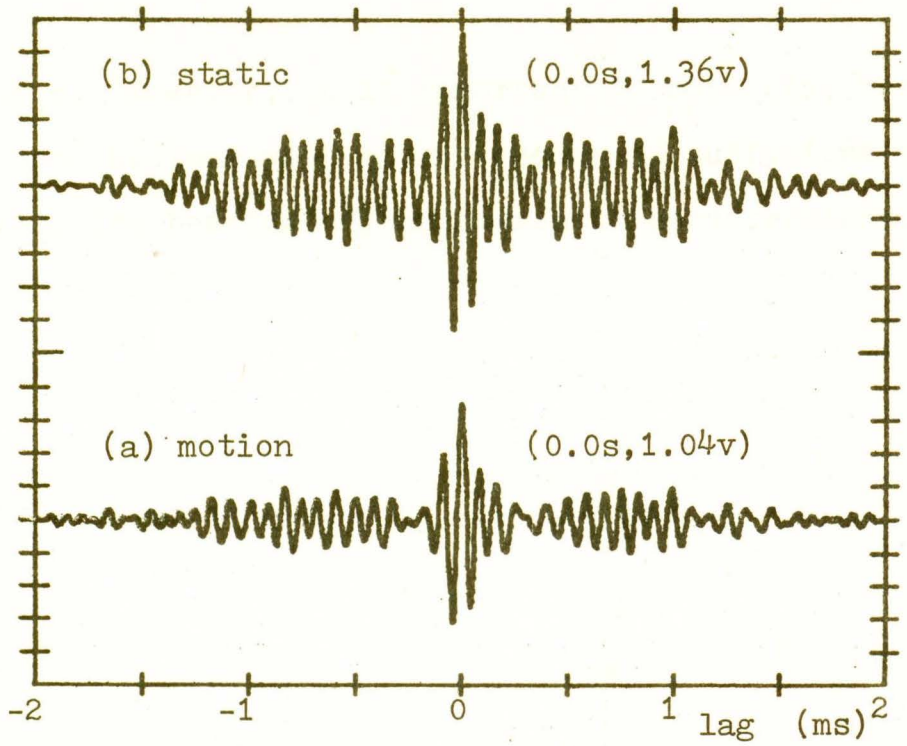

FIG. 7.5 Cross correlograms obtained with the longitudinal reflector in the 'low' position.

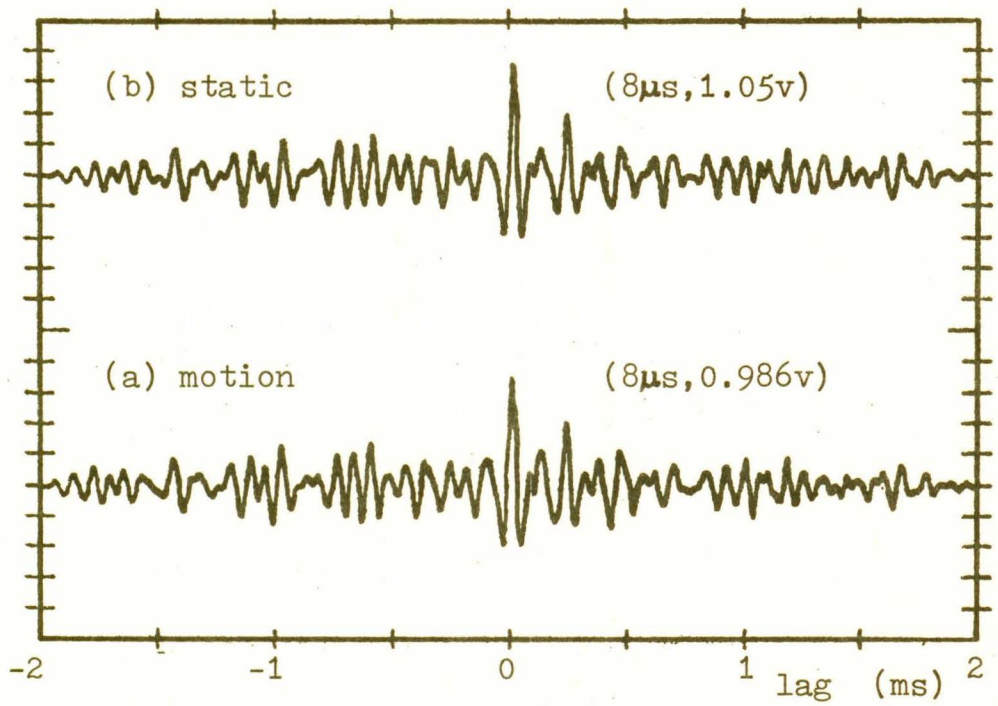

FIG. 7.6 Correlograms obtained with the transverse reflector in the 'high' position.

source. However, it is important to note that the correlation obtained with source motion is sufficient to enable the bearing of the source to be determined.

8. COHERENCE, WITH REFLECTORS AND A MOVING SOURCE

8.1 Arrangement of Apparatus

To examine how coherence is affected by reflection and source motion, the model parameters and procedures for obtaining the coherence function are those described in Chapter 6 (see Fig. 6.6). The horn speaker is oriented so that it is pointed approximately at the centre of the reflecting panel when it is at the mid-point of that portion of the arc over which sampling occurs, viz., at about 78 degrees in this case. The sound-absorbing hood shown in Fig. 7.1 blocks the direct path from speaker to microphone in the same way as for the cross correlation experiments of Chapter 7.

8.2 The Effects of Different Reflecting Surfaces

Figure 8.1 shows the coherence at the source frequency, as a function of time, when different reflectors are in position. Each of the points represent a statistical mean of three coherence functions computed under identical conditions and the ordinates shown for times 0.84, 1.26, 1.68,... seconds are those coherences calcualted for 2, 3, 4,... samplings.

Curve (a), the result for the plane reflector, is nearly identical to the result shown in Fig. 6.8 when no reflecting surface was used. This similarity occurs

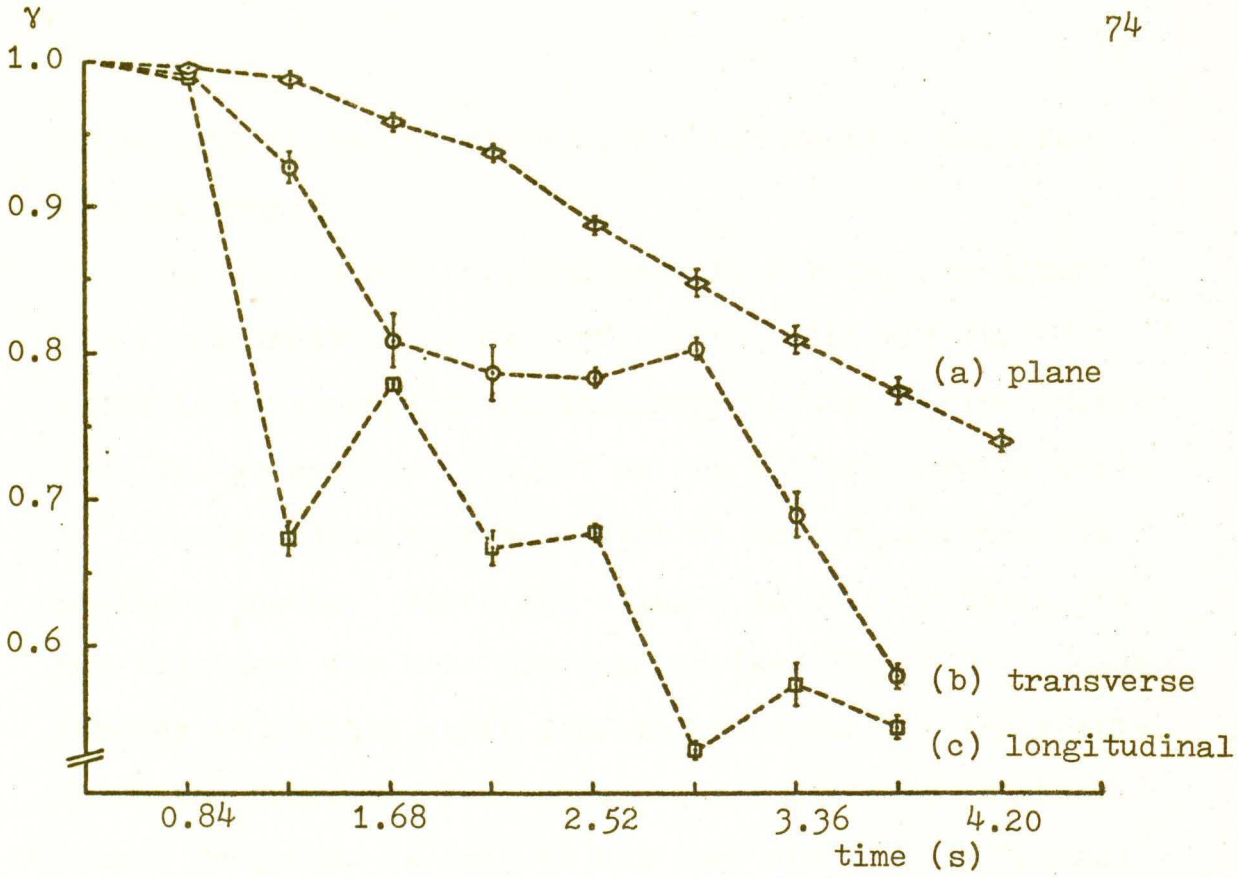

FIG. 8.1 Coherence at the source frequency for different reflectors.

since both cases involve only one propagation path for each microphone.

Curves (b) and (c), the results for the one-dimensional quadratic residue surface, show the effects of multiple path propagation and larger order Doppler shifts (2-3 Hz, as opposed to 0.067 Hz for the plane reflector).

The acoustic energy arrives at each microphone via different paths. Hence the changes in Doppler shift are not identical for both microphones (see Fig. 8.2). These changes in Doppler shift degrade the coherence indirectly. Since the frequency resolution of the analyser at this source frequency is only 50 Hz, they are seen as changes in the phase relationship between the signals. In addition, the superpositioning of these Doppler shifted signals with the non-shifted signals creates amplitude variations at each microphone whose frequencies depend on the degree of Dopper shift (see Kinsler & Frey[21]). Hence the Doppler shifts are also seen as changes in the power ratio.

This textured surface enables the sound to arrive at the microphones via several reflected paths. The interaction of sounds arriving via different paths creates interference patterns whose spatial relationship to the microphones changes as the source moves. Hence changes in the power ratio of the signals occur

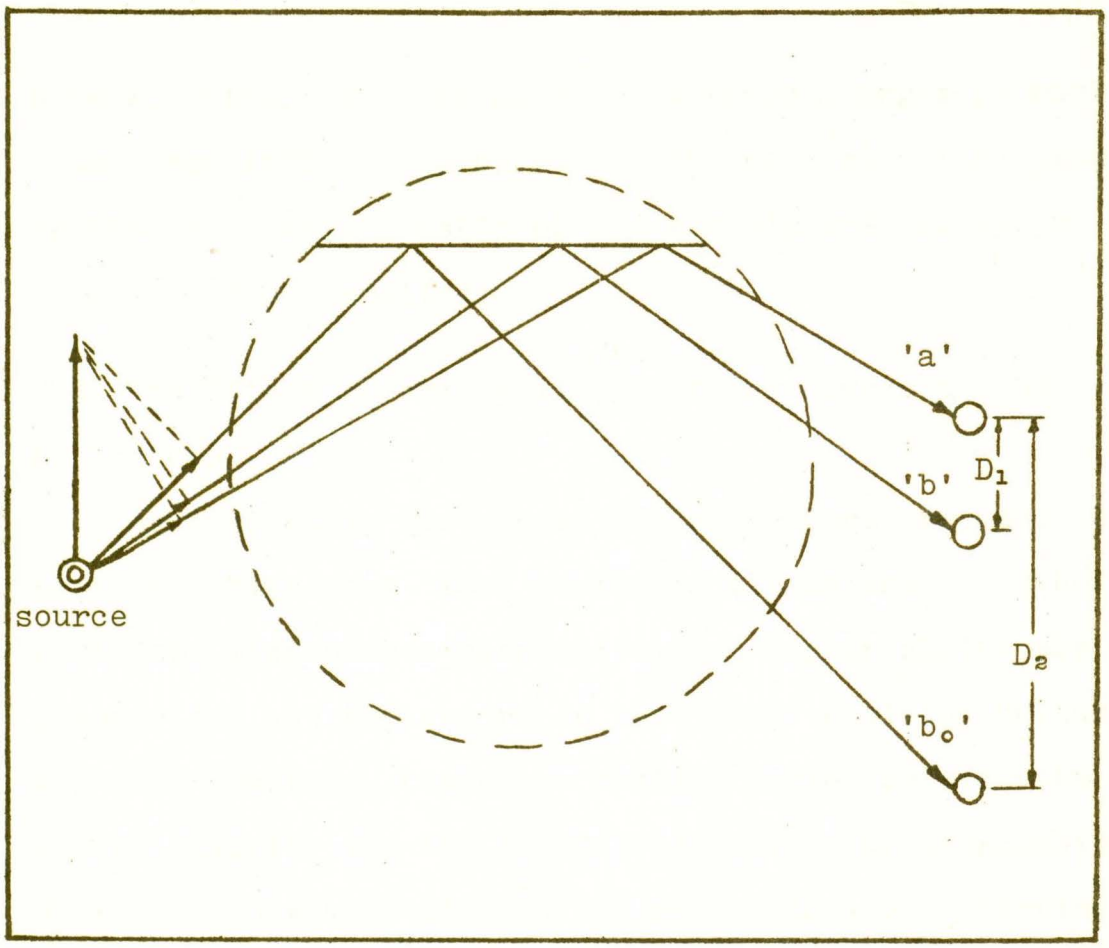

FIG. 8.2 Array-source geometry showing the sound arriving at the microphones via different reflected paths. The sound rays that arrive via different reflected paths possess different components of the source velocity and hence different Doppler shifts. Only two microphones are used in this study. Microphone 'b_o' illustrates the relationship between the difference in Doppler shift at the microphones and their separation.

between samplings. The absence of these changes probably causes the inflections on curves (b) and (c) since changes in the phase relationship of the signals are likely to occur for each sampling.

8.3 The Effect of the Proximity of the Source to the Reflectors

As previously discussed, the reflectors are used in both the 'high' and 'low' positions (20 cm and 40 cm beneath the microphones respectively). Dopper shifts are greater for the reflectors in the 'high' position because, for this position, there are smaller angles between the source velocity and the initial directions of progagation of the sound waves which, after reflection or scattering by the textured reflector, are received by the microphones. The greater Doppler shifts result in a coherence which is lower than that obtained when the same reflector is used in the 'low' position. Figure 8.3 illustrates this effect with the longitudinal reflector.

8.4 The Effect of Ridges

The magnitude of the Doppler shifts produced by the transverse reflector can be increased by adding narrow reflecting ridges. These additional surfaces simulate the large-order surface variations or ridges observed in the Arctic (see Table VI).

Two ridges are positioned as shown in Fig. 8.4 and

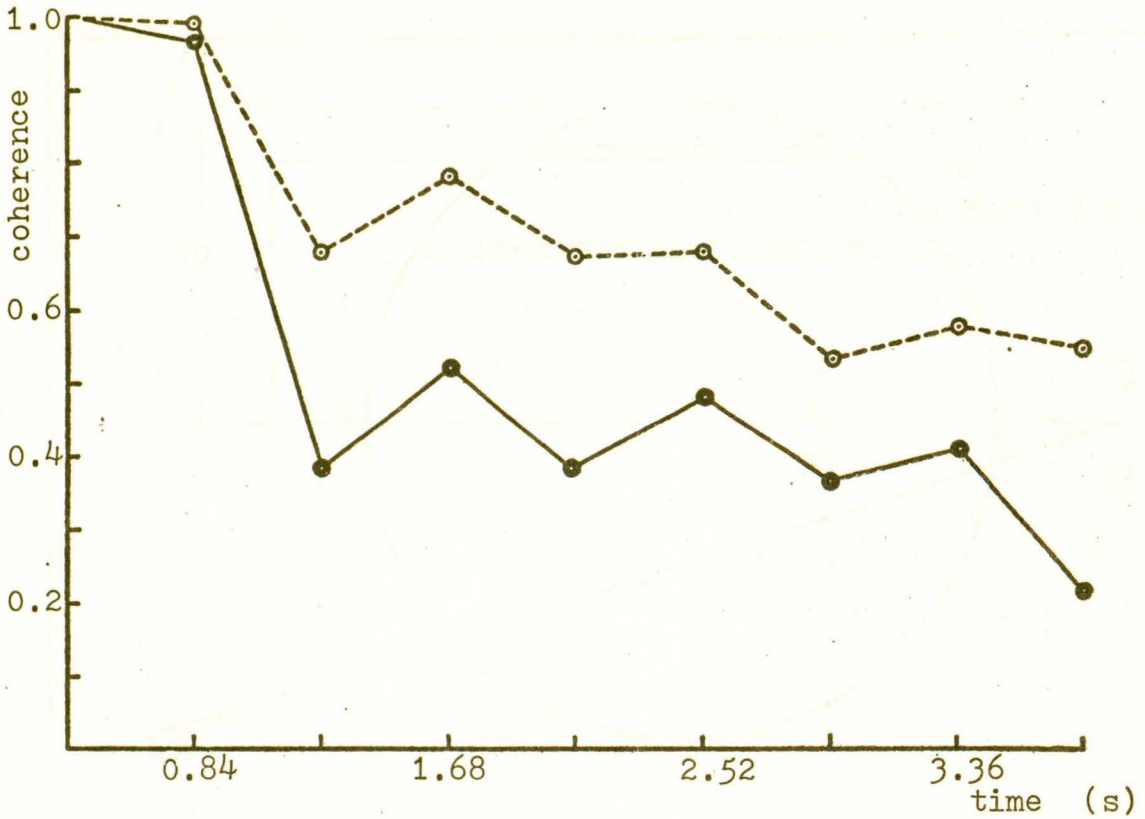

FIG. 8.3 Coherence as a function of time illustrating the effect of reflector height for the longitudinal reflector.

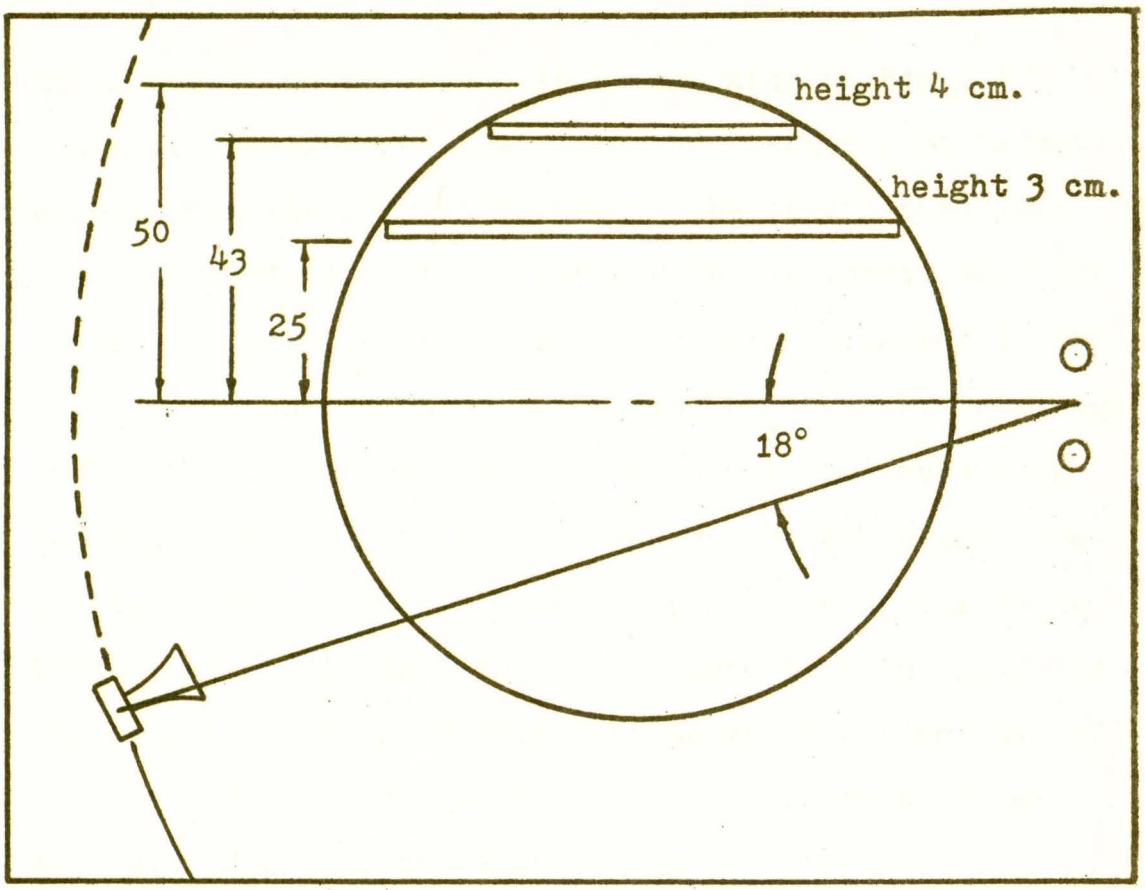

FIG. 8.4 Plane reflector showing the position of the ridges. All dimensions are in centimeters.

their effect on coherence is illustrated in Figs. 8.5 and 8.6. As expected the ridges have their most dramatic effect when the reflectors are in the 'high' position.

The variation of coherence with frequency, when the ridges are positioned on the transverse reflector in the 'low' position, is shown for various numbers of samplings in Fig. 8.7. In contrast to the results observed with no reflector (Fig. 6.6) the coherence at the source frequency is never greater than the coherence of the electrical noise. It is important to note that in the field the coherence of the source must be greater than that of the electrical and/or ambient noise in order to be observed. (However, see Section 1.3 para 2.)

8.5 The Effect of Increasing the Microphone Separation

The model parameters are based on satisfying a nominal field time-difference rate of change of 6.7 μs/s as discussed in Chapter 2. Since this is a conservative estimate, the microphone separation can be increased without adjusting the other model parameters. For example, a separation of 10 cm represents a time-difference rate of change of 19.3 μs/s (for r=1.5 m v=0.1 m/s). This estimate is well within the limits of the time-difference rate of change shown in Table II.

Figure 8.8 illustrates the effect on coherence of an increase in microphone separation when the plane re-

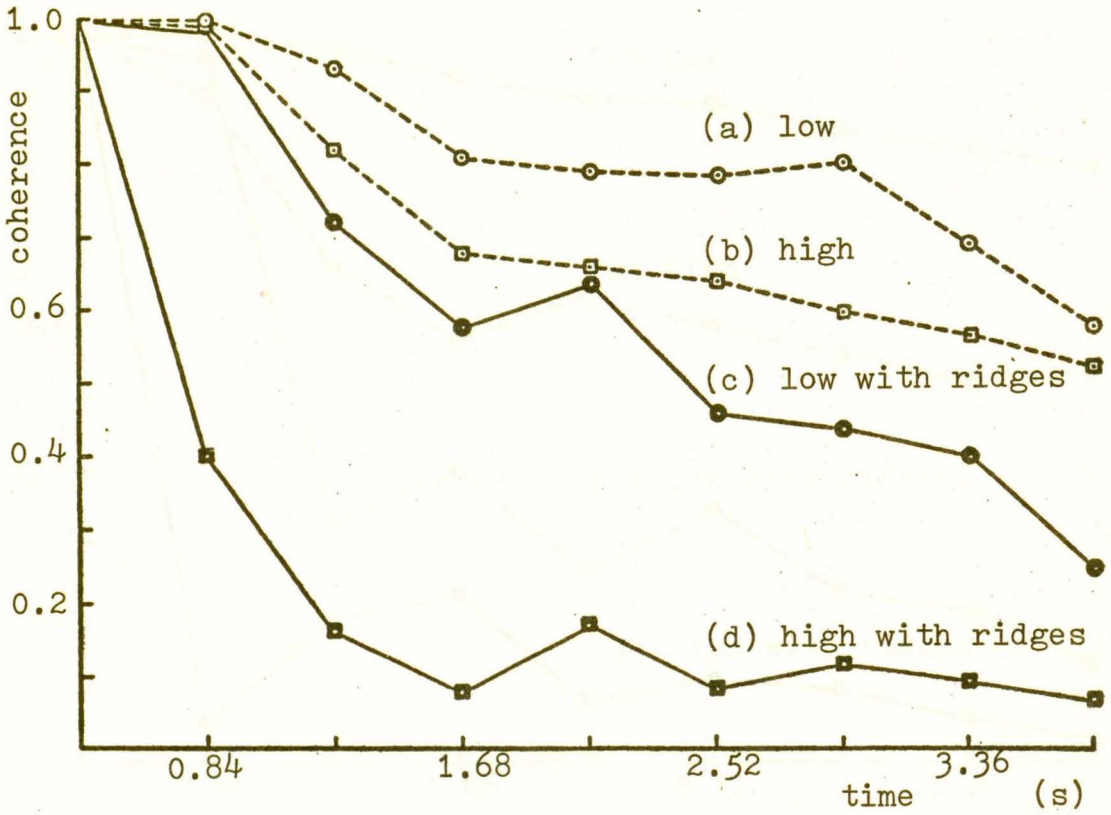

FIG. 8.5 Coherence with the transverse reflector (ridges).

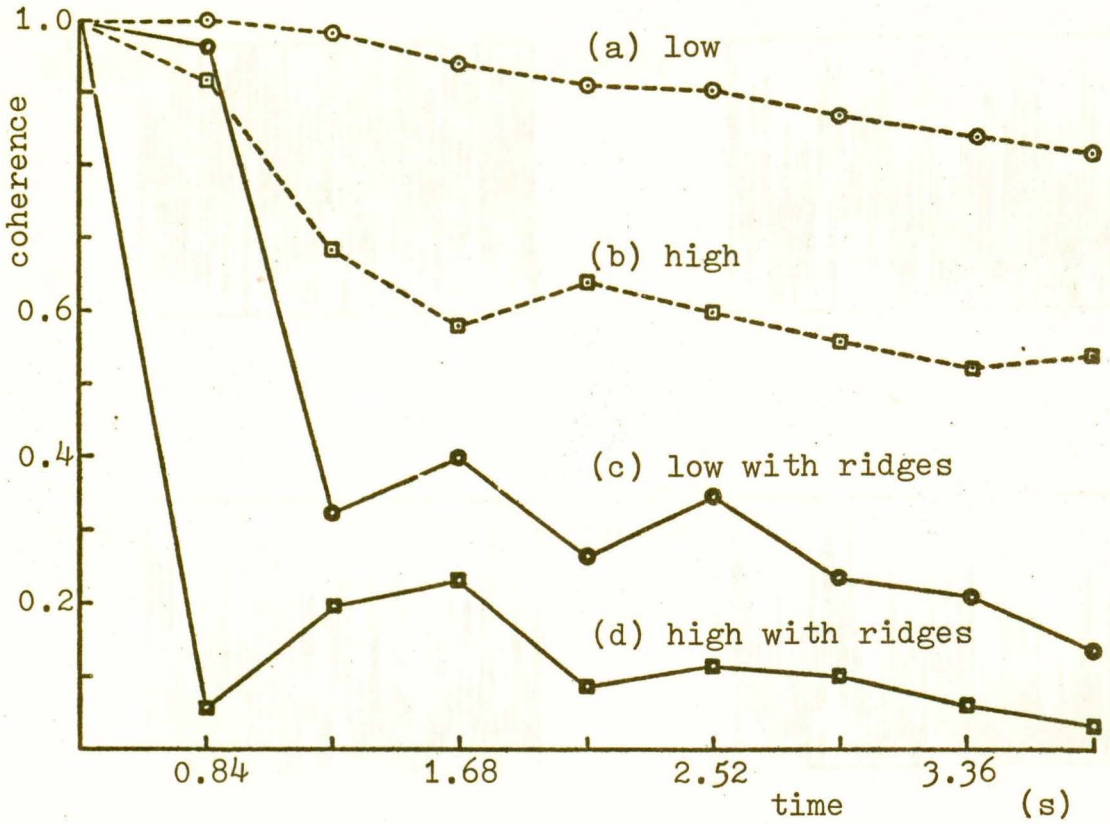

FIG. 8.6 Coherence with the two-dimensional reflector showing the effect of ridges.

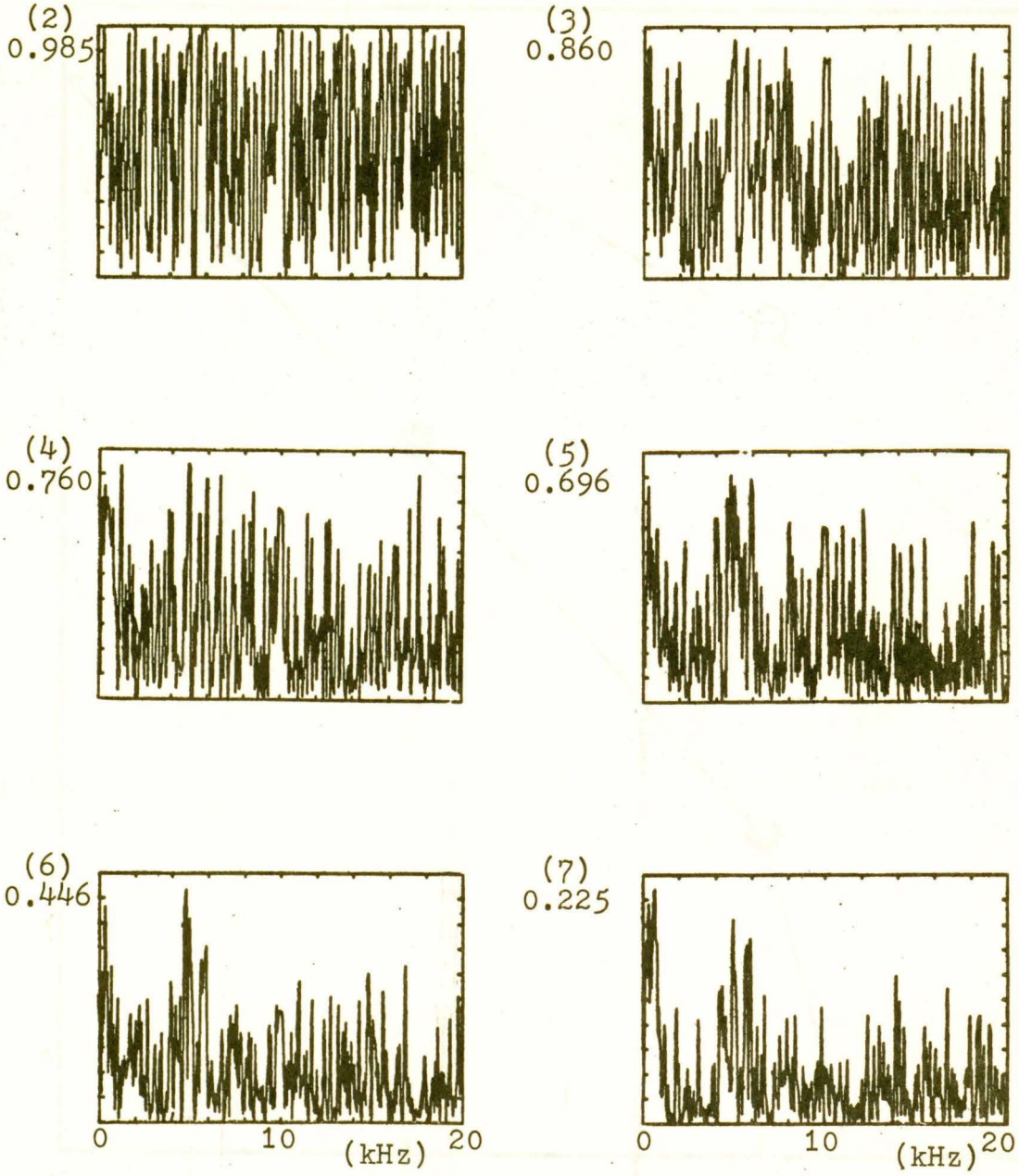

FIG. 8.7 Coherence for the transverse reflector in the 'high' position with ridges. The number of samplings is shown in brackets, with the updated coherence at the source frequency (10 kHz) below.

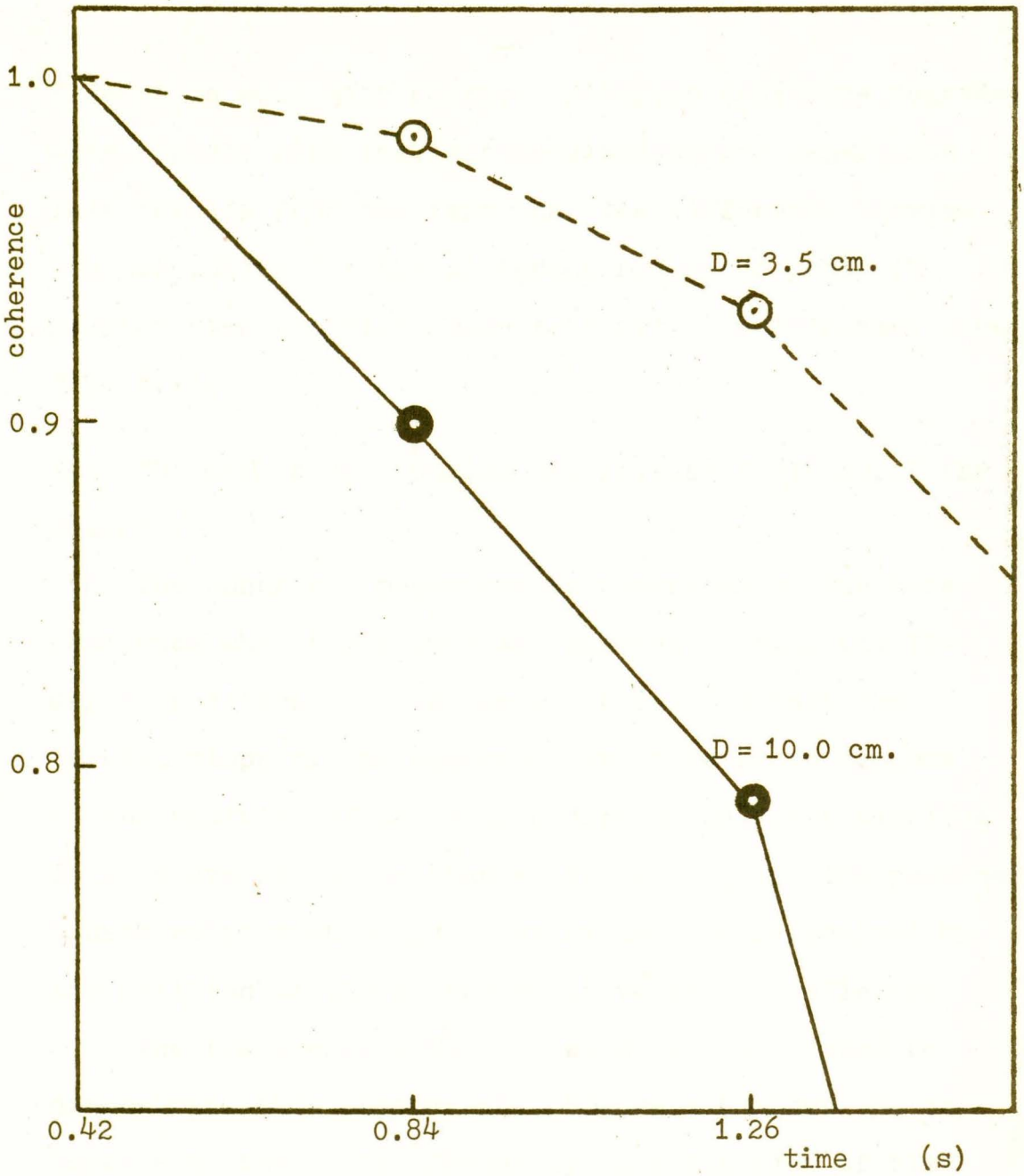

FIG. 8.8 Coherence showing the effect of microphone separation when the plane reflector is in the 'high' position with ridges.

flector is used with ridges. Note: the coherence degrades more rapidly with the increased microphone separation. This results from the fact that the difference between Doppler shifts for the different reflected paths is greater when the microphone separation is increased (see Fig. 8.2).

8.6 The Effect of Changing the Initial Position of the Source

The coherence measurements described so far have commenced when the source was passing through the 72-degree position. It is important to note that the initial slope of the coherence vs. time plots depends on the position of the source during the first sampling. This occurs since the changes in the degradation phenomena (phase relationship and power ratio) are determined by the position of the source relative to the reflector.

The transverse reflector with ridges is used to demonstrate this phenomenon. Figure 8.9 shows the coherence at the source frequency as a function of time when two different initial sampling positions are used. For curve (a) the sampling commences when the source is in the 72-degree position, while for curve (b) the sampling commences 400 ms after the source has passed this position. Note the similarity of these curves to that in Chapter 5 (Fig. 5.1). This result confirms that

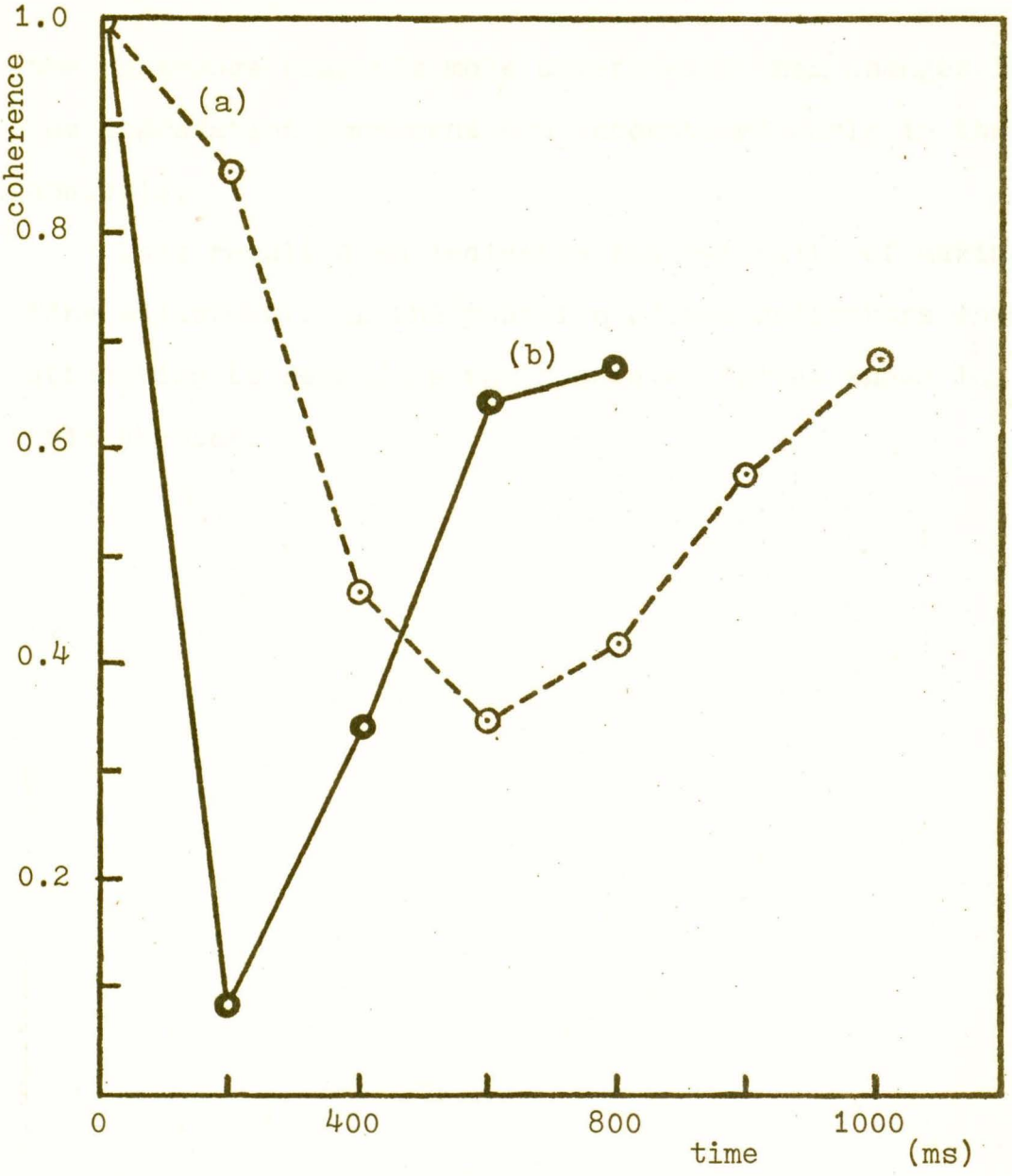

FIG. 8.9 Coherence, the effect of the initial sampling.

the coherence responds more drastically when changes in the degradation phenomena are encountered early in the analysis.

This result also indicates the necessity of making fine adjustments in the position of the reflectors when attempting to reproduce the coherence curves shown in this chapter.

9. COMPARISON OF CROSS CORRELATION AND COHERENCE

9.1 Introduction

As discussed in Chapter 7 it is not possible to obtain an exact quantitative measurement of the degradation in cross correlation. However, the cross correlation and coherence results may be obtained under similar conditions and the degradation in these two measurements compared. To ensure that conditions are as nearly identical as possible, measurements of cross correlation and coherence are obtained on alternate rotation cycles of the source. The two-dimensional reflector with ridges and the model parameters v=0.1 m/s, D=3.5 cm and r=1.5 m are used for all comparison measurements.

The measurements are obtained using first a pure tone and then a frequency-modulated (FM) sinusoid. In the former, the cross-correlation function is periodic and hence only the presence of the source can be observed; while the latter produces a strong main correlation peak that enables the bearing of the source to be calculated. The acoustic energy from both of these sources is localized in the frequency domain. Therefore, they are both ideal sources to observe coherence.

9.2 Results Using a Pure Tone Source

Figure 9.1 shows the coherence of a pure tone at

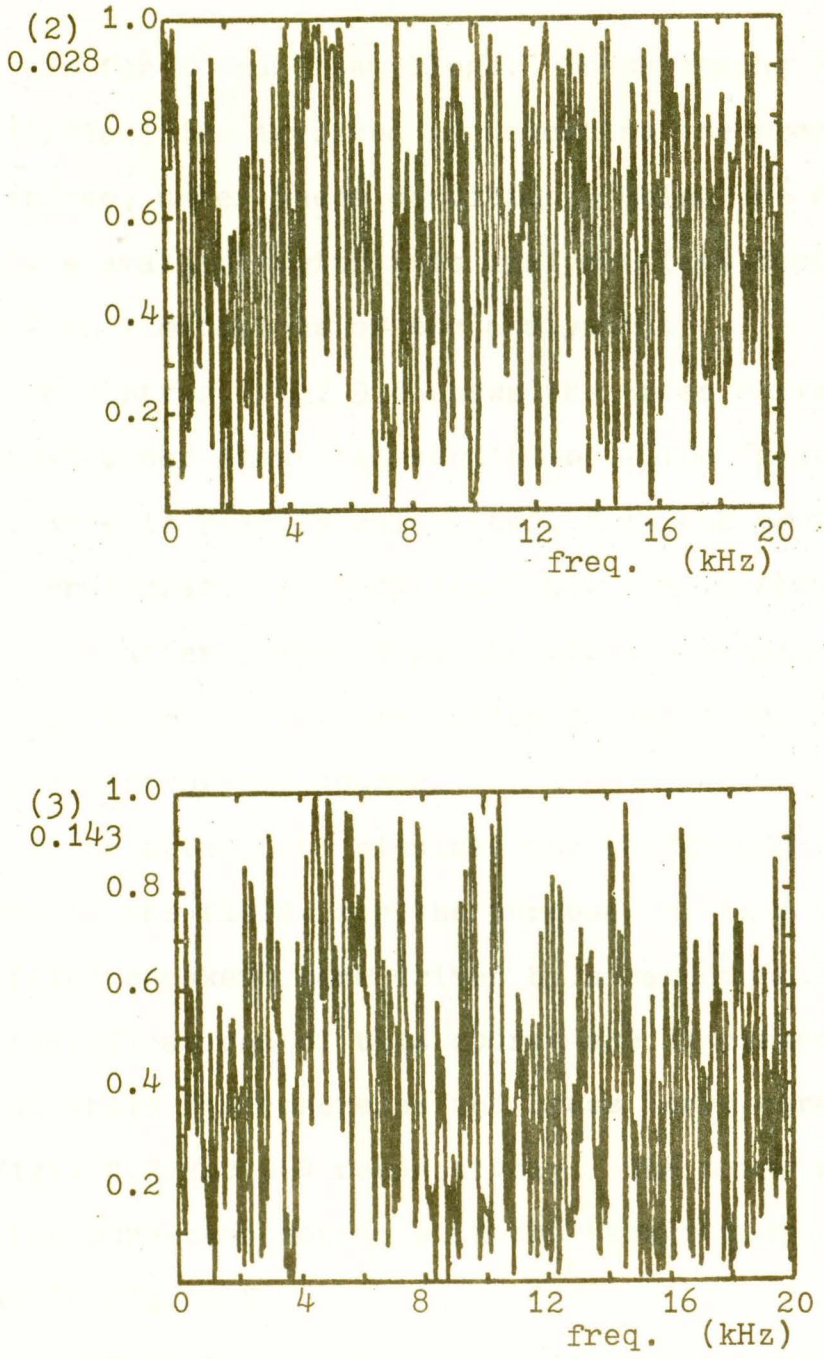

FIG. 9.1 Coherence, with a pure-tone source at 9.95 kHz. The number of samplings appears in brackets with the updated coherence below.

9.95 kHz for 2 and 3 samplings. These graphs illustrate the difficulties involved in detecting the presence of the source, under these conditions, using the coherence estimate available with this analyser (see Section 1.3 para 2 on limitations of the analyser).

In contrast Fig. 9.2 shows the cross correlation obtained under identical conditions. The frequency of the source is readily calculated, from the period of the correlogram, as 40 cycles/0.004 s = 10 kHz. Note that even after 5 samplings the signals remain correlated, although there is some reduction in magnitude due to the displacement of the source.

In an attempt to simulate the background noise observed in the field, for the purposes of this comparison, two fixed speakers were driven by a random noise source. The specifications of this source are discussed in Appendix H1 while its coherence and cross correlogram are shown in Figs. 9.3 and 9.4 respectively. The power spectrum for the pure-tone source with the background noise is shown in Fig. 9.5.

As shown in Fig. 9.6 the existence of the source under these conditions can not be determined by coherence. In contrast, the cross correlogram, Fig. 9.7, suggests the presence of a narrow-band source at approximately 10 kHz. It should be pointed out that it is not

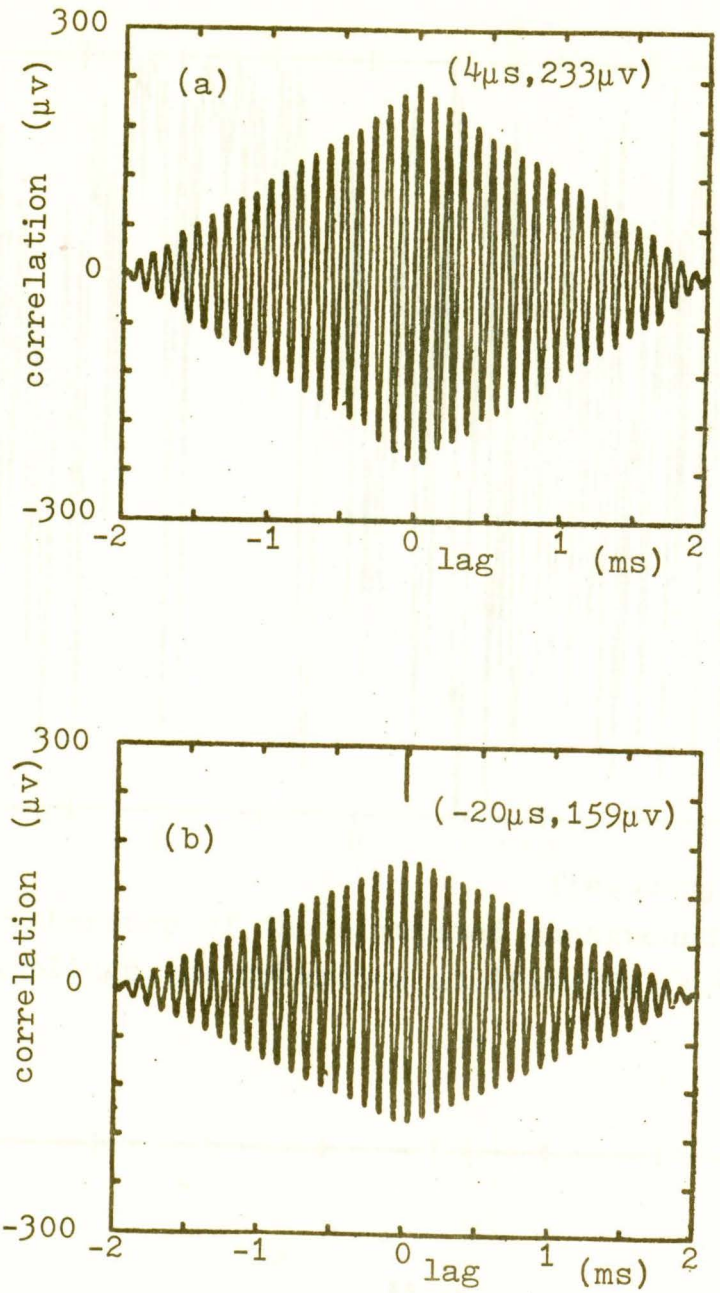

FIG. 9.2 Cross correlation with a pure-tone source at 9.95 kHz; (a) 1 sampling, (b) 5samplings. The co-ordinates of the central peak are shown in brackets.

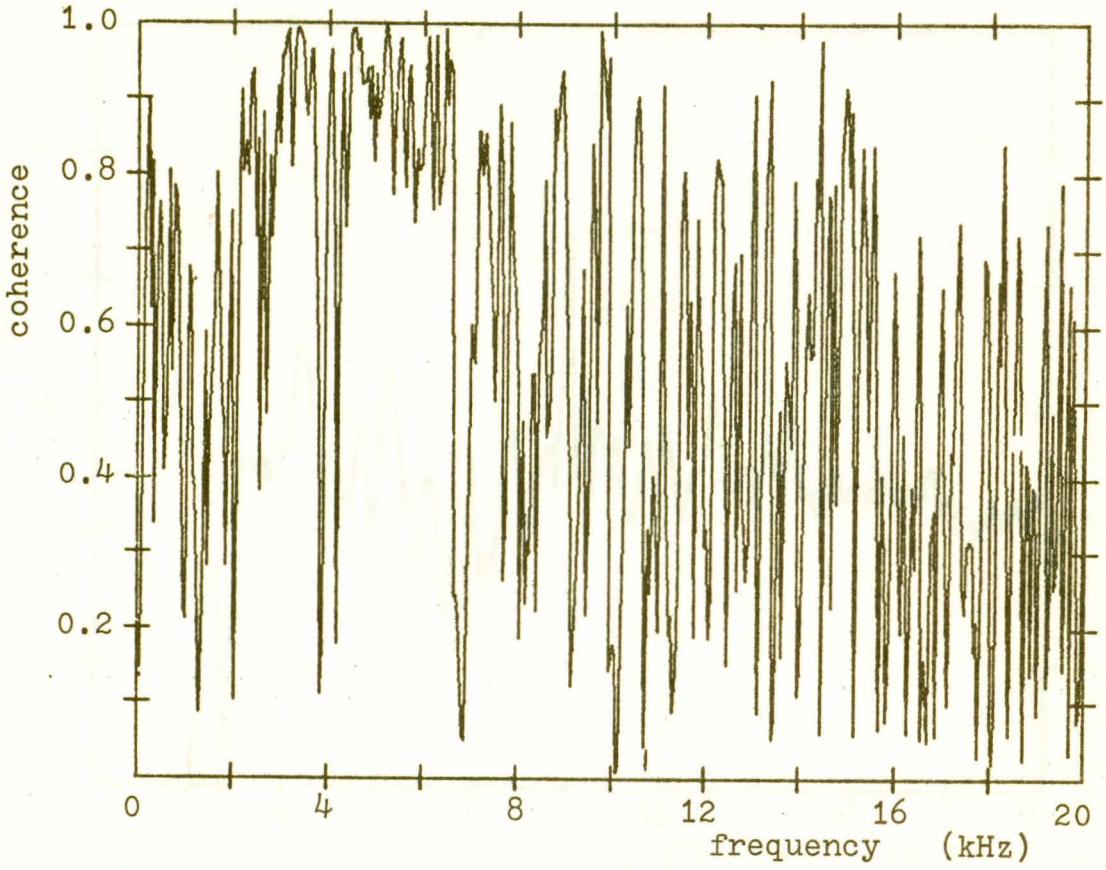

FIG. 9.3 Coherence of the simulated background noise. After 3 samplings the coherence at 10.7 kHz is 0.332.

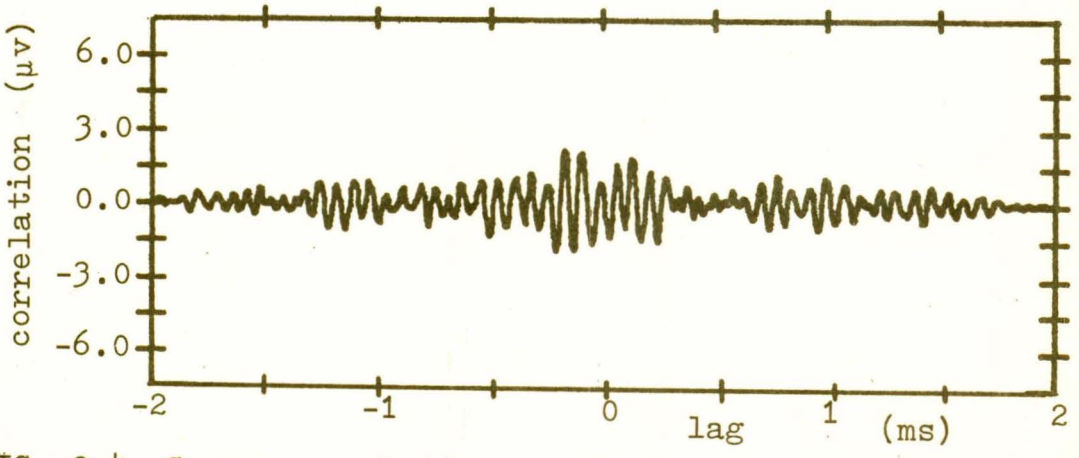

FIG. 9.4 Cross correlation of simulated background noise.

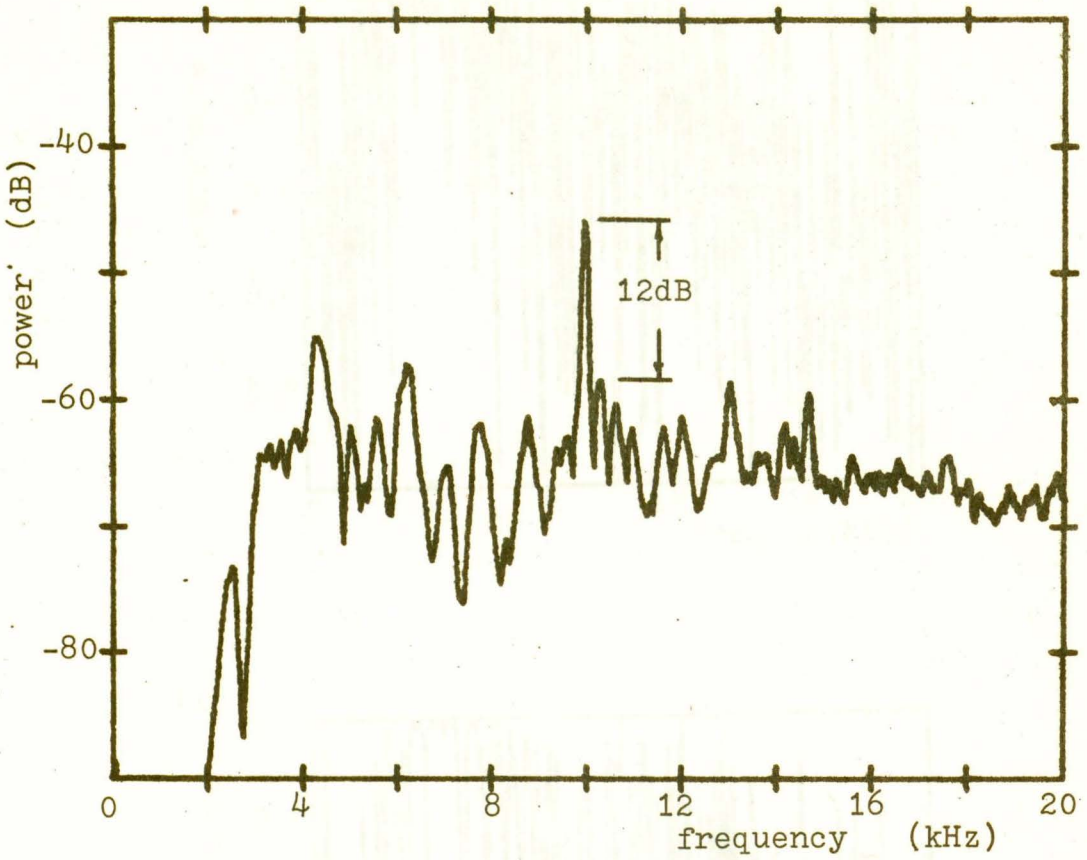

FIG. 9.5 Power spectrum of the pure-tone source with the background noise.

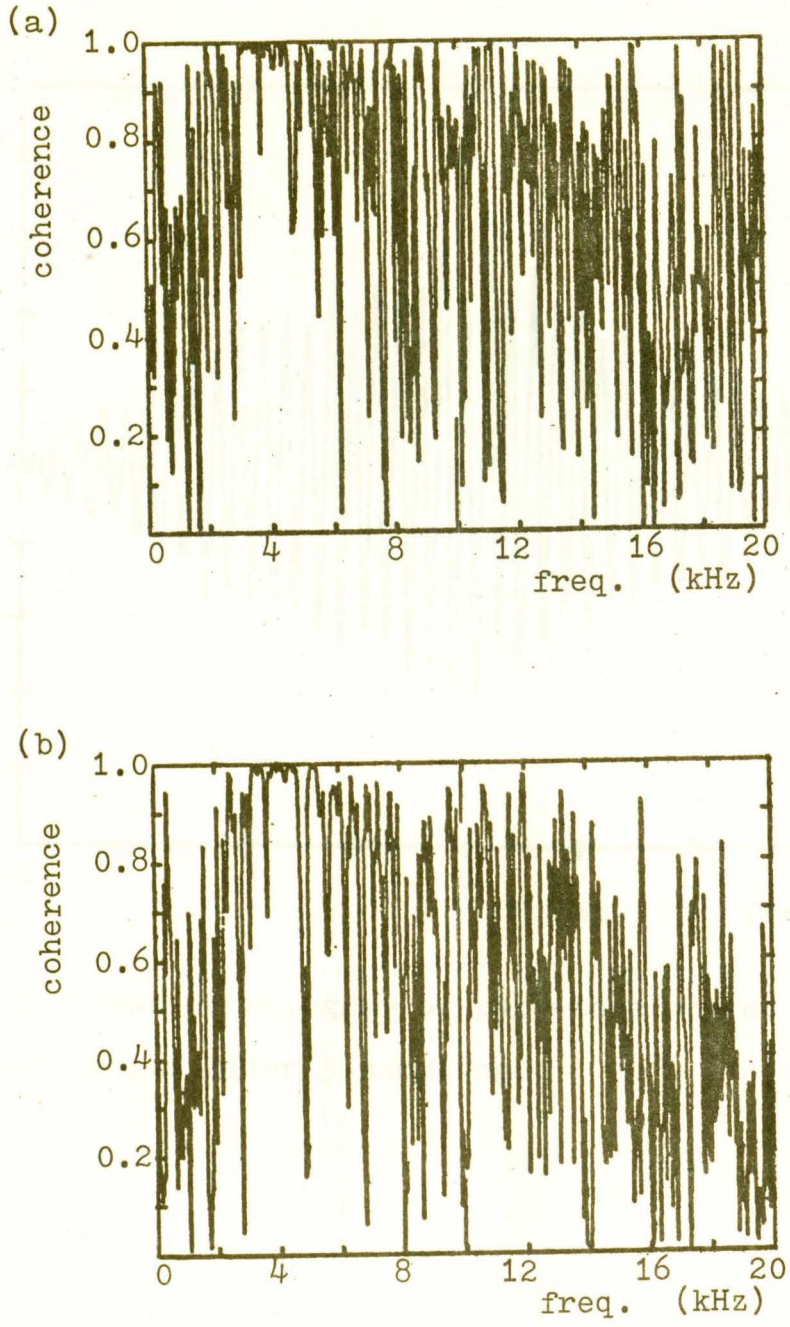

FIG. 9.6 Masking effect of the background noise on the coherence of a pure-tone at 9.95 kHz; (a) 2 samplings, (b) 3 samplings.

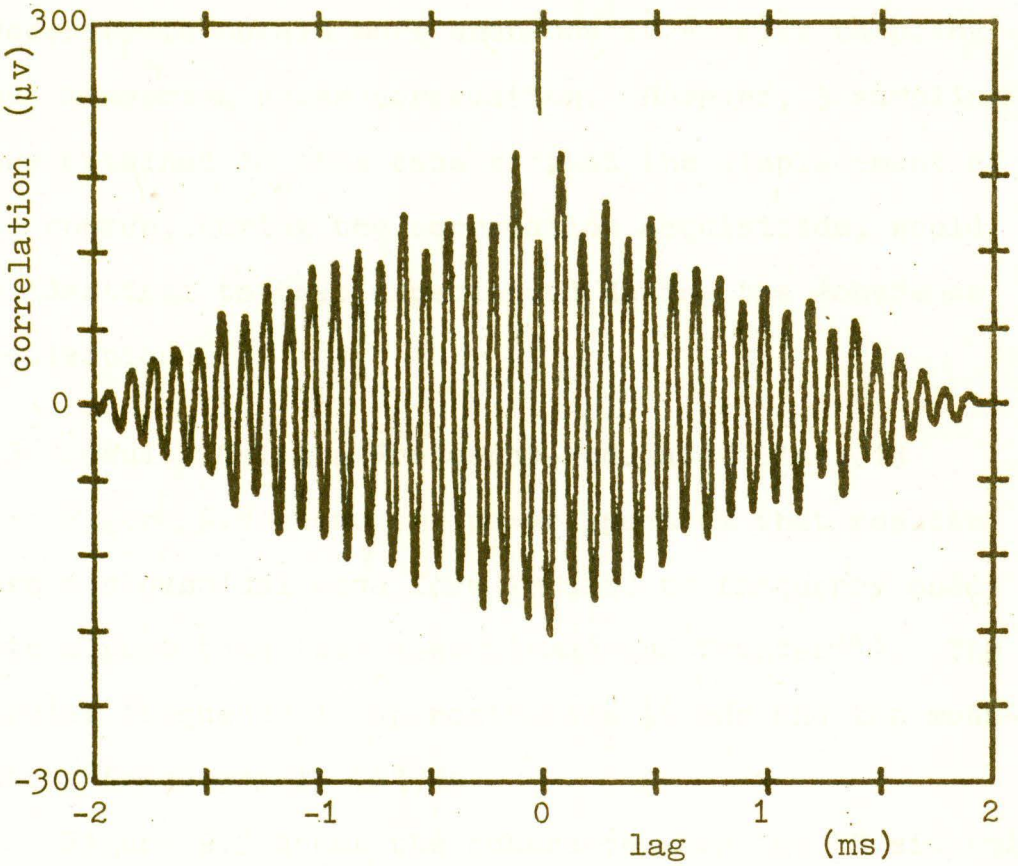

FIG. 9.7 Cross correlogram of pure-tone source with the background noise after 3 samplings.

necessary to obtain more than one 1024-point sampling when measuring cross correlation. However, 3 samplings were obtained in this case so that the displacement of the source, during the correlation acquisition, would be identical to that experienced during the coherence acquisition.

9.3 Results Using a Frequency-Modulated Sinusoid

Figure 9.8 shows the power spectrum that results when a sinusoidal wave form is used to frequency modulate a pure tone (see also Ziemer and Tranter[20]). The carrier frequency is approximately 10 kHz and the modulating frequency is 500 Hz.

Figure 9.9 shows the coherence when the FM sinusoid is used as a source. The effect of the ridges can be seen at the higher frequencies in the result shown for 4 samplings.

The coherence of the energy at the lower frequencies is of an acceptable standard to permit the detection of the source. However, if larger order ridges were present or if the source were composed only of high frequencies, ie., above 9 kHz, then the presence of the source could not be detected with coherence.

Figure 9.10 shows the cross correlograms obtained under the same conditions. As in the case with pure tone source, the presence of the source is readily de-

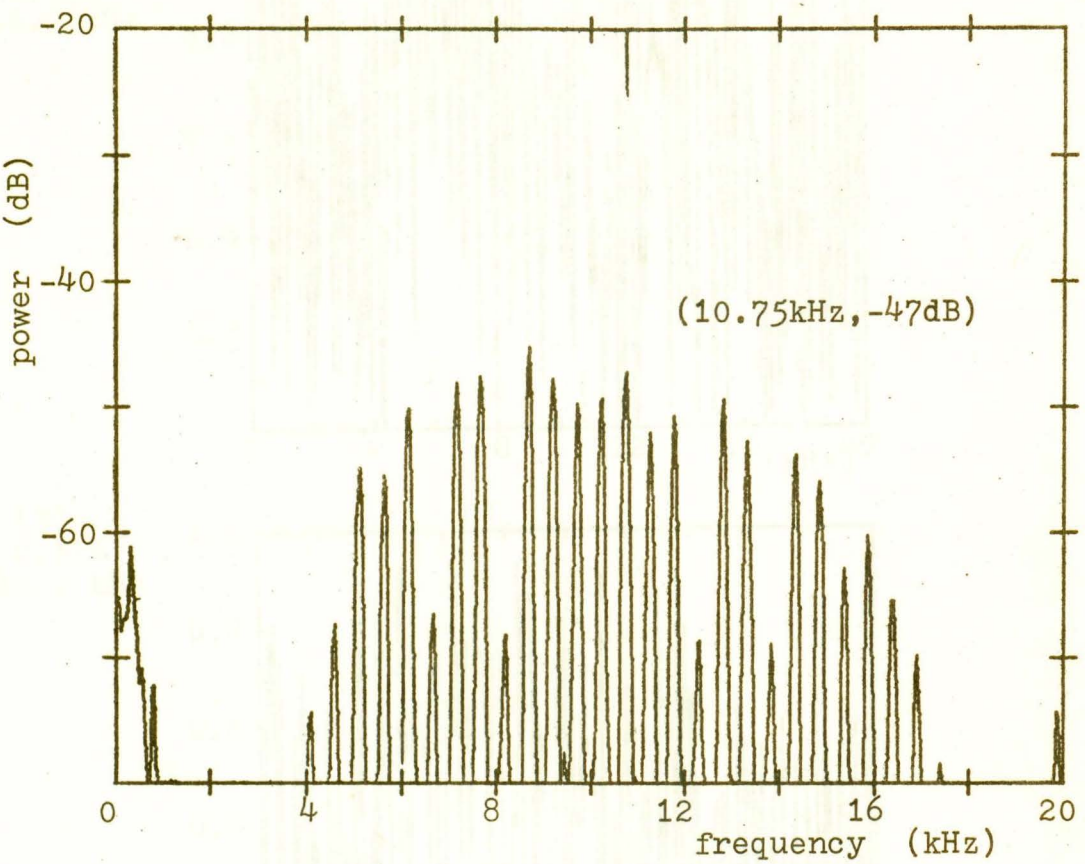

FIG. 9.8 Power spectrum of the frequency-modulated sinusoid after 10 samplings.

(2)
$\gamma = 0.851$
at 10.7 kHz

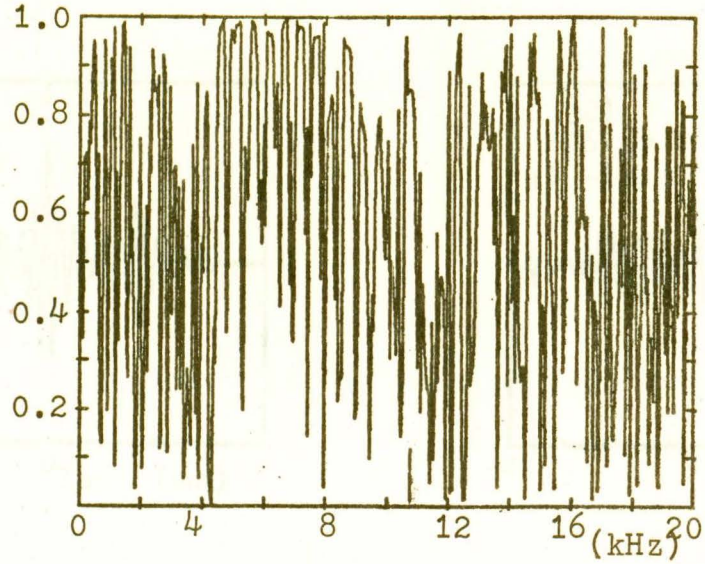

(3)
$\gamma = 0.529$
at 10.7 kHz

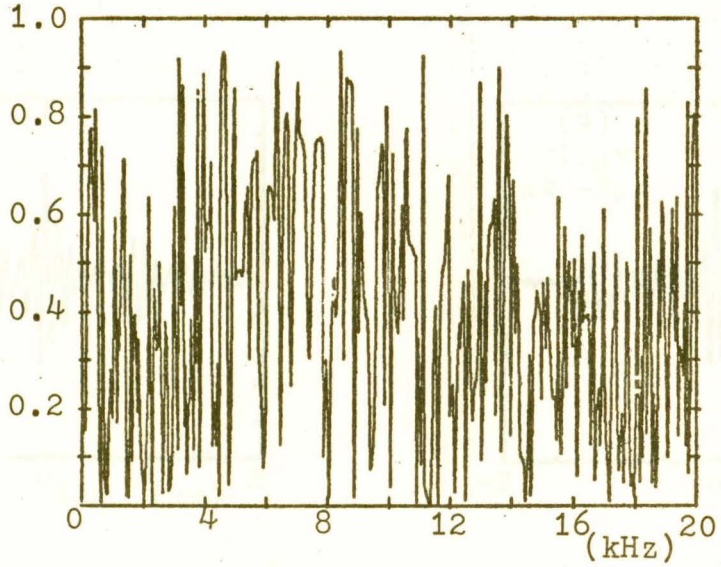

(4)
$\gamma = 0.519$
at 10.7 kHz

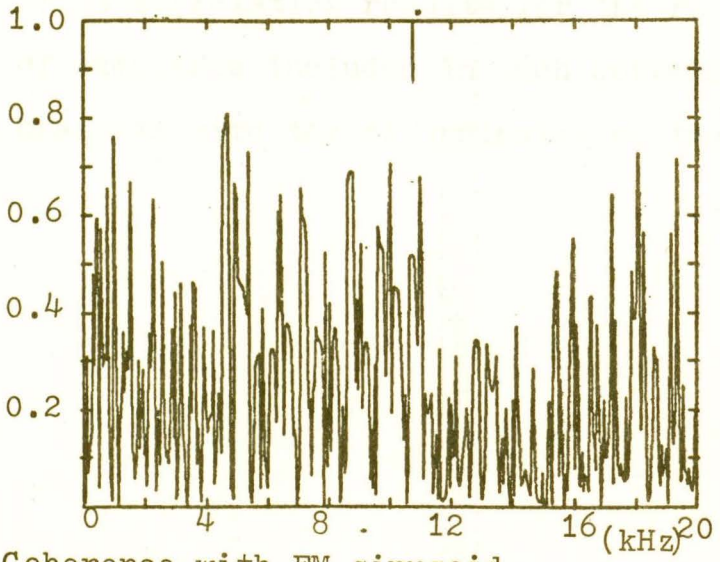

FIG. 9.9 Coherence, with FM sinusoid

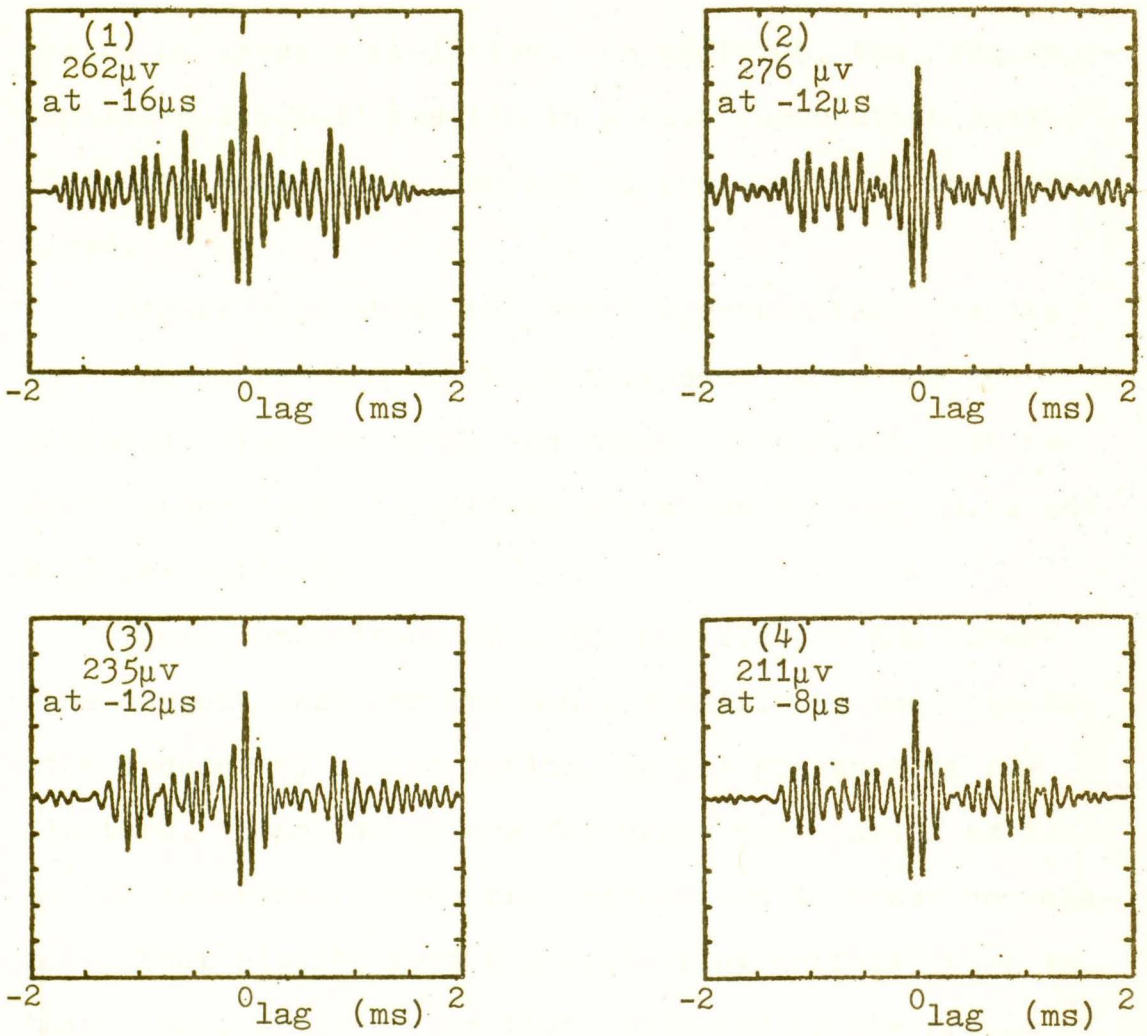

FIG. 9.10 Cross-correlation results for the FM sinusoid. The number of samplings included in each correlation appears in brackets with the co-ordinates of the main peak below.

tected by cross correlation. In addition, the frequency-modulated sinusoid results in a main correlation peak that also enables the bearing of the source to be determined.

Figure 9.11 shows the power spectrum that results when the background noise is introduced with the FM sinusoid. The coherence and cross correlation that results under these conditions are shown in Figs. 9.12 and 9.13 respectively.

These comparisons of cross correlation and coherence suggest that for the model conditions, the degradation induced by source motion, in the presence of reflectors, is not as severe for cross correlation as it is for coherence. Thus the degradation in cross correlation, that results from the reflecting surfaces used in this study, is less than that indicated by the graphs of coherence presented in Chapter 8.

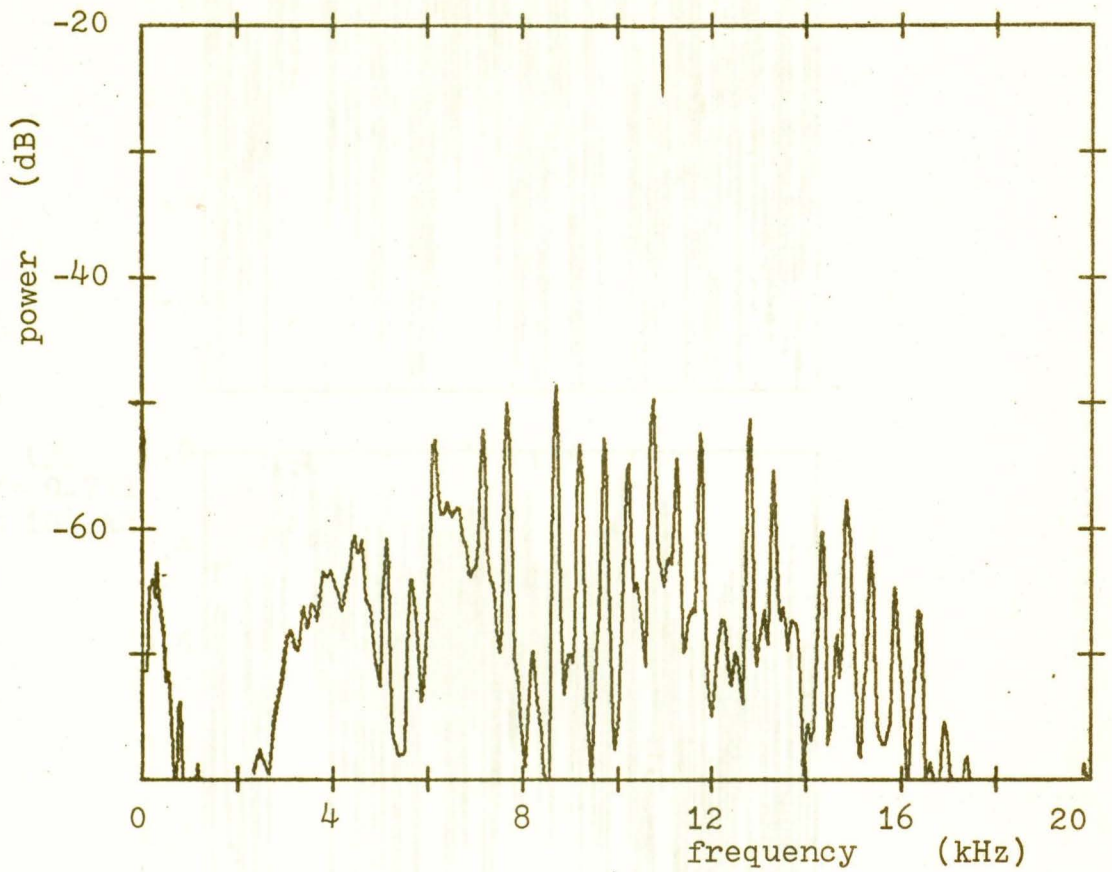

FIG. 9.11 Power spectrum of the FM sinusoid with the background noise after 100 samplings.

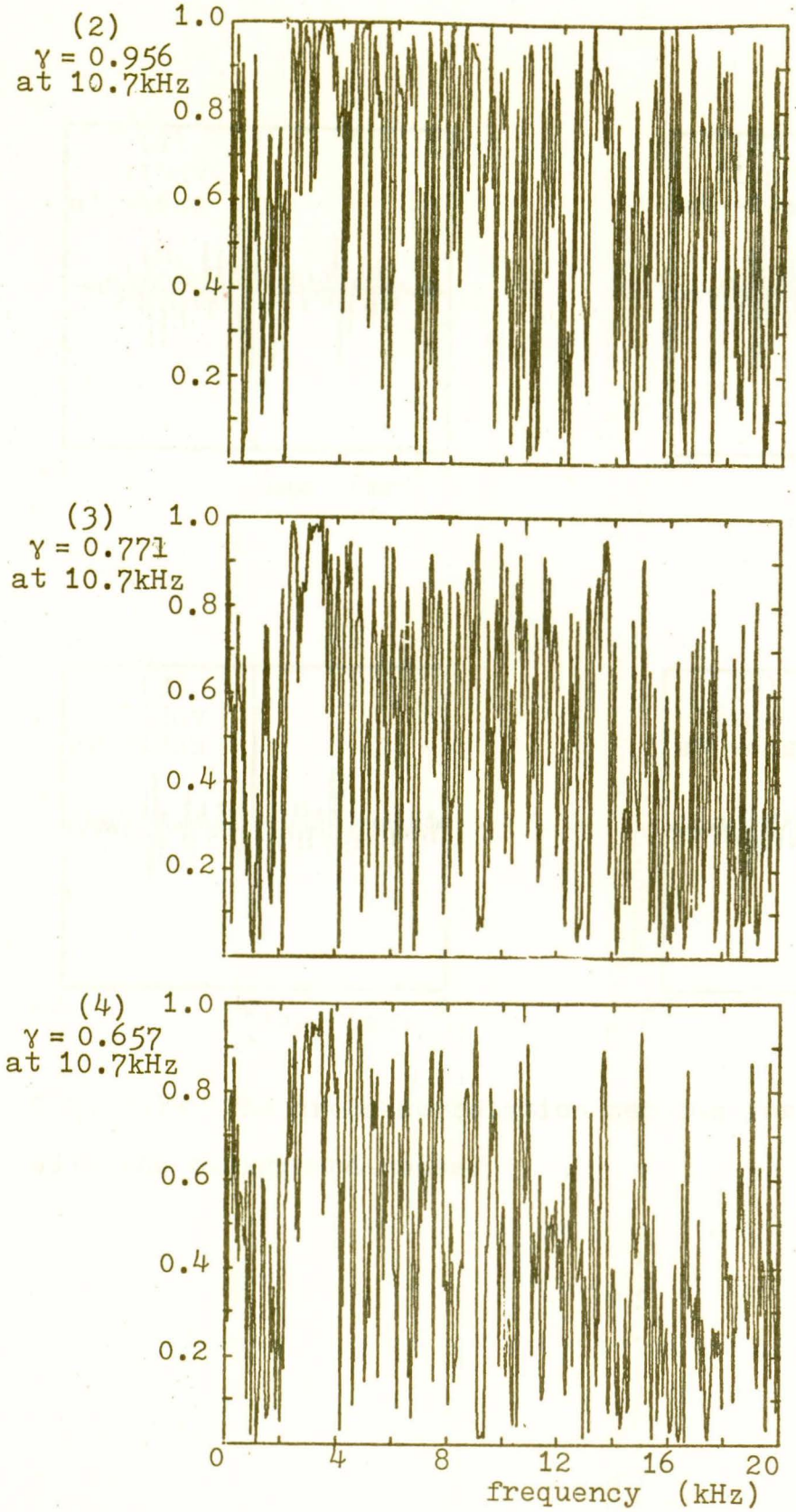

FIG. 9.12 Coherence, with the FM sinusoid and background.

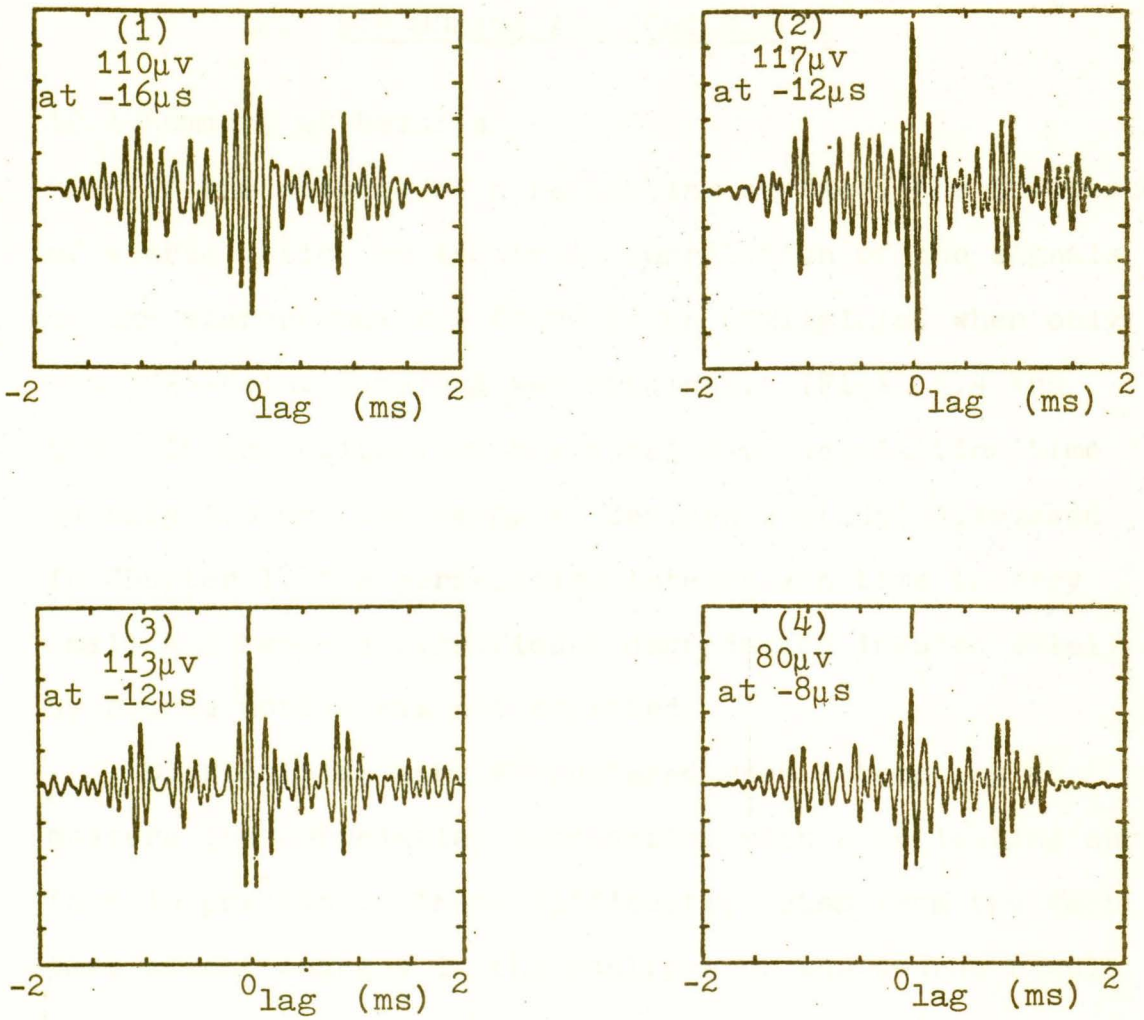

FIG. 9.13 The cross-correlation results for the FM sinusoid with the background noise.

10. DISCUSSION AND CONCLUSIONS

10.1 Summary of Results

In the absence of a reflecting surface, the influence of source motion on the cross-correlation of the signals at the microphones was found to be negligible, when only one 1024-point sampling was obtained. (Figs. 6.4 and 615) In this situation the total data acquisition time is only 4.0 ms. In terms of Gerlach's study, discussed in Chapter 1, the correlation integration time is very small and hence a significant degradation induced solely by source motion was not expected.

Difficulties were encountered when attempting to measure the correlation degradation with a reflecting surface in position. These difficulties stem from the fact that slight changes in the position of the source result in dramatic changes in the spatial relationship of the interference patterns at the microphones. Hence a quantitative measure of the correlation degradation, induced by source motion in the presence of a reflecting surface, was not obtained. However the signals at the microphones were observed to have a finite correlation even under the most severe conditions. (See Fig. 9.13 for example)

However, a quantitative measure of the coherence degradation was readily available, primarily because of the normalization of the coherence function. The value

of the coherence at the source frequency was plotted as a function of time when different reflectors were present. These graphs illustrate the dependence of the coherence on three model parameters; the proximity of the source to the reflector, the separation of the microphones, and the vertical components of the reflecting surface. In addition, it was observed that the response of the coherence to the relative changes in power at the source frequency depends on the number of samplings that have already been considered when the relative changes are encountered (see for example Fig. 8.8).

10.2 Factors Influencing Coherence

It is clear from the analysis of the coherence function in Section 5.2 that the degradation in coherence results from two phenomena; (a) changes in the phase relationship of the signals and, (b) changes in their power ratio. In this study changes in the phase relationship of the signals resulted primarily from changes in their Doppler shift, while changes in the power ratio resulted from changes in the acoustic interference patterns at the microphones.

To a certain degree the severity of the degradation resulting from these changes can be controlled by the model parameters. For example, it was found that increasing the vertical components of the reflectors or

placing the reflectors closer to the source adversely effected the coherence by increasing the changes in Doppler shifts which were not identical for both microphones. However, this is of little significance to the detection problem since these parameters can not be controlled in the field.

A more realizable control of coherence degradation was found to be microphone separation. Increasing this separation enhances the probability that the acoustic energy arrives at the microphones via different paths and hence possess different Doppler shifts at each microphone. In addition, if the reflecting surface produces acoustic interference patterns consisting of alternate zones of high and low intensity, then the probability that the microphones experience opposing changes in intensity, as the source moves, is also enhanced. Thus it is desirable, from the standpoint of maximizing the coherence of the source, to have a receiver separation that is small compared to the wavelength of the interference. However, in the field, factors such as the gain of the array and the degradation in coherence of the ambient noise are also effected by the separation of the sensors and hence must also be considered when selecting the minimum sensor separation.

10.3 Apparent Advantages of Cross Correlation

In an attempt to determine the degradation in cross correlation, relative to that experienced for coherence, a number of experiments were designed to compare these techniques under identical conditions. The results of these comparisons, presented in Chapter 9, indicate that cross correlation is a better technique for detecting the presence of a moving source when reflecting surfaces are present. This results from the fact that, although the ability to detect the presence of the source with cross correlation is adversely affected by changes in the phase relationship of the signals, it is not detrimentally affected by the changes in the power ratio which severely affect the ability to detect the source with coherence.

It should be pointed out that this conclusion may not remain valid under field conditions, or when a more sophisticated instrument is used to obtain the spectral estimates. In the model study, processing the signals in real time results in a sampling time that represents only a small portion of the total acquisition time. However if the same signal analyser were used to process the field signals in real time, the sampling time would then represent a very large portion of the total acquisition time. This occurs since a much larger sampling time is required for the lower field frequen-

cies while the calculation time required by the analyser is reduced.

As discussed in Chapter 1 the coherence estimates are limited by the capabilities of the analyser. Had it been possible to apply adaptive smoothing to the power estimate a satisfactory coherence may have been available after only one sampling. Hence further investigation is required with a more sophisticated analyser to determine which technique (cross correlation or coherence) is less affected by the presence of the reflecting surfaces.

In an attempt to verify the apparent superiority of cross correlation at field frequencies a second study is currently being conducted. This second investigation uses tape recorded data obtained in this study. The source frequency is reduced by re-recording the signals on a high speed recorder and re-playing them at a much lower speed. In this way the signals are analyzed using a sampling time which represents a large portion of the total acquisition time.

Preliminary results from the second study appear to confirm the conclusions drawn in this study. As well, these results suggest that the rate at which the coherence degrades is not changed when the sampling time represents a large portion of the total acquisition time (see Appendix H2).

APPENDIX A

A1 Sound Propagation in the Ocean

Compressional waves are propagated in a fluid with a speed whose square is proportional to the ratio of the fluid's elasticity and density. In the ocean these parameters are a complicated function of salinity, temperature, and pressure. An empirical equation for the velocity of sound is given by Wilson[22] as

$$C = 1499.2 + C_t + C_p + C_s - C_{s,t,p} \qquad \text{(A-1)}$$

where

$C_t = 4.6233T - 5.4585 \times 10^{-2}T^2 + 2.822 \times 10^{-4}T^3 - 5.07 \times 10^{-7}T^4$,

$C_p = 1.60518\times10^{-1}p + 1.0279\times10^{-5}p^2 + 3.451\times10^{-9}p^3 - 3.503\times10^{-12}p^4$,

$C_s = 1.391(S-35) - 7.8 \times 10^{-2}(S-35)^2$.

$C_{s,t,p} = (S-35)(-1.197\times10^{-2}T + 2.61\times10^{-4}p - 1.96\times10^{-2}p^2 - 2.09\times10^{-6}pT) + p(-2.796\times10^{-4}T + 1.3302\times10^{-5}T^2 - 6.644\times10^{-8}T^3) + P^2(-2.391\times10^{-7}T + 9.286\times10^{-10}T^2) - 1.745\times10^{-10}p^3T$ and s,t,p represent the measured values of salinity, temperature and pressure. In general sound speed in the ocean increases with increases in salinity, temperature and depth (pressure), with temperature changes dominating the equation near the surface. As a result, sound at different depths propagates with different speeds and these variations of sound speed with depth are in turn dependent on location and time of year.

A typical velocity gradient for temperate waters[23] is shown in Fig. A-1. The upper portion of the curve (0-1000 m) shows the effect of temperature changes while the lower portion indicates the effect of increasing pressure. These variations in sound speed with depth result in the sound's being refracted almost continuously as it propagates in the ocean. Hence the sound follows a curved path and rarely travels in a straight line for any distance.

The radius of curvature of each segment of a curved path a sound ray may follow can be calculated by applying Snell's law. A simple relationship for computing the radii of curvature, for a given velocity profile, is developed by Kinsler and Fay[24] as

$$R = \frac{C_o}{-g} = \frac{C}{-g\cos\theta} \qquad \text{(A-2)}$$

where θ is the angle made with the horizontal at a depth where the speed of sound is c, g is the velocity gradient and C_o is the sound speed at a depth where the ray would become horizontal. By calculating the radius of curvature of each segment, the actual path a ray of sound would follow, when transmitted at a particular depth, can be determined.

A2 Sound Channels in General

As shown in Figure A-1 the velocity of sound attains a minimum value at some depth (normally of the order of

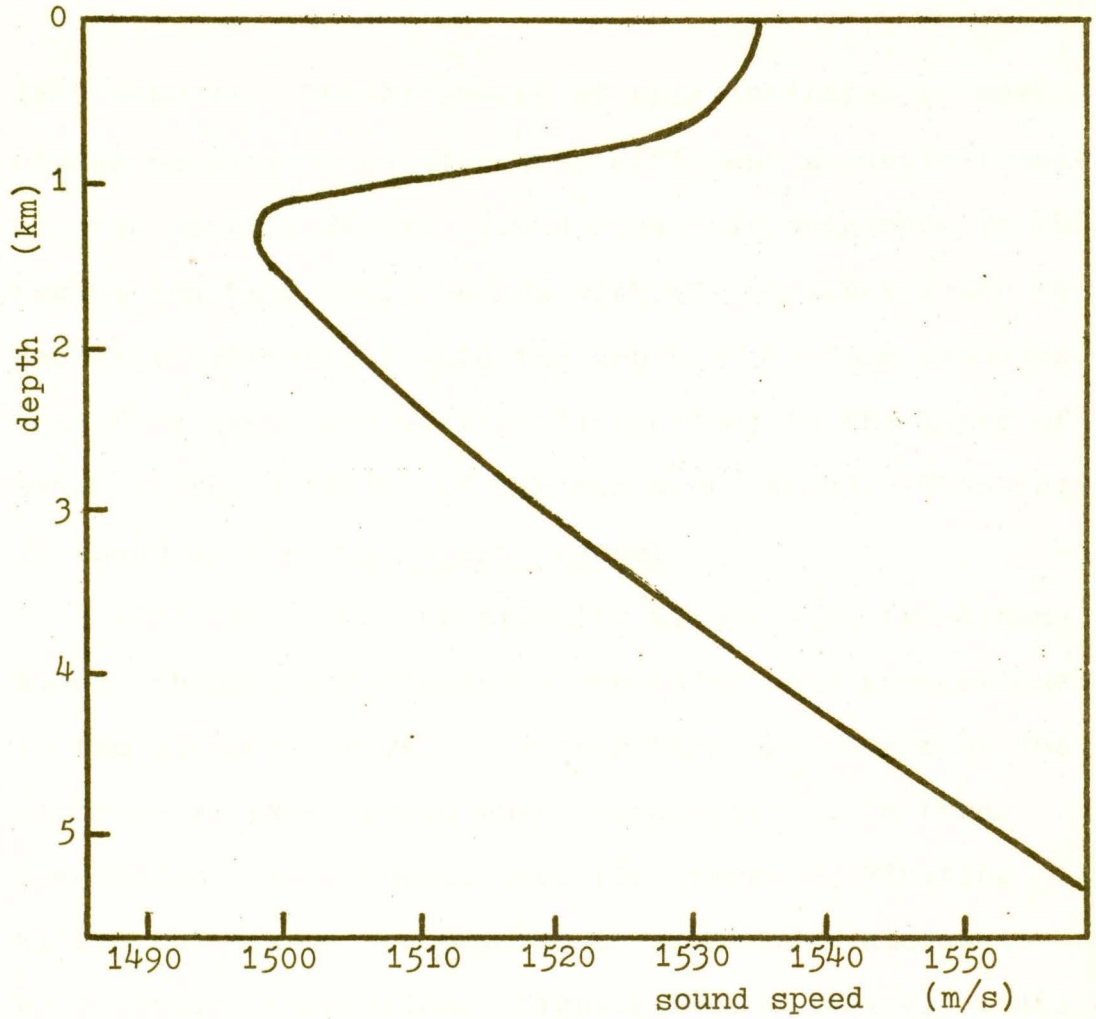

FIG. A-1 Typical depth variation of sound speed for temperate waters. Note the influence of temperature variations near the surface (0 - 1km) while at depths beyond 2km pressure is the dominating factor.

1000 meters). The existence of this condition in most oceans results in particularly efficient acoustic transmission at this depth. Sound rays that originate in this region and make small angles with the horizontal are repeatedly refracted toward the depth of minimum velocity. Therefore their propagation is confined to the layer of water in the vicinity of minimum sound speed. This region is known as the deep sound channel.

Acoustic energy propagating within this two-dimensional channel experiences a spreading loss proportional to the distance travelled rather than the square of the distance as experienced when propagation is in three dimensions. As a result acoustic energy originating within the channel propagates to tremendous distances with little attenuation. Signals from relatively small explosive sources within the channel have been detected up to several thousand miles from the source.[25]

In Arctic waters the axis of the deep sound channel lies at or near the surface. Figure A-2 shows the curved propagation paths that sound follows when transmitted at a depth of 800 ft in the Arctic.[26] Note that most of the sound reaches long distances only after repeated reflections from the rough surface of the ice.

These reflections have a severe effect on the frequency composition of the energy arriving at a remote sensor. Acoustic energy with wavelengths of the order

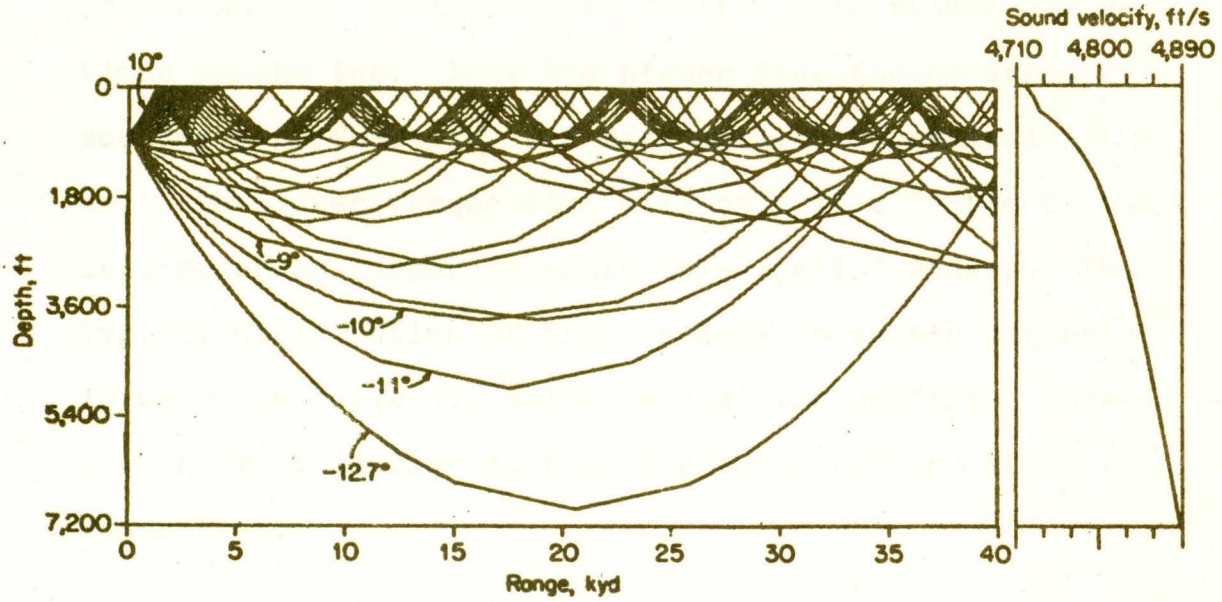

FIG. A-2 Ray diagram for sound transmission in ice-covered Arctic waters. The rays, drawn with 10° intervals, illustrate some of the many paths that sound can follow when transmitted at a depth of 800 ft.

of the surface variations is scattered in random directions by the ice. Thus the higher frequencies are scattered profusely by the many smaller irregularities while the lower frequencies will only be effected by the less numerous larger irregularities called ridges. The typical distribution of these ridges in Arctic waters[27] is shown in Table VI, while typical ice profiles, showing the many smaller surface fluctuations[28] are shown in Figure A-3.

TABLE VI The occurrence of ridges in Arctic water

Drafts in excess of (feet)	Average per mile
60	0.1
38	1
24	4
15	10

The Arctic sound channel is analogous to a shallow-water channel overlaying a soft mud-bottom.[29] The shallow-water layer can be thought of as corresponding to the upper 350 m of water, while the sub-bottom sediments are represented by the water beneath 350 m. Sound propagation in shallow-water channels has been widely investigated and solutions of the wave equation in a medium bounded by two sides are given by different authors.

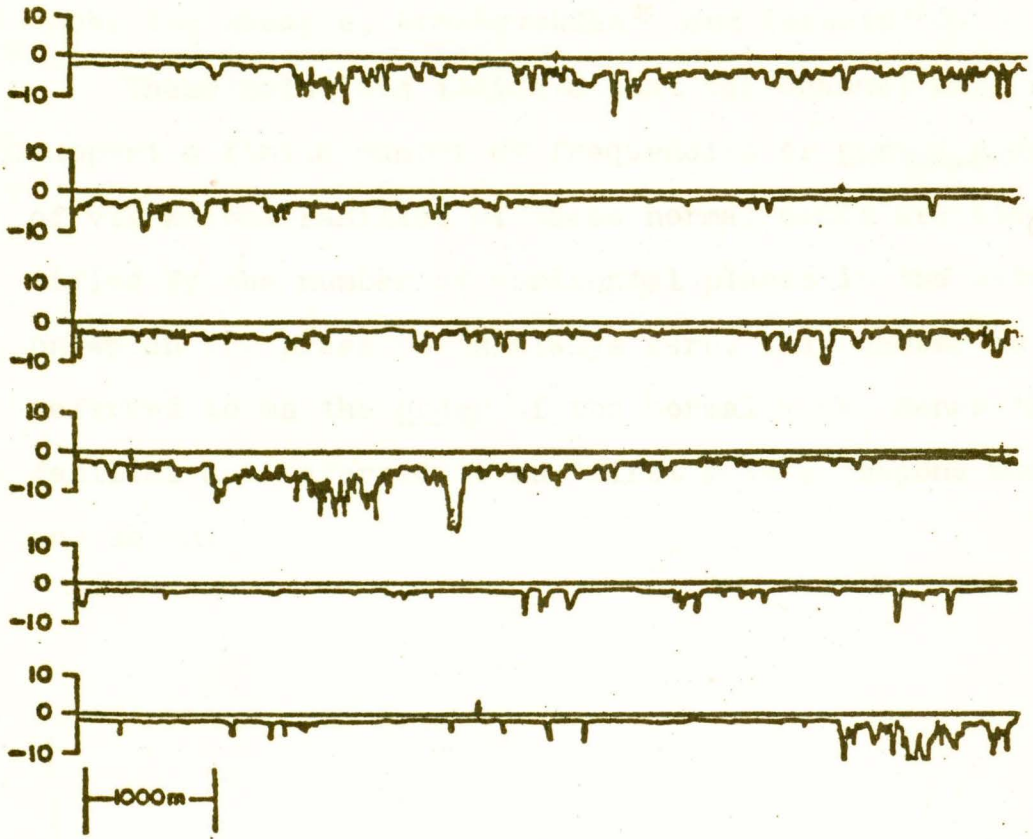

FIG. A-3 Profiles of the under surface of the ice.

(See, for example, Brekhovskikh[30] and Pekeris[31]).

These solutions indicate that the channel will only support a finite number of frequencies or normal modes of vibration. Families of these normal modes are identified by the number of horizontal planes in the water on which the pressure is always zero. This number is referred to as the order of the normal mode. Hence the families are referred to as "first mode", "second mode", and so on.

APPENDIX B

B1 The Drive Unit

A partial cut-away view of the drive unit is shown in Fig. 3.3. The drive unit can be divided into two major components, the bearing assembly and the motor assembly.

The primary function of the bearing assembly is to support the rotating arm and thus eliminate vertical stresses on the motor assembly. The bearings are mounted in a 7.6 cm diameter plastic cylinder. This cylinder also serves to support the microswitch which is actuated by a disc mounted on the shaft to which the rotating arm is fastened. A moveable pin which can be placed at 5 degree intervals on the circumference of the disc enables the microswitch to be actuated at different positions of the rotating arm. This device is used to control the electrical input to the analyser.

The second major component of the drive unit, the motor assembly, consists of an 1800-rpm motor with a series of reduction gears which reduce its angular velocity to 0.75 rpm. By replacing the first gear in the assembly with a gear of approximately one-half its diameter, the angular velocity can be further reduced to 0.33 rpm. The motor has two starting windings which remain in the circuit during its operation. By revers-

ing the connections to these starting windings, the direction of rotation can be reversed. This is accomplished by means of the toggle switch mounted on the top of the reduction gear box.

APPENDIX C

C1 Sound Reflection

When a sound wave is reflected at the interface between two fluids, for example air and water, the acoustic pressure of the reflected wave at the boundary is either in phase with that of the incident wave at the boundary or 180° out of phase.[32] This results since the specific acoustic impedance z of each fluid is a real quantity given by $\rho_o c$ where ρ_o is the equilibrium density of the respective medium and c its sound velocity. However the reflection of a sound wave in air produced at a solid surface is somewhat more involved.

The normal specific acoustic impedance z_n of the solid is defined as the ratio of acoustic pressure acting on the surface to the associated particle velocity normal to the surface. Since acoustic pressure is not always in phase with particle velocity at the surface of a solid, the normal specific acoustic impedance may be complex. In this case, the pressure amplitude of the reflected wave is also complex and consequently the reflected wave at the boundary may either lead or lag the incident wave by angles ranging from 0° to 180°.

C2 Diffuse Scattering Properties of the Quadratic-Residue Reflector

A wavelet of wavelength λ will experience a phase

shift, upon travelling down and up one of the wells, given by[33]

$$\phi_n = 4\pi d_n/\lambda \qquad \text{(C-1)}$$

where $d_n = S_n\,(\lambda_o/2N)$ is the depth of the n^{th} well. This results in the wavelets being reflected with a complex amplitude given by

$$a_n = \exp[-2\pi i\, S_n\, \lambda_o/\lambda N] \qquad \text{(C-2)}$$

When the quantity λ_o/λ is an integer, the Fourier transform of a_n for $(-\infty \leq n \leq +\infty)$ is equal to 1/N. This means that the energies scattered into different (discrete) directions are equal. Thus the quadratic-residue surface is an ideal wide-angle scatterer for a broad range of wavelengths.

APPENDIX D

D1 The Effect of Truncating the Signals

Consider two periodic functions given by

$$f(t) = A \cos(\omega_o t + \phi)$$

$$g(t) = B \cos \omega_o t$$

Their cross-correlation, given by Eq. 5.1 in periodic form is

$$C(\tau) = \frac{1}{2\pi} \int_{-\pi}^{\pi} A \cos(\omega_o(t+\tau)+\phi)\ B \cos \omega_o t \quad dt$$

Using the identity, $\cos \alpha \cos \beta = \frac{1}{2} \cos(\alpha-\beta) + \frac{1}{2} \cos(\alpha+\beta)$, the expression for cross correlation results in

$$C(\tau) = \frac{AB}{2} \cos(\omega_o \tau - \phi) \qquad \text{(D-1)}$$

The Fourier transform of this expression results in an expression for the cross-power of the two functions

$$P_{ab} = \frac{AB}{2} \{\delta(\omega - \omega_o)e^{j\phi} + \delta(\omega+\omega_o)e^{-j\phi}\} \qquad \text{(D-2)}$$

where $\delta(\omega)$ is defined as

$$\lim_{\varepsilon \to 0} \begin{cases} 0 & \omega < -\frac{\varepsilon}{2} \\ \frac{1}{\varepsilon} & -\frac{\varepsilon}{2} < \omega < \frac{\varepsilon}{2} \\ 0 & \omega > \frac{\varepsilon}{2} \end{cases}$$

Consider the same signals, only now truncated at time $|t| = \frac{Tm}{2}$ as shown in Fig. D-1. To obtain the cross correlation using Eq. (5.4) the Fourier transforms of the signals are required. The Fourier transform of $g(t)$ results in

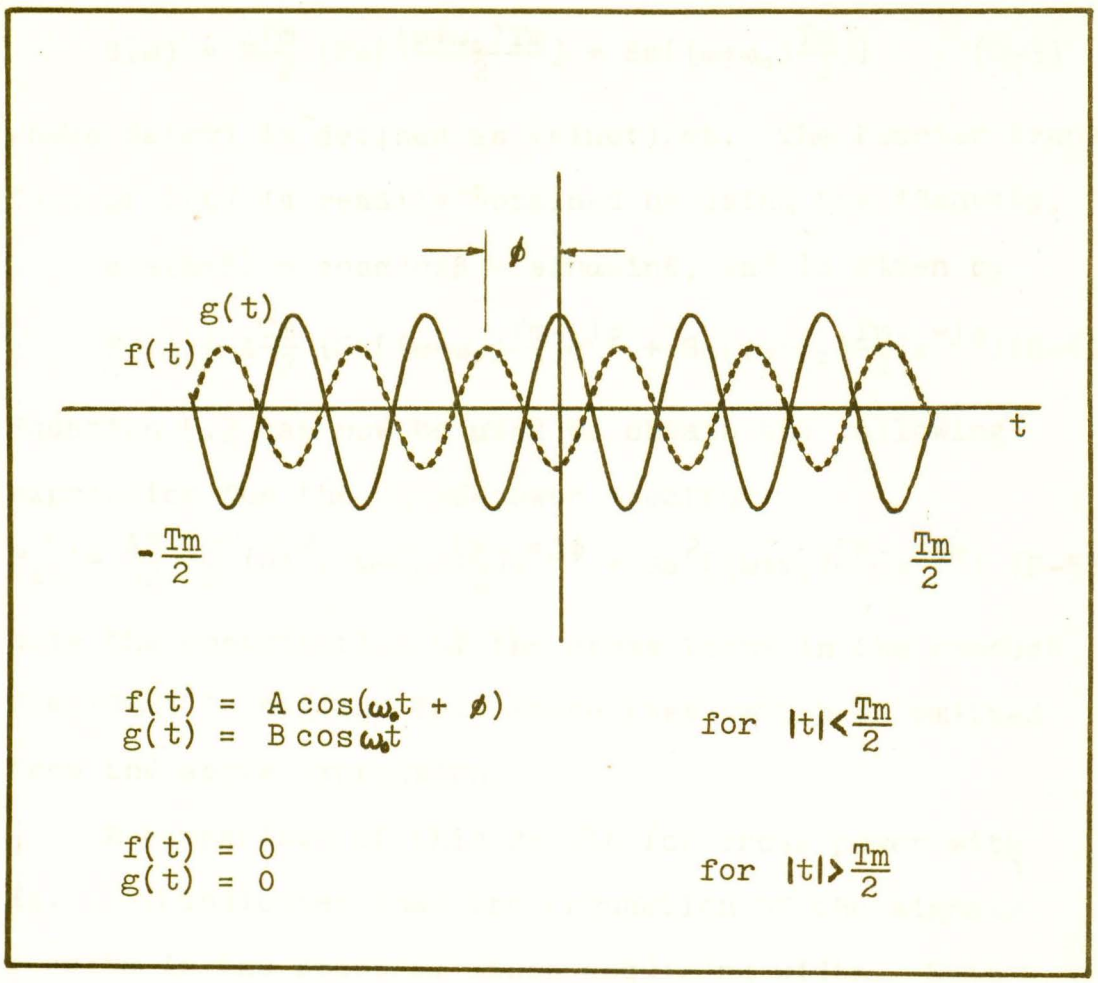

FIG. D-1 Truncated cosine signals.

$$G(\omega) = B\frac{Tm}{2}\{Sa[\frac{(\omega+\omega_o)Tm}{2}] + Sa[(\omega+\omega_o)\frac{Tm}{2}]\} \qquad (D\text{-}3)$$

where $Sa(\omega t)$ is defined as $(\sin\omega t)/\omega t$. The Fourier transform of $f(t)$ is readily obtained by using the identity, $\cos(\alpha+\beta) = \cos\alpha\cos\beta - \sin\alpha\sin\beta$, and is given by

$$F(\omega) = A\frac{Tm}{2}\{Sa[(\omega-\omega_o)\frac{Tm}{2}]e^{j\phi} + Sa[(\omega+\omega_o)\frac{Tm}{2}]e^{-j\phi}\} \qquad (D\text{-}4)$$

Equation 5.3 can now be used to obtain the following expression for the cross-power spectrum:

$$P_{ab} = \frac{AB}{2}\frac{Tm}{2}\{Sa^2[(\omega-\omega_o)\frac{Tm}{2}]e^{+j\phi} + Sa^2[(\omega+\omega_o)\frac{Tm}{2}]e^{-j\phi}\} \qquad (D\text{-}5)$$

Note the contribution of the cross terms in the product $F(\omega)\cdot G(\omega)$ is negligible. Hence they have been omitted from the above expression.

A comparison of this result for cross power with Eq. (D-2) indicates that the truncation of the signals results in the spectral lines acquiring width. Note that as Tm approaches infinity Eq. (D-5) approaches Eq. (D-2).

An alternate expression for cross-correlation can now be obtained by taking the inverse Fourier transform of Eq. (D-5). It is useful to use the Fourier transform pairs (b) and (c) given in Appendix D2. The resulting cross-correlation for the truncated signals is given by

$$C(\tau) = \left(1 - \frac{|\tau|}{Tm}\right)\frac{AB}{2}\cos(\omega_o\tau - \phi) \qquad (D\text{-}6)$$

It is important to note that as Tm approaches infinity, Eq. (D-6) the truncated result approaches the

continuous result, Eq. (D-1).

D2 Fourier Transform Pairs

a) $f(t) = \begin{cases} A & |t| < \frac{T}{2} \\ 0 & |t| < \frac{T}{2} \end{cases}$ $\qquad F(\omega) = AT\ Sa(\omega T)$

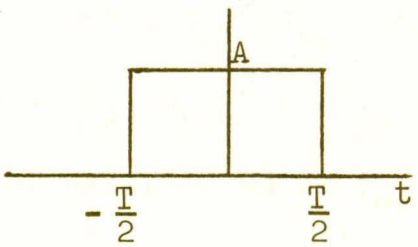

'boxcar' function

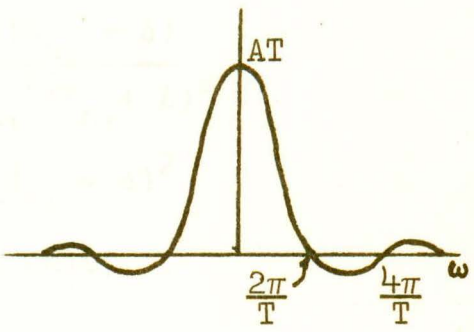

sample function

b) $f(t) = \begin{cases} (1 - \frac{|\tau|}{a})\ b & -a<\tau<a \\ 0 & \text{otherwise} \end{cases}$ $\qquad F(\omega) = ab\ Sa^2(\frac{\omega a}{2})$

c) $f(t) = g(t)e^{j\omega_o \tau}$ $\qquad F(\omega) = G(\omega - \omega_o)$

D3 The Influence of Power Changes on Coherence

Consider the sampling of two time sequences f_k and g_k whose power changes with respect to time. Assume their Fourier transforms F_n and G_n possess only real components, ie. $F_n \cdot F_n^* = F_n^2$.

Let the Fourier transforms obtained from the second sampling be related to the first so that $F_{n2} = F_{n1} + \Delta$

and $G_{n_2} = G_{n_1} + \delta$. Therefore the coherence that results after two samplings is given by

$$\gamma_{n_2} = \frac{[F_{n_1} G_{n_1} + (F_{n_1} + \Delta)(G_{n_1} + \delta)]^2}{[F_{n_1}^2 + (F_{n_1} + \Delta)^2][G_{n_1}^2 + (G_{n_1} + \delta)^2]}$$

$$= \frac{B + 2 F_{n_1} G_{n_1} (F_{n_1} + \Delta)(G_{n_1} + \delta)}{B + F_{n_1}^2 (G_{n_1} - \delta)^2 + G_{n_1}^2 (F_{n_1} + \Delta)^2}$$

where $B = (F_{n_1} G_{n_1})^2 + (F_{n_1} + \Delta)^2 (G_{n_1} + \delta)^2$

Two cases exist in which γ_{n_2} can be unity.

Case #1

i) $2 F_{n_1} G_{n_1} (F_{n_1} + \Delta)(G_{n_1} + \delta) = 0$

and ii) $F_{n_1}^2 (G_{n_1} + \delta)^2 + G_{n_1}^2 (F_{n_1} + \Delta)^2 = 0$

This leads to a solution where F_{n_1} and F_{n_2} equal zero or G_{n_1} and G_{n_2} equal zero, ie. only one signal exists.

Case #2

$$2F_{n_1} G_{n_1} (F_{n_1}+\Delta)(G_{n_1}+\delta) = F_{n_1}^2 (G_{n_1}+\delta)^2 + G_{n_1}^2 (F_{n_1}+\Delta)^2$$

This results in a situation where

$$\frac{(F_{n_1} + \Delta)^2}{(G_{n_1} + \delta)^2} = \frac{F_{n_1}^2}{G_{n_1}^2} = \frac{F_{n_2}^2}{G_{n_2}^2}$$

In other words if the changes in the Fourier transforms of the two signals are such that $\Delta/\delta = F_{n_1}/G_{n_1}$ the coherence will remain at unity. Therefore, it is the changes in the ratio of the power of the two signals that ad-

versely affects coherence.

D4 The Effect of Phase Changes on Coherence

Consider the two time series described by $f(t)$ and $f(t + \phi_m/\omega_o)$. Their Fourier transforms may be expressed $F(\omega)$ and $F(\omega)e^{j\phi_m}$. When the two series are sampled their coherence after one sampling can be expressed as $\gamma_1(\omega) = |F(\omega)\cdot F(\omega)e^{-j\phi_1}|^2/F^2(\omega)\cdot F^2(\omega) = 1$. If their phase relationship changes by an equal amount for each successive sampling then their coherence after m samplings can be expressed as

$$\gamma_m(\omega) = \frac{\sin^2(m\Delta\phi/2)}{m^2\sin^2(\Delta\phi/2)} \qquad \text{(D-8)}$$

where $\Delta\phi$ is the phase change between successive samplings.

The phase relationship of the signals is given in Section 2.2 as $\phi = (2\pi\ f\ D/c)\cos\theta$. For the model parameters and system geometry used in the coherence measurements (see Fig. 6.6) the phase change between samplings $\Delta\phi$ is 0.17 rad. Thus, when the phase changes resulting from changes in the angular position of the source are the only forces degrading coherence, the coherence after m samplings is given by

$$\gamma_m(\omega) = \frac{\sin^2(0.085\ m)}{7.2\text{x}10^{-3}m^2} \qquad \text{(D-9)}$$

D5 The Coherence Time Window

As previously stated the changes in the power spectra are inconsistent with a stationary process when the source is in motion. Since the process may be nearly stationary for very short time records it is desirable to have the length of each sampling as small as possible. However, the resolution of the function in the frequency domain is inversely proportional to the length of the sampling. Therefore, to provide adequate frequency resolution, a 20 ms sampling time was chosen as a compromise. Several coherence functions were obtained with the 20 ms time window and compared to those obtained, under identical conditions, with a 4 ms window. One comparison is shown in Table VII and in Fig. D-2. The source is the FM sinusoid described in Chapter 9. The two-dimensional reflector (with ridges) was in position and the coherence shown is that of the component at 8.95 kHz after 5 samplings.

TABLE VII The effect of different time windows on coherence.

run #	γ at 8.95 kHz for 20 ms T.W.	γ at 8.95 kHz for 4 ms T.W.
1	0.827	0.827
2	0.857	0.878
3	0.876	0.884
4	0.886	0.897
5	0.873	0.864
6	0.865	0.877
7	0.870	0.875
8	0.855	0.871
9	0.865	0.886
10	0.896	0.891

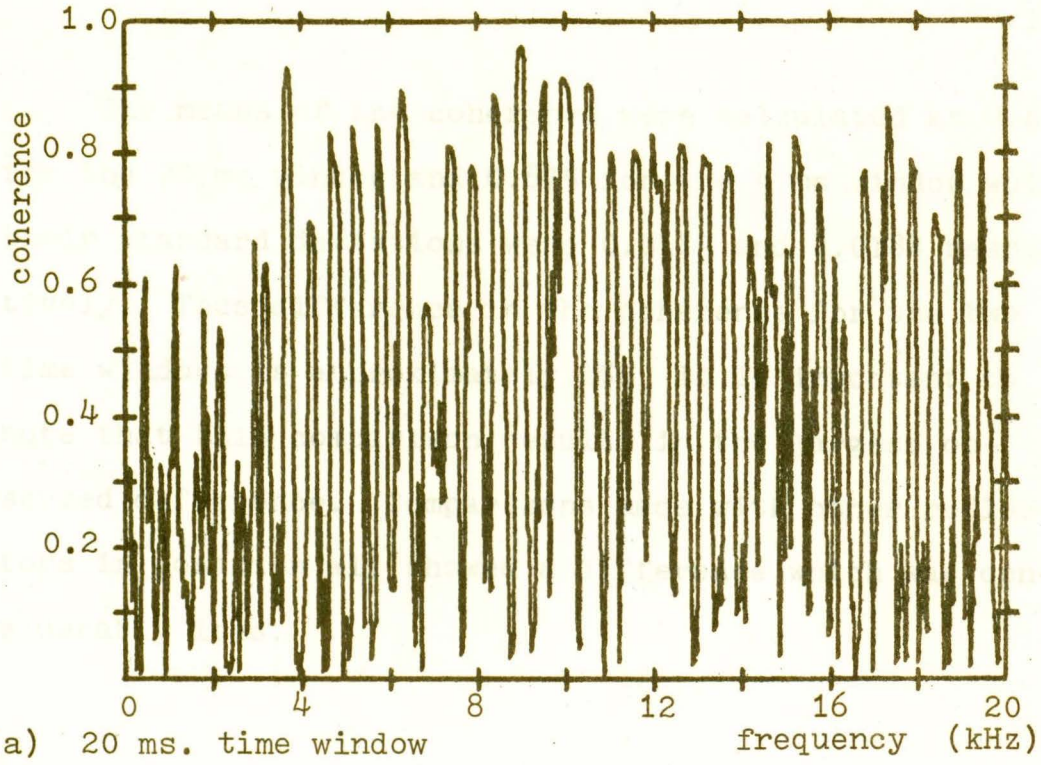

(a) 20 ms. time window

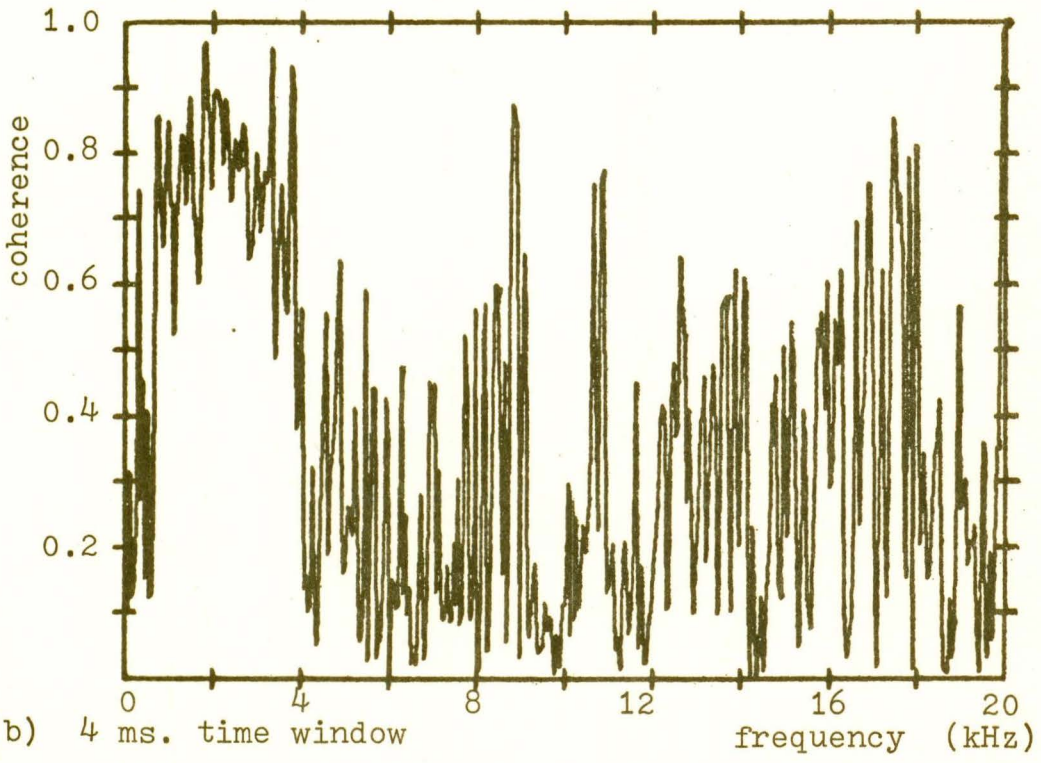

(b) 4 ms. time window

FIG. D-2 The effect of the time window on the resolution of the coherence.

The means of the coherence were calculated as 0.866 for the 20 ms window and 0.875 for the 4 ms window while their standard deviations were 0.0189 and 0.0184 respectively. Thus difference in the coherence for the two time windows is approximately 1%. It is important to note that this comparison results in the largest observed difference. Comparisons made with other reflectors in position all showed a difference which was considerably less.

APPENDIX E

E1 Determining the Beamwidth of the Speaker

For the purposes of determining its beamwidth the speaker was mounted on the central supporting shaft of the moving source apparatus and one of the microphones was placed on the end of the rotating arm. The analyser was programmed to compute the power spectrum of the signal received by the microphone when a pure tone was used as a source (8 kHz). The magnitude of the power spectrum was recorded for various angular positions of the rotating arm. This procedure was repeated for a pure tone at 14 kHz and the beamwidths at each frequency were calculated.

Figure E-1 shows the resulting radiation patterns for these two frequencies which represent the approximate band limits of the pink noise source used in the experiments. By convention, the bandwidth is calculated at the half power points of the radiation pattern (3dB down). The resulting beamwidths are 56 and 40 degrees for the 8 and 14 kHz tones respectively. These calculations indicate that it is not necessary to remove the analysing equipment from the anechoic chamber during the experiments; although precautions must be taken to ensure that the equipment is not within the beam immediately before or during the sampling of the signals.

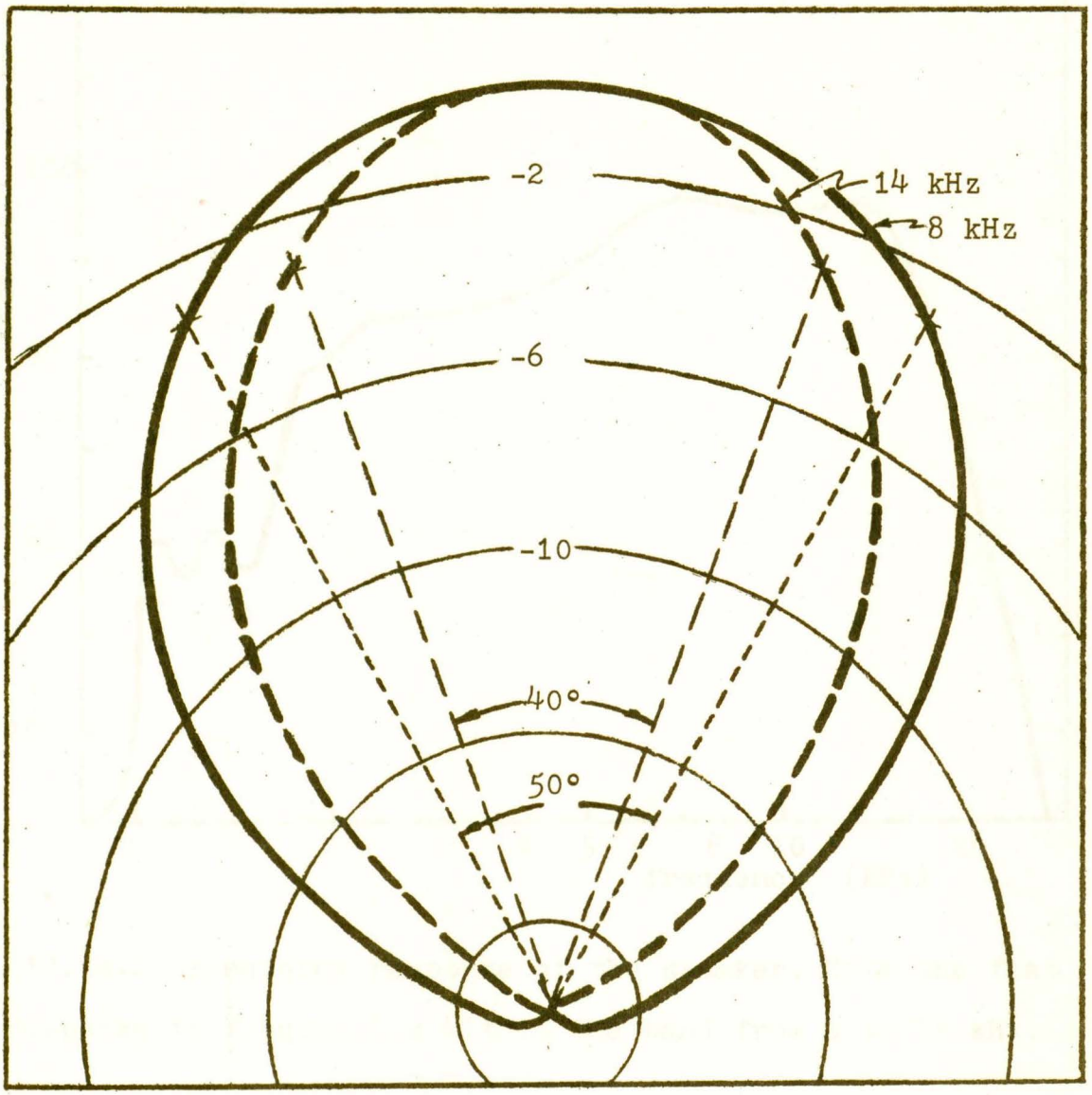

FIG. E-1 Radiation patterns of speaker for source frequencies 8 and 14 kHz. The concentric circles indicate the relative intensity of the beam in decibels.

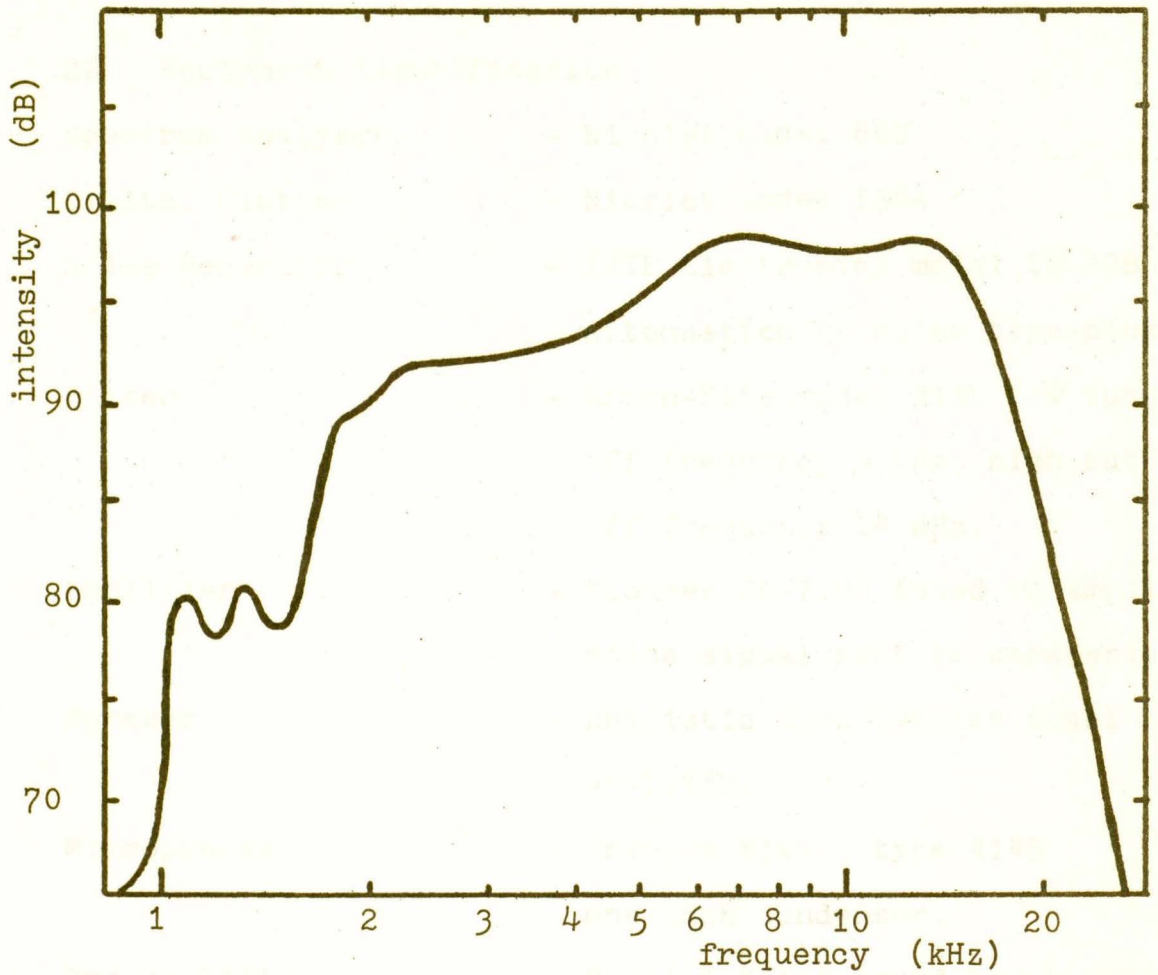

FIG. E-2 Frequency response of the speaker. Note the flat response to frequencies within the band from 8 to 14 kHz.

E2 Equipment Identification

Spectrum Analyser	- Nicolet model 660
Digital Plotter	- Nicolet model 136A
Noise Generator	- IVIE Electronics model TE-20B attenuation-0, noise type-pink.
Filter	- Krohn-Hite model 3100 low cut-off frequency 9 kHz, high cut-off frequency 14 kHz.
Amplifier	- Pioneer SA-7100 (used to amplify noise signal sent to speaker).
Speaker	- Realistic Horn Tweeter model 40-1278B.
Microphones	- Bruel & Kjaer, type 4145 one inch condenser.
Pre-amplifier	- Bruel & Kjaer sound level meter type 2209 (used to amplify output from microphone A).
Pre-amplifier	- Bruel & Kjaer Heterodyne Analyser type 2010 (used to amplify output from microphone B).

APPENDIX F

F1 The Doppler Effect

Consider a sound source moving with velocity v relative to a microphone as shown in Fig. F-1. Let c, f and λ refer to the sound wave as it passes through the medium (air) and let θ be the angle between the velocity vector $\vec{v}$ and the line from the source to the microphone. The component of $\vec{v}$ in the direction of the microphone is then $v\cos\theta$.

The wavelength λ observed at the microphone is then given by $\lambda = (c + v\cos\theta)/f_o$, where f_o is the frequency of the sound in the reference frame in which the source is at rest. Therefore the frequency observed at the microphone is given by $f = f_o(1 + \frac{v}{c}\cos\theta)^{-1}$. To terms in $(v/c)^2$ this expression can be approximated as

$$f \simeq f_o(1 - \frac{v}{c}\cos\theta) \qquad \text{(F-1)}$$

Thus the frequency of the source observed at the microphone is changed by an amount equal to

$$\Delta f \simeq - f_o \frac{v}{c}\cos\theta \qquad \text{(f-2)}$$

and is referred to as the Doppler shift.

F2 The Error Involved in the Frequency Difference Approximation

The term $[1 + (D/2r)^2]^{-\frac{1}{2}}$ in Eq. 6.4 can be expanded as follows:

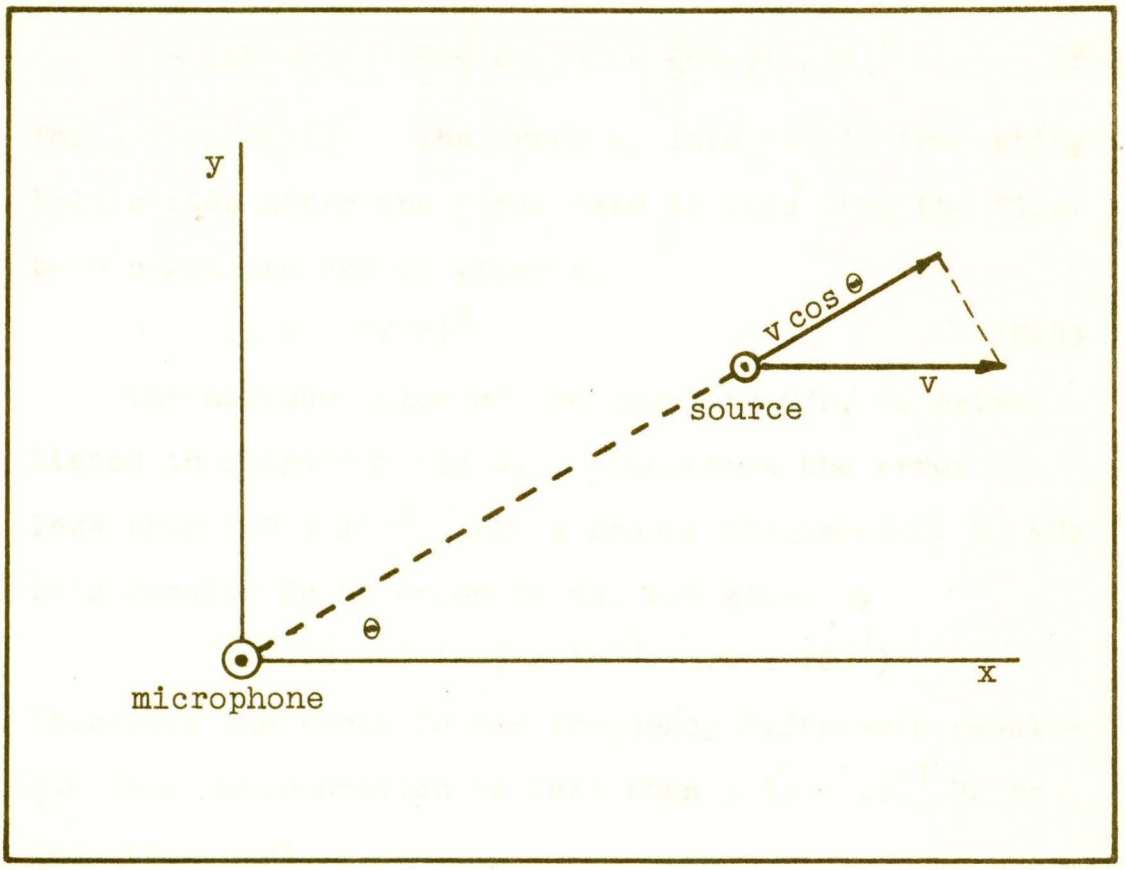

FIG. F-1 Sound source moving relative to a microphone.

$$1 - \tfrac{1}{2}(D/2r)^2 + \frac{1.3}{2.4}(D/2r)^4 - \frac{1.3.5}{2.4.6}(D/2r)^6 + \ldots \quad \text{(F-3)}$$

for $-1 < (D/2r)^2 \leq 1$. The error ε_o involved in truncating this series after the first term is less than the first term neglected and is given by

$$\varepsilon_o < \tfrac{1}{2}(D/2r)^2 \quad \text{(F-4)}$$

The maximum value of the quantity D/r, as established in Chapter 2 is 0.2. Therefore the error is less than 5.0×10^{-3}. For a source frequency of 10 kHz this results in an error in Eq. 6.4 given by

$$\varepsilon < 10{,}000\ (6.7 \times 10^{-6})(5.0 \times 10^{-3})$$

Therefore the error in the frequency difference resulting from the truncation is less than 3.35×10^{-4} Hz or less than 0.5%.

F3 Degradation in Correlation Induced by the Doppler Effect

Consider a moving pure tone source passing through a point on the perpendicular bisector of the array as shown in Fig. 6.1. The frequency of the signal at microphone 'a' is increased to $f_a = f_o + \Delta f$ and that at microphone 'b' is reduced to $f_b = f_o - \Delta f$. If the source signal is defined as $f_o(t) = A \cos\omega_o t$ then the signals received at the respective microphones are $f_a(t) = A \cos\omega_a t$ and $f_b(t) = A \cos\omega_b t$ where $\omega_o = 2\pi f_o$ is the angular frequency of the source, $\omega_b = \omega_o - \Delta\omega$ and $\omega_a = \omega_o + \Delta\omega$.

For the purposes of calculating the cross correlation a period given by $T = 2\pi/\omega_o$ is assumed. Therefore an approximate expression for cross correlation is given by

$$C(\tau) \simeq \frac{A^2}{T} \int_o^T \cos \omega_b(t+\tau) \cos\omega_a t \quad dt \qquad \text{(F-5)}$$

where $T = 2\pi/\omega_o$.

Using the identities $\cos a \cos b = \frac{1}{2}\{\cos(a-b) + \cos(a+b)\}$ and $\cos(a+b) = \cos a \cos b - \sin a \sin b$ the integral is expanded as

$$C(\tau) \simeq \frac{A^2}{2T} \cos \omega_o\tau \int_o^T (\cos 2\Delta\omega t + \cos 2\omega_o t)\, dt$$

$$- \frac{A^2}{2T} \sin \omega_o\tau \int_o^T (\sin 2\Delta\omega t + \sin 2\omega_o t)\, dt \qquad \text{(F-6)}$$

where $2\Delta\omega = \omega_b - \omega_a$ and $2\omega_o = \omega_b + \omega_a$.

Upon completing the integration the resulting cross correlation is expressed as

$$C(\tau) \simeq \frac{A^2}{2} \cos \omega_o\tau \; Sa(4\pi\frac{\Delta\omega}{\omega_o})$$

$$+ A^2\pi\frac{\Delta\omega}{\omega_o} \sin \omega_o\tau \; Sa^2(2\pi\frac{\Delta\omega}{\omega_o}) \qquad \text{(F-7)}$$

where $Sa(\omega)$ is defined as $\frac{\sin\omega}{\omega}$;

the coefficient of the cross correlation $C(o)$ is then given by

$$C(o) \simeq \frac{A^2}{2} Sa(4\pi\frac{\Delta\omega}{\omega_o}) \qquad \text{(F-8)}$$

The correlation coefficient for signals of identical frequency is simply $A^2/2$. Therefore the difference in

the correlation coefficient that results from a Doppler shift can be written as

$$\Delta C(o) \simeq \frac{A^2}{2} [1 - Sa(4\pi \frac{\Delta f}{f_o})] \qquad (F-9)$$

APPENDIX G

G1 The Accuracy of Re-positioning the Source for the Static Comparison

The position that the moving source was in when the electrical signals were sampled is determined by the "lag" of the main correlation peak. Since the lag is read to the nearest 4.0 μs an uncertainty of ± 2μs is introduced into the result. For a sound velocity of 3.46×10^5 mm/s this represents an uncertainty in the path difference S of 3.46×10^5 mm/s x 2×10^{-6} s = ± 0.692 mm. When the source distance r is much greater than the microphone separation D, $S/D \simeq \cos\theta = \sin(\frac{\pi}{2} - \theta)$ (see Fig. 2.1). Since the length of the arc $a = r(\frac{\pi}{2} - \theta)$ the following relationship exists between the path difference S and the displacement of the source a,

$$a \simeq \sin^{-1}(S/D) \cdot r \qquad (G\text{-}1)$$

Therefore the uncertainty in the path difference of ± 0.692 mm results in an uncertainty in the displacement of the source of ± 2.9 cm when the microphone separation is 3.5 cm.

As a result of this uncertainty the position of the source for the static correlogram is not necessarily identical to the position it was in when the electrical signals were sampled with the moving source. A difference in the source position results in a significant

change in the intensity of sound at the microphones between the static and moving tests. This occurs since small changes in the source position result in corresponding spacial changes in the zones of high and low intensity in the vicinity of the microphones.

APPENDIX H

H1 Simulating Background Noise

Since the background noise in the field is generated by a variety of sources and arrives at the receivers from a number of directions it is generally non-coherent. To simulate this situation in the model, band limited random noise (1 to 8 kHz) was used to frequency-modulate a sinusoidal waveform. The output from the modulator was recorded and used to drive two moving-coil speakers positioned at opposite ends of the microphone array as shown in Fig. H-1. A quantity of acoustic absorbing material was placed between the microphones in an attempt to confine the output of each speaker to the respective microphone. In this way a significant time-delay is established between the arrival of the noise at the two microphones. Since the noise is composed of frequencies which are randomly changing, the time-delay results in a rapid degradation in coherence of the background noise at the microphones.

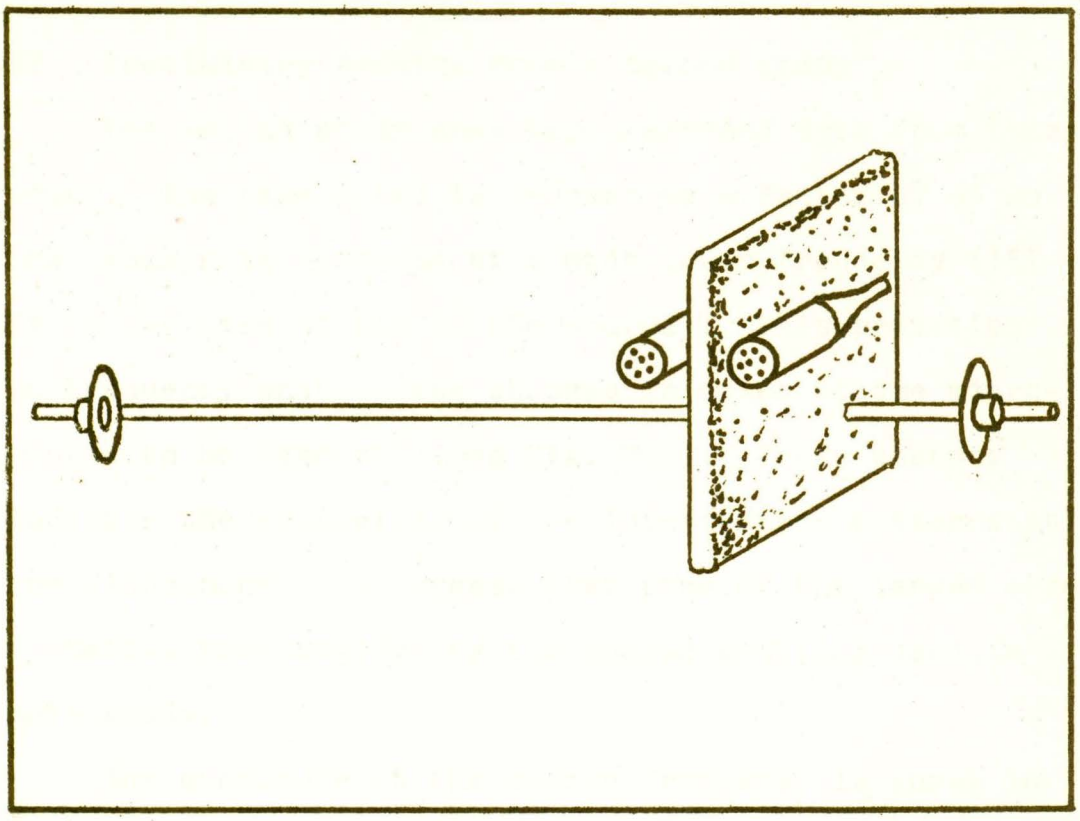

Fig. H-1 The microphone array showing the background noise speakers and the sound-absorbing material used to isolate their output to their respective microphones.

H2 Preliminary Results From a Second Study

The second study uses tape recorded data from this study. The tape speed is reduced by a factor of 64 so the source is observed at a much lower frequency (157 Hz in the case of the 10 kHz source). This reduction in frequency enables the changes in power at the microphones to be observed (see Fig. H-2). These changes indicate the complexity of the interference patterns at the microphones and suggest that some of the larger order anomalies were avoided by the spaced sampling used in this study.

The coherence at the source frequency is shown in Fig. H-3 for two different sampling ratios (ie., sampling time:total acquisition time). Curve (a) is the result for the tape recorded 10 kHz source, therefore the sampling ratio is identical to that used in this study (ie., 0.02s/0.42s = 0.05). Curve (b) was obtained from the same tape when its speed was reduced by a factor of 64. The sampling ratio is 2.0s/2.17s = .92. These curves suggest that the coherence results shown in this study would not have shown a significant improvement had it been possible to use a larger sampling ratio.

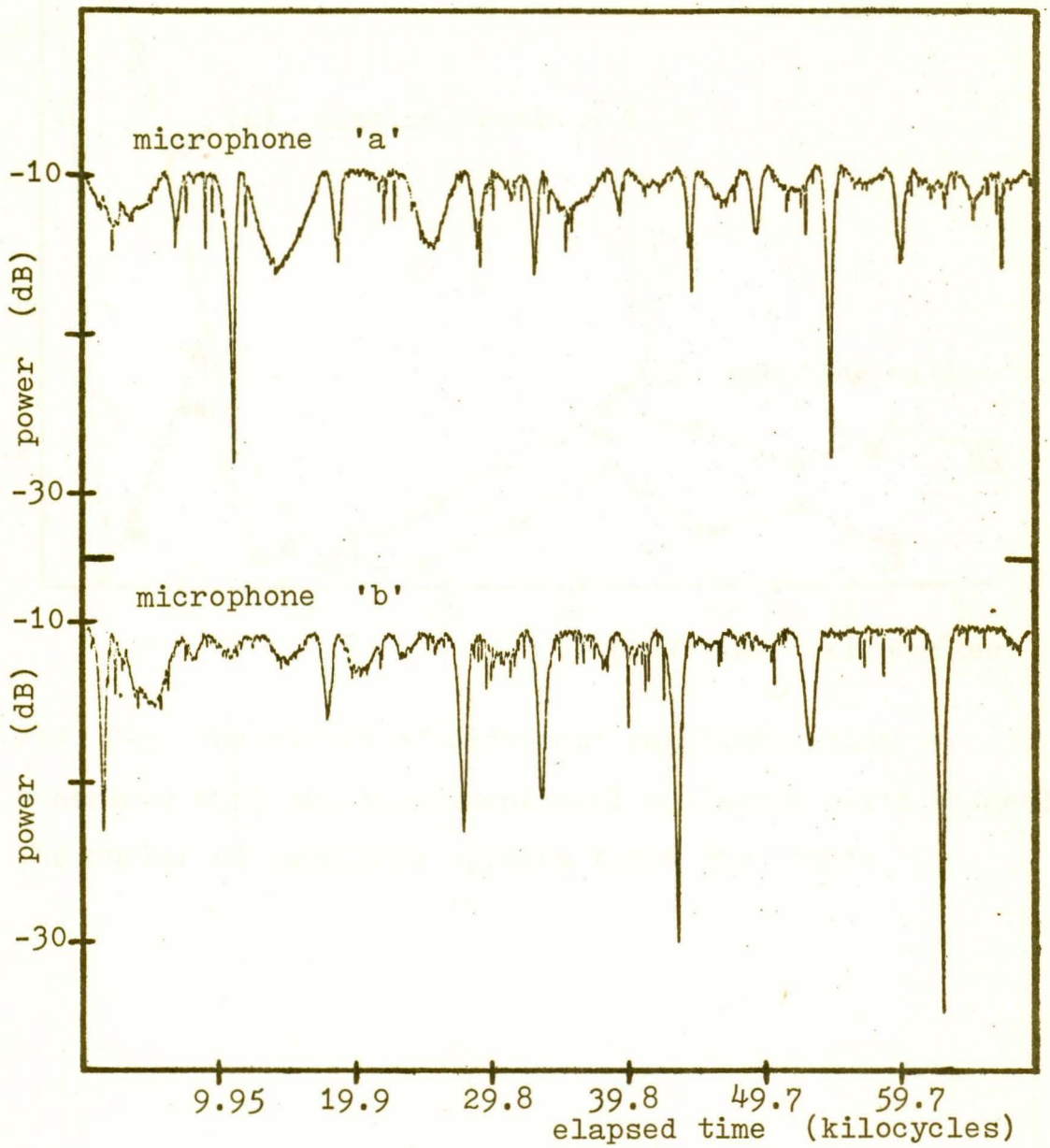

FIG. H-2 Power at the microphones as a function of time when the two-dimensional reflector (with ridges) is in position. The graph commences when the source is in the 72° position. The elapsed time is measured in cycles of the pure-tone source so that graphs made with different tape speed reductions can be compared.

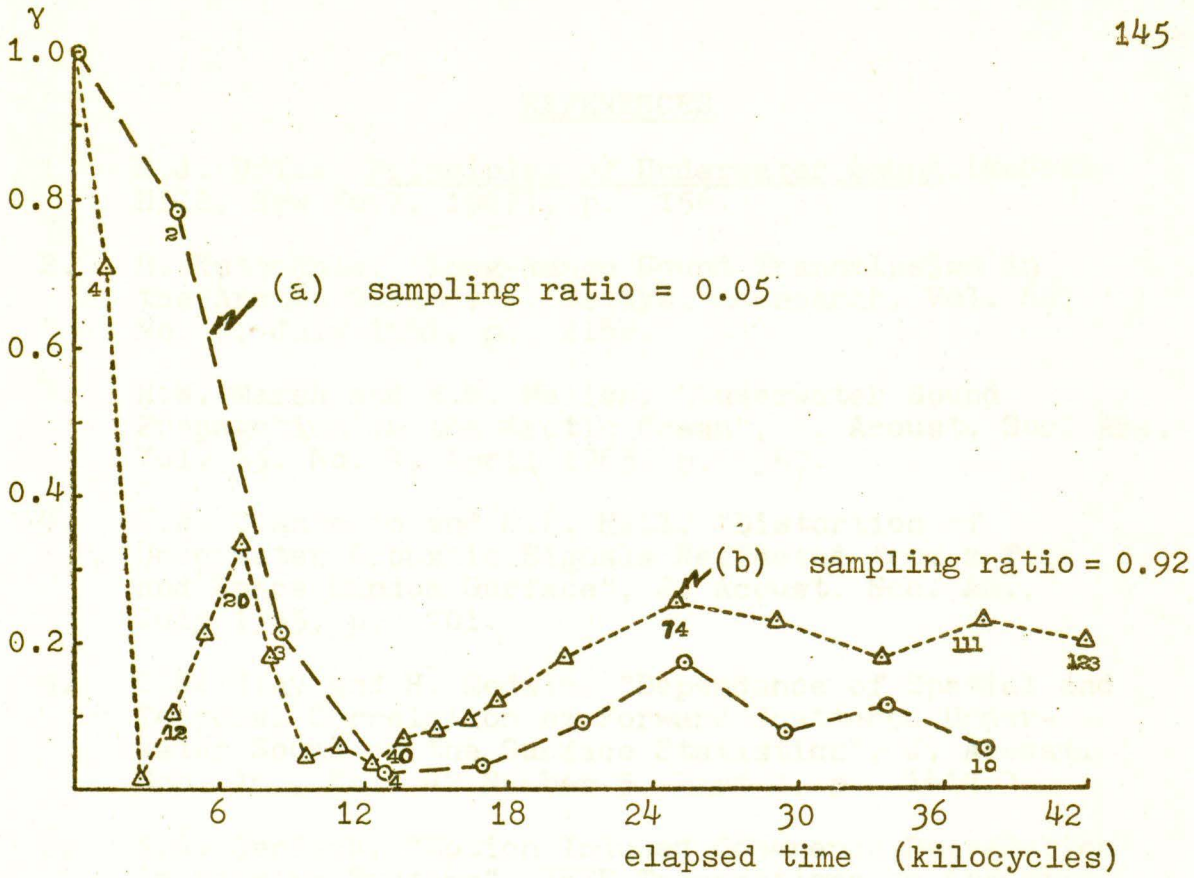

FIG. H-3 The effect of different sampling ratios on coherence with the two-dimensional reflector (with ridges). The number of samplings appears below the points.

REFERENCES

1. R.J. Urick, Principles of Underwater Sound,(McGraw-Hill, New York, 1967), p. 156.

2. H. Kutschale, "Long-Range Sound Transmission in the Arctic Ocean", J. Geohys. Research, Vol. 66, No. 7, July 1961, p. 2189.

3. H.W. Marsh and R.H. Mellen, "Underwater Sound Propagation in the Arctic Ocean", J. Acoust. Soc. Am., Vol. 35, No. 4, April 1963, p. 560.

4. R.A. D'Antonio and R.F. Hill, "Distortion of Underwater Acoustic Signals Reflected from a Time and Space Random Surface", J. Acoust. Soc. Am., July 1965, p. 701.

5. C.S. Clay and H. Medwin, "Dependance of Spatial and Temporal Correlation of Forward Scattered Underwater Sound on the Surface Statistics", J. Acoust. Soc. Am., Vol. 47 Number 5, Part 2, p. 1412.

6. A.A. Gerlach, "Motion Induced Coherence Degredation in Passive Systems", IEEE Transactions on Acoustics, Speech, and Signal Processing, Vol. ASSP-26, No. 1, Feb. 1978, p.p. 1-15.

7. R.P. Flanagan and N.L. Weinberg, "Effects of Source Motion on an Acoustic Signal in the Frequency, Time, and Space Domains", J. Acoust. Soc. Am., Vol. 67, No. 5, May 1980, p. 1532.

8. H.J. Young, "Measurements of Underwater Signal Phase Stability Using a Moving Source", J. Acoust. Soc. Am., Vol. 67, No. 6, June 1980, p. 2025

9. G.M. Jenkins and D.G. Watts, Spectral Analyses and its Applications, (Holden-Day, San Francisco, 1968), p. 230.

10. D.J. Thomson, "Spectrum Estimation Techniques for Characterization and Development of WT 4 Waveguide-11", The Bell System Technical Journal, Dec. 1977, p. 1983.

11. G.M. Jenkins and D.G. Watts, Spectral Analyses and its Applications, (Holden-Day, San Francisco, 1968), p. 356.

REFERENCES (con't)

12. B. Kleiner and R.D. Martin and D.J. Thomson, "Robust Estimation of Power Spectra", Journal of the Royal Statistical Society, Series B, Vol. 41, No. 3, 1979, p. 313.

13. R.H. Mellen and H.W. Marsh, "Underwater Sound Reverberation in the Arctic Ocean", J. Acoust. Soc. Am., Vol. 35, No. 10, Oct. 1963, p. 1615.

14. M.R. Shroeder, "Binaural Dissimilarity and Opitimum Ceilings For Concert Halls: More Lateral Sound Diffusion", J. Acoust. Soc. Am., Vol. 65, No. 4, Apr. 1979, p. 958.

15. E.R. Kanasewich, Time Sequence Analysis in Geophysics (Univ. of Alberta Press, Alberta, 1975), p. 83.

16. ibid., p. 119

17. ibid., p. 84

18. ibid., p. 84

19. ibid., p. 121

20. R.E. Ziemer and W.H. Tranter, Principles of Communications, (Houghton Mifflin Company, New Jersey, 1076), p. 116.

21. L.E. Kinsler and A.R. Frey, Fundamentals of Acoustics, (John Wiley and Sons, New York, 1962), p. 13.

22. H.J. McLellan, Elements of Physical Oceanography, (Pergamon Press, Toronto, 1965), p. 117.

23. H.J. McLellan, Elements of Physical Oceanography, (Pergamon Press, Toronto, 1965), p. 118.

24. L.E. Kinsler and A.R. Frey, Fundamentals of Acoustics, (John Wiley and Sons, New York, 1962), p. 466.

25. R.J. Urick, Principles of Underwater Sound, (McGraw-Hill, New York, 1967), p. 146.

26. R.J. Urick, Principles of Underwater Sound, (McGraw-Hill, New York, 1967), p. 158.

REFERENCES (con't)

27. R.H. Mellen and H.W. Marsh, "Underwater Sound Reverberation in the Arctic Ocean", J. Acoust. Soc. Am., Vol. 35, No. 10, Oct. 1963, p. 1618.

28. Arctic Submarine Laboratory, San Diego, Ca.

29. H. Kutschale, "Long-Range Sound Transmission in the Arctic Ocean", J. Geophys. Research, Vol. 66, No. 7, July 1961, p. 2193.

30. L.M. Brekhvoskikh, Waves in Layered Media, (Academic Press Inc., New York, 1960) Chap. 5.

31. C.L. Pekeris, "Theory of Propagation of Explosive Sound in Shallow Water", Geol. Soc. Am. Memo 27, 1948.

32. L.E. Kinsler and A.R. Frey, Fundamentals of Acoustics, (John Wiley and Sons, New York, 1962) p. 128.

33. M.R. Shroeder, "Toward Better Acoustics For Concert Halls", Physics Today, Vol. 33, No. 10, Oct. 1980, p. 29.

VITA

Surname: HUTTON Given Names: JAMES PATRICK

Place of Birth: OWEN SOUND, ONT. Date of Birth: 20-09-49

Educational Institutions Attended, with Dates of Entering and leaving:

NOVA SCOTIA INSTITUTE OF TECHNOLOGY 1974 to 1975

ROYAL ROADS MILITARY COLLEGE, VICTORIA 1975 to 1979

UNIVERSITY OF VICTORIA, B.C. 1979 to 1981

Degrees, Diplomas, Etc., Awarded, with Dates and Names of Institutions:

B.Sc. 1979 ROYAL ROADS MILITARY COLLEGE

Honors and Awards:

University of Victoria Fellowship, 1979/80 and 1980/81

Publications: NONE

PARTIAL COPYRIGHT LICENSE

I hereby grant the right to lend my thesis or dissertation (the title of which is shown below) to users of the University of Victoria Library, and to make single copies only for such users or in response to a request from the library of any other university, or similar institution, on its behalf or for one of its users. I further agree that permission for extensive copying of this thesis for scholarly purposes may be granted by me or a member of the University designated by me. It is understood that copying or publication of this thesis for financial gain shall not be allowed with out my written permission.

Title of Thesis:

DEGRADATION OF COHERENCE AND CORRELATION WHEN SOUND FROM A MOVING SOURCE IS REFLECTED FROM SOLID SURFACES

Author:

[redacted]

James P. Hutton

July 31 1981